Electronic Supplementary Material (ESI) for New Journal of Chemistry.

Supplementary Information

Copper(II) Complexes of CuN_4S Core: Selective Cytotoxicity to Cancerous Cells, ROS Generation and Induction of Apoptosis

Kakoli Malakar[a,†], Balasubramaniam Selvakumaran[b,†], Mariappan Murali[b,*], Pitchan Arul Prakash[c], Somasundaram Sangeetha[b,d], Winaki P. Sohtun[a], Mohamed Sultan Mohamed Jaabir[c], Marappan Velusamy[c,*]

[a]Department of Chemistry, North Eastern Hill University, Shillong 793 022, India

[b]Coordination and Bioinorganic Chemistry Research Laboratory, Department of Chemistry, National College (Autonomous), Tiruchirappalli 620 001, Tamil Nadu, India

[c]Department of Biotechnology and Microbiology, National College (Autonomous), Tiruchirappalli 620 001, Tamil Nadu, India

[d]Department of Chemistry, Tamilavel Umamaheswaranar Karanthai Arts College, Thanjavur 613 002, Tamil Nadu, India

[†]Both authors are equally contributed.

[*]Corresponding authors: Mariappan Murali: murali@nct.ac.in; ma66mu@gmail.com
Marappan Velusamy: mvelusamy@nehu.ac.in; mvelusamy@gmail.com

Table S1 Selected crystal data and structure refinement parameters for [Cu (L1-L4)(phen)]ClO_4.

	1	**2**	**3**	**4**
Crystal system	triclinic	triclinic	monoclinic	triclinic
Empirical Formula	$C_{20}H_{16}ClCuN_5O_4S_2$	$C_{23}H_{21}ClCuN_6O_4S_2$	$C_{26}H_{20}ClCuN_5O_4S_2$	$C_{24}H_{18}ClCuN_5O_4S_2$
Space group	P-1	P-1	P21/n	P-1
a/Å	7.832(4)	9.728(12)	11.0470(5)	9.5643(4)
b/Å	11.671(7)	11.627(14)	12.7855(6)	11.7487(6)
c/Å	25.344(14)	12.805(15)	38.4549(14)	12.3580(7)
α/°	91.825(19)	77.374(13)	90	99.801(2)
β/°	97.631(19)	69.379(12)	97.2820(10)	101.321(2)
γ/°	98.431(18)	84.417(13)	90	109.2430(10)
Volume/$Å^3$	2268(2)	1322(3)	5387.6(4)	1243.47(11)
Z	2	2	4	2
$\rho_{calc}g/cm^3$	1.621	1.508	1.572	1.612
μ/mm^{-1}	1.303	1.129	1.110	1.196
F(000)	1124.0	612.0	2600.0	614.0
Radiation, (MoKα) λ	0.71073	0.71073	0.71073	0.71073
2θ range for data collection/°	3.81 to 57.888	4.472 to 55.584	3.836 to 56.706	3.796 to 56.926
Index ranges	$-10 \le h \le 10$, $-15 \le k \le 15$, $-34 \le l \le 33$	$-12 \le h \le 12$, $-15 \le k \le 15$, $-16 \le l \le 16$	$-14 \le h \le 14$, $-17 \le k \le 17$, $-51 \le l \le 46$	$-12 \le h \le 12$, $-15 \le k \le 15$, $-16 \le l \le 16$
Independent reflections	11472, $R_{int} = 0.1439$, $R_{sigma} = 0.1124$	6118, $R_{int} = 0.1890$, $R_{sigma} = 0.1526$	13433, $R_{int} = 0.0544$, $R_{sigma} = 0.0350$	6251, $R_{int} = 0.0277$, $R_{sigma} = 0.0185$
Data/restraints/parameters	11472/0/596	6118/0/328	13433/0/712	6251/0/406
Goodness-of-fit on F^2	1.517	0.912	1.031	1.033
Final R indexes [I > = 2σ (I)]	$R_1 = 0.1623$, $wR_2 = 0.4331$	$R_1 = 0.0776$, $wR_2 = 0.1865$	$R_1 = 0.0476$, $wR_2 = 0.1123$	$R_1 = 0.0341$, $wR_2 = 0.0910$
Final R indexes [all data]	$R_1 = 0.2224$, $wR_2 = 0.4727$	$R_1 = 0.1411$, $wR_2 = 0.2125$	$R_1 = 0.0792$, $wR_2 = 0.1264$	$R_1 = 0.0437$, $wR_2 = 0.0966$
Largest diff. peak/hole / e $Å^{-3}$	1.32/-2.44	1.16/-0.81	0.65/-0.52	0.43/-0.42

Table S1a Selected crystal data and structure refinement parameters for [Cu (L5-L7)(phen)]ClO_4.

	5	**6**	**7**
Crystal system	triclinic	monoclinic	triclinic
Empirical Formula	$C_{23}H_{17}ClCuN_6O_4S_2$	$C_{19}H_{17}ClCuN_6O_4S_2$	$C_{23}H_{19}ClCuN_6O_4S_2$
Space group	P-1	$P2_1/n$	P-1
a/Å	9.6470(5)	8.091(2)	8.0120(17)
b/Å	11.4872(6)	27.271(7)	11.649(2)
c/Å	12.3607(6)	11.092(3)	13.796(3)
α/°	98.975(2)	90	98.427(11)
β/°	99.686(2)	110.960(3)	99.066(11)
γ/°	109.761(2)	90	94.234(11)
Volume/$Å^3$	1236.82(11)	2285.6(10)	1251.6(5)
Z	2	4	2
$\rho_{calc}g/cm^3$	1.623	1.617	1.610
μ/mm^{-1}	1.204	1.295	1.190
F(000)	614.0	1132.0	618.0
Radiation, (MoKα) λ	0.71073	0.71073	0.71073
2θ range for data collection/°	3.87 to 57.156	4.206 to 58.408	3.028 to 57.478
Index ranges	$-12 \le h \le 12$, $-15 \le k \le 15$, $-16 \le l \le 16$	$-11 \le h \le 10$, $-37 \le k \le 37$, $-15 \le l \le 15$	$-10 \le h \le 10$, $-15 \le k \le 15$, $-18 \le l \le 18$
Independent reflections	6221, $R_{int} = 0.0364$, $R_{sigma} = 0.0239$	6068, $R_{int} = 0.0929$, $R_{sigma} = 0.0502$	6411, $R_{int} = 0.0677$, $R_{sigma} = 0.0517$
Data/restraints/parameters	6221/0/334	6068/0/299	6411/0/336
Goodness-of-fit on F^2	1.028	1.028	1.045
Final R indexes [I > = 2σ (I)]	$R_1 = 0.0396$, $wR_2 = 0.1021$	$R_1 = 0.0472$, $wR_2 = 0.1048$	$R_1 = 0.0436$, $wR_2 = 0.1025$
Final R indexes [all data]	$R_1 = 0.0546$, $wR_2 = 0.1106$	$R_1 = 0.0930$, $wR_2 = 0.1247$	$R_1 = 0.0771$, $wR_2 = 0.1172$
Largest diff. peak/hole / e $Å^{-3}$	0.52/-0.40	0.50/-0.45	0.47/-0.47

Table S2 Selected bond lengths (Å) and bond angles (°).

1		**2**		**3**		**4**	
Cu1-N1	2.057(8)	Cu1-N1	2.048(5)	Cu1-N1	2.054(2)	Cu1-N1	2.2217(15)
Cu1-N2	1.954(7)	Cu1-N2	1.952(5)	Cu1- N2	1.953(2)	Cu1-N2	1.9431(15)
Cu1-N3	2.011(7)	Cu1-N3	1.999(5)	Cu1-N3	1.999(2)	Cu1-N3	1.9993(16)
Cu1-N4	2.242(7)	Cu1-N4	2.222(5)	Cu1-N4	2.188(2)	Cu1-N4	2.1656(16)
Cu1-S1	2.290(3)	Cu1-S1	2.294(3)	Cu1-S1	2.310(8)	Cu1-S1	2.2838(6)
N2-Cu1-N3	176.6(3)	N2-Cu1-S1	84.35(15)	N2-Cu1-S1	83.45(7)	N2-Cu1-N3	173.52(6)
N2-Cu1-N1	80.1(3)	N2-Cu1-N3	176.43(19)	N2-Cu1-N1	79.31(9)	N2-Cu1-N4	103.95(6)
N3-Cu1-N1	101.3(3)	N2-Cu1-N4	102.63(19)	N2-Cu1-N3	177.39(1)	N3-Cu1-N4	80.09(7)
N2-Cu1-N4	97.8(3)	N2-Cu1-N1	80.02(19)	N2-Cu1-N4	99.12(9)	N2-Cu1-N1	78.07(6)
N3-Cu1-N4	79.1(3)	N3-Cu1-S1	98.15(15)	N1-Cu1-S1	148.10(7)	N3-Cu1-N1	107.47(6)
N1-Cu1-N4	91.2(3)	N3-Cu1-N4	79.09(19)	N1-Cu1-N4	107.03(9)	N4-Cu1-N1	85.98(6)
N2-Cu1-S1	83.5(3)	N3-Cu1-N1	96.92(19)	N3-Cu1-S1	98.94(7)	N2-Cu1-S1	83.14(5)
N3-Cu1-S1	95.8(2)	N4-Cu1-S1	107.51(16)	N3-Cu1-N1	99.02(9)	N3-Cu1-S1	90.49(5)
N1-Cu1-S1	159.5(2)	N1-Cu1-S1	158.94(14)	N3-Cu1-N4	79.40(9)	N4-Cu1-S1	118.11(4)
N4-Cu1-S1	103.1(2)	N1-Cu1-N4	89.700(2)	N4-Cu1-S1	102.04(6)	N1-Cu1-S1	152.59(4)

Table S2a Selected bond lengths (Å) and bond angles (°).

5		**6**		**7**	
Cu1-N1	2.2845(17)	Cu1-N1	2.077(3)	Cu1-N1	2.035(2)
Cu1-N2	1.9409(18)	Cu1-N2	1.961(3)	Cu1-N2	1.967(2)
Cu1-N3	1.9854(19)	Cu1-N3	2.010(2)	Cu1-N3	2.000(2)
Cu1-N4	2.1421(19)	Cu1-N4	2.233(3)	Cu1-N4	2.209(2)
Cu1-S1	2.2798(7)	Cu1-S1	2.309(9)	Cu1-S1	2.3037(9)
N2-Cu1-N3	175.14(8)	N2-Cu1-N3	173.39(10)	N2-Cu1-N3	174.36(9)
N2-Cu1-N4	103.70(8)	N2-Cu1-N4	107.70(10)	N2-Cu1-N4	95.98(9)
N3-Cu1-N4	80.76(8)	N3-Cu1-N4	78.81(10)	N3-Cu1-N4	79.68(9)
N2-Cu1-S1	83.16(6)	N2-Cu1-S1	82.88(8)	N2-Cu1-S1	83.79(7)
N3-Cu1-S1	92.85(6)	N3-Cu1-S1	94.49(8)	N3-Cu1-S1	100.36(7)
N4-Cu1-S1	122.03(5)	N4-Cu1-S1	104.32(7)	N4-Cu1-S1	98.88(6)
N2-Cu1-N1	77.46(7)	N2-Cu1-N1	80.59(10)	N2-Cu1-N1	80.37(9)
N3-Cu1-N1	105.09(7)	N3-Cu1-N1	100.51(10)	N3-Cu1-N1	96.94(9)
N4-Cu1-N1	84.85(7)	N1-Cu1-N4	93.02(10)	N1-Cu1-N4	102.09(9)
S1-Cu1-N1	150.18(5)	N1-Cu1-S1	159.00(8)	N1-Cu1-S1	154.84(7)

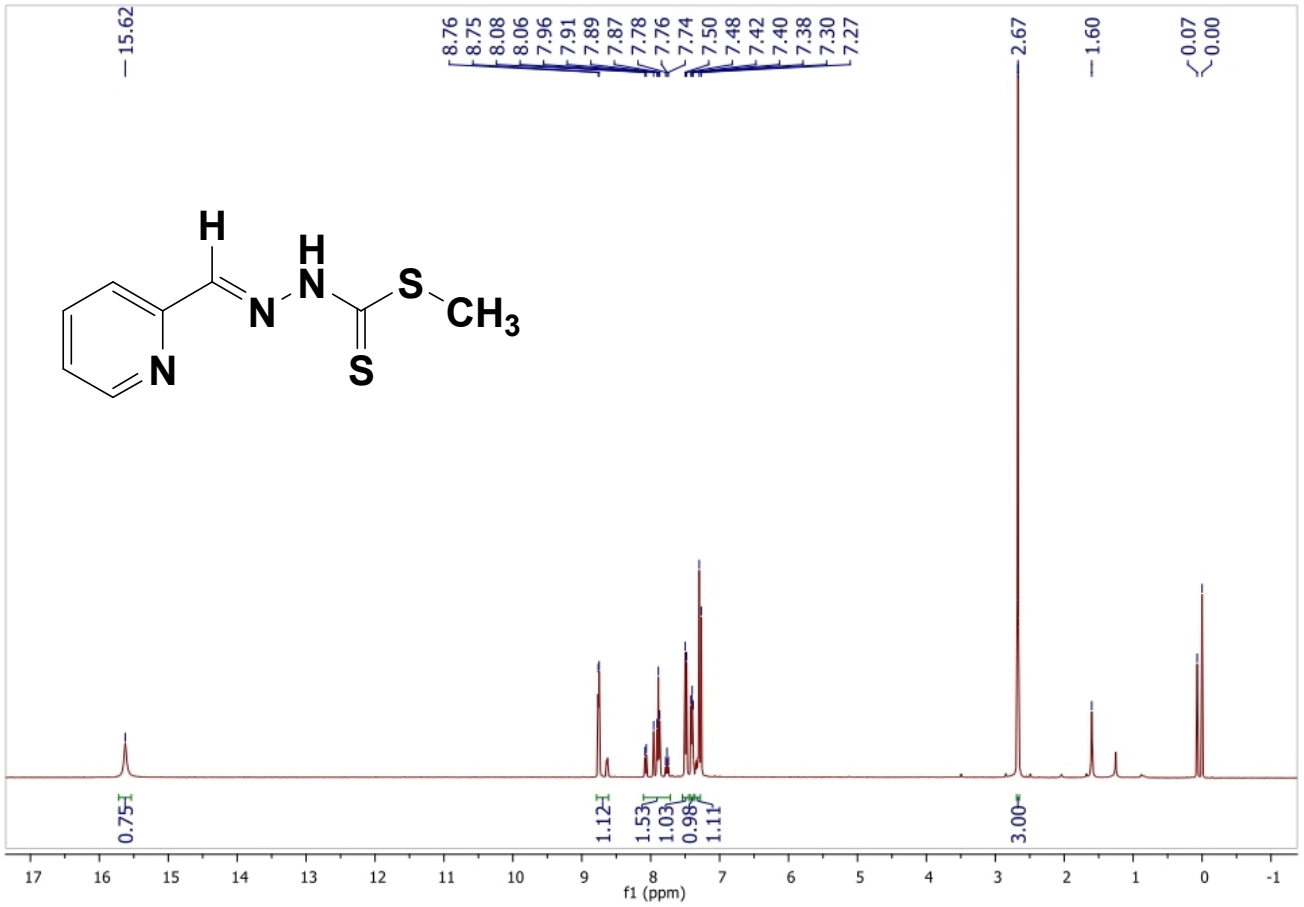

Figure S1. ^{1}H NMR spectrum of H(L1) in $CDCl_3$

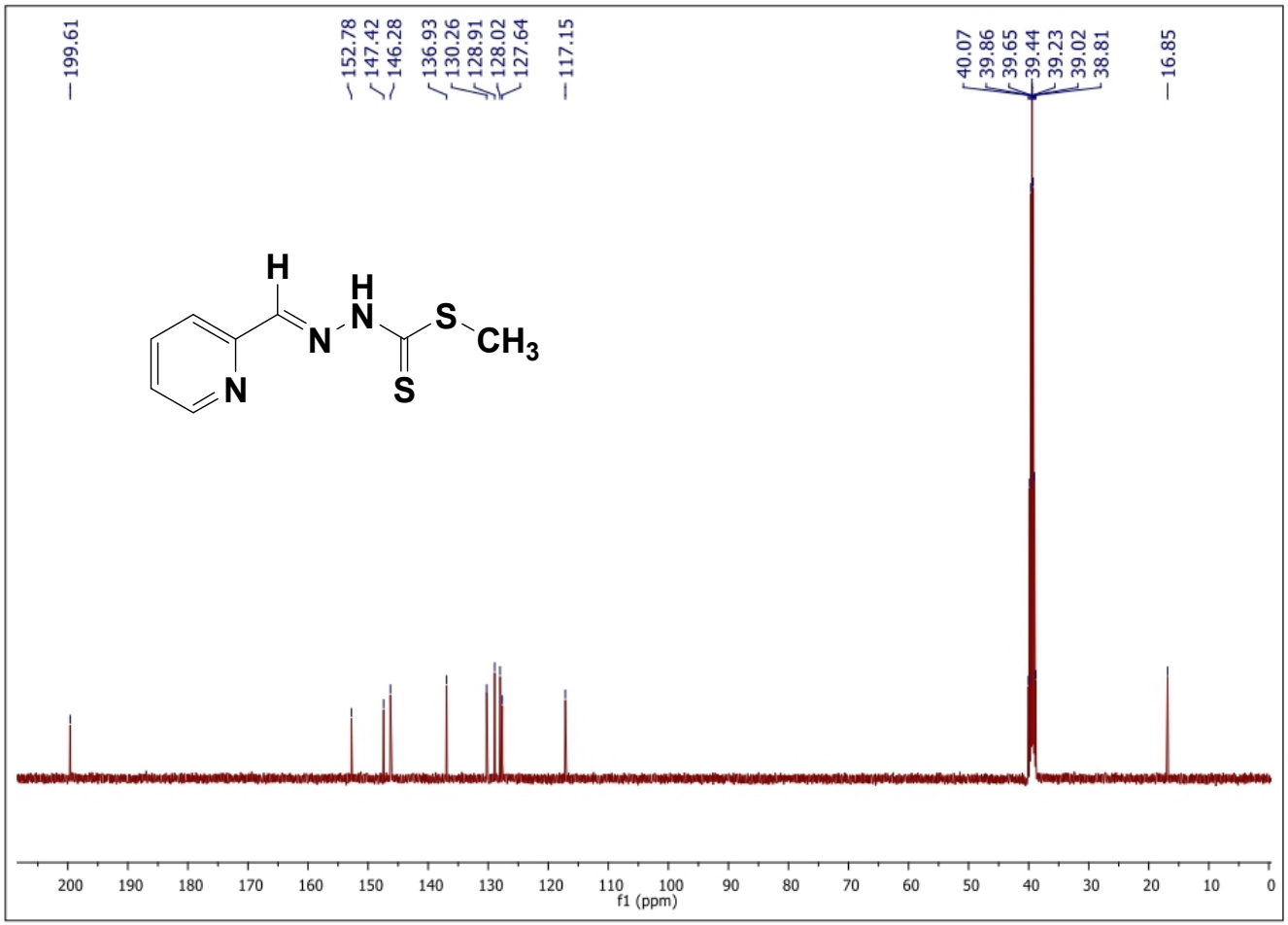

Figure S2. ^{13}C NMR spectrum of H(L1) in $CDCl_3$.

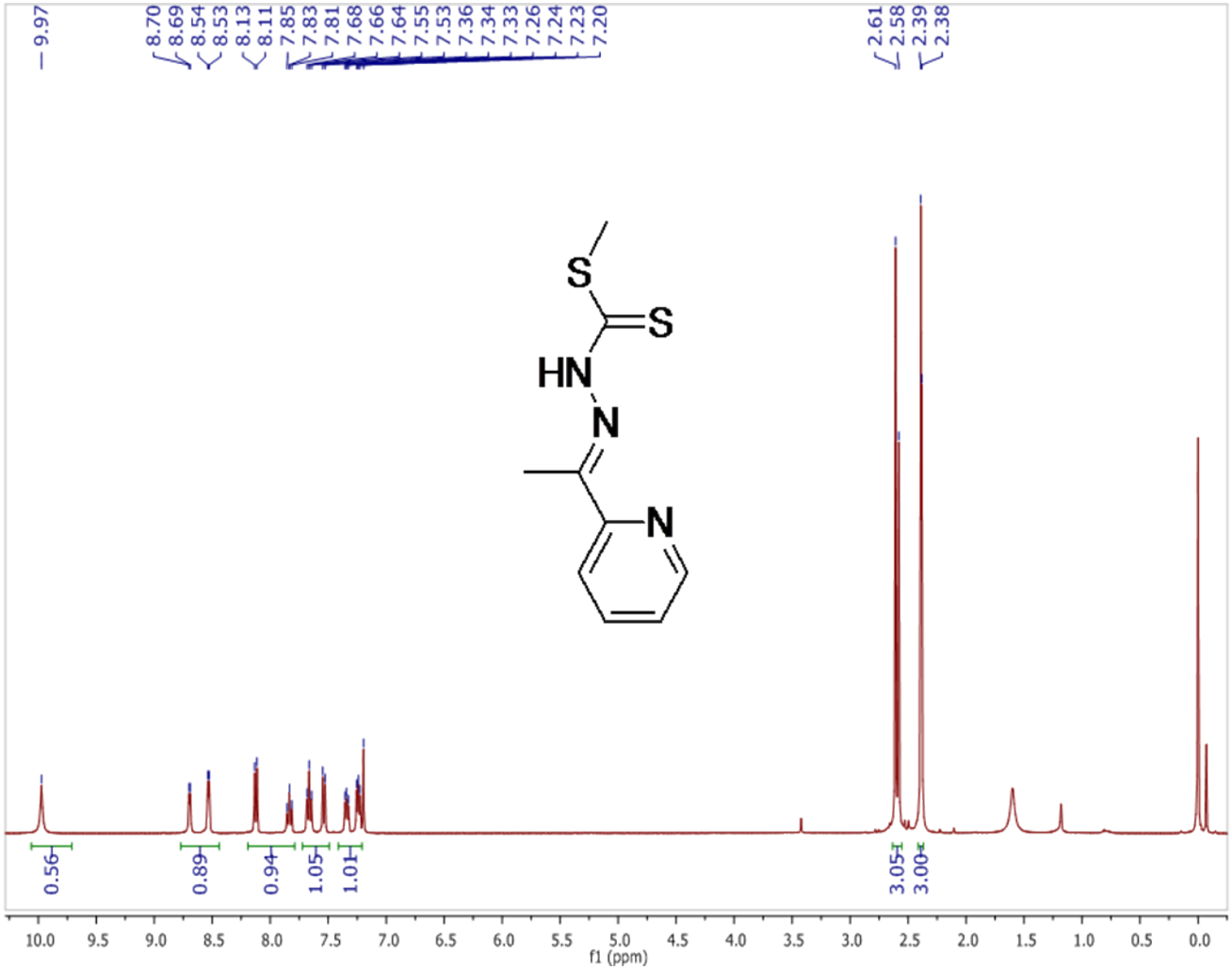

Figure S3. ^{1}H NMR spectrum of H(L2) in $CDCl_3$

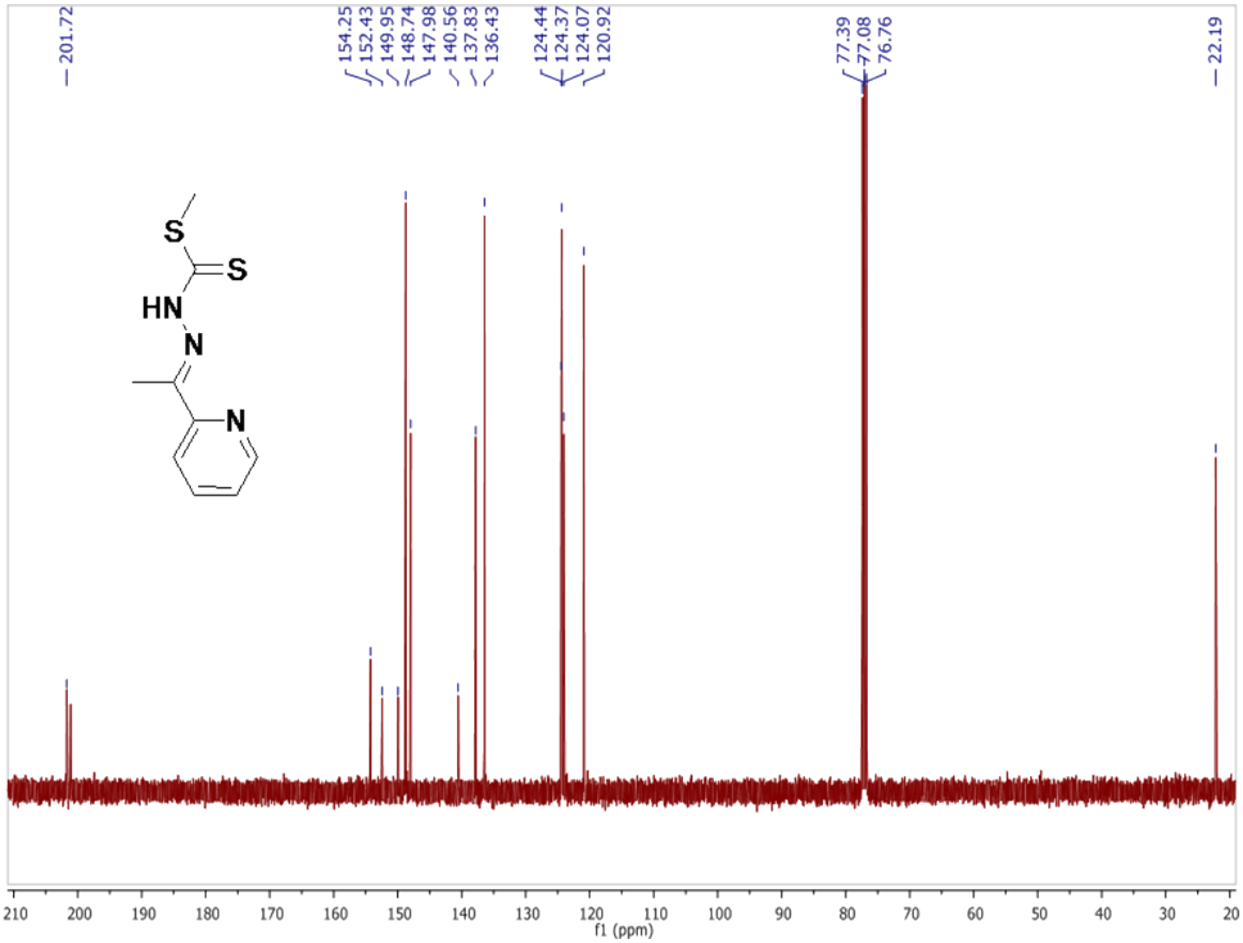

Figure S4. ^{13}C NMR spectrum of H(L2) in $CDCl_3$

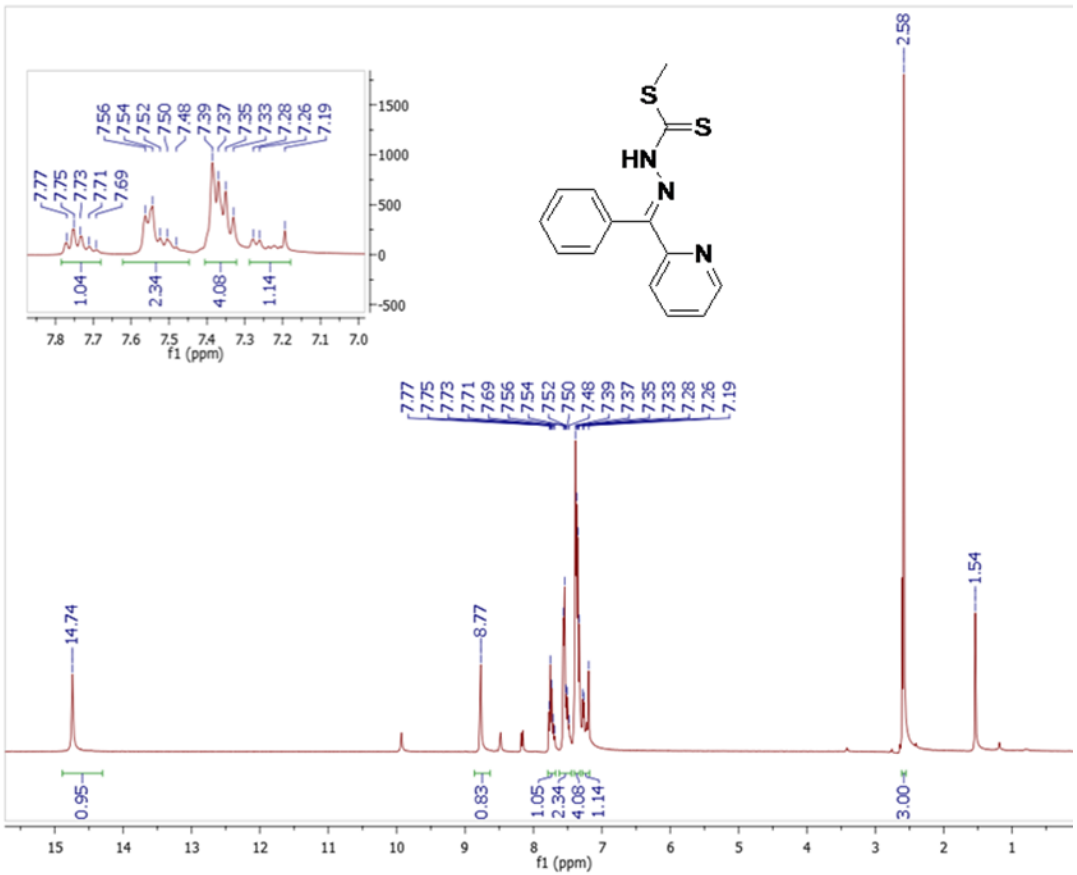

Figure S5. ^{1}H NMR spectrum of H(L3) in $CDCl_3$

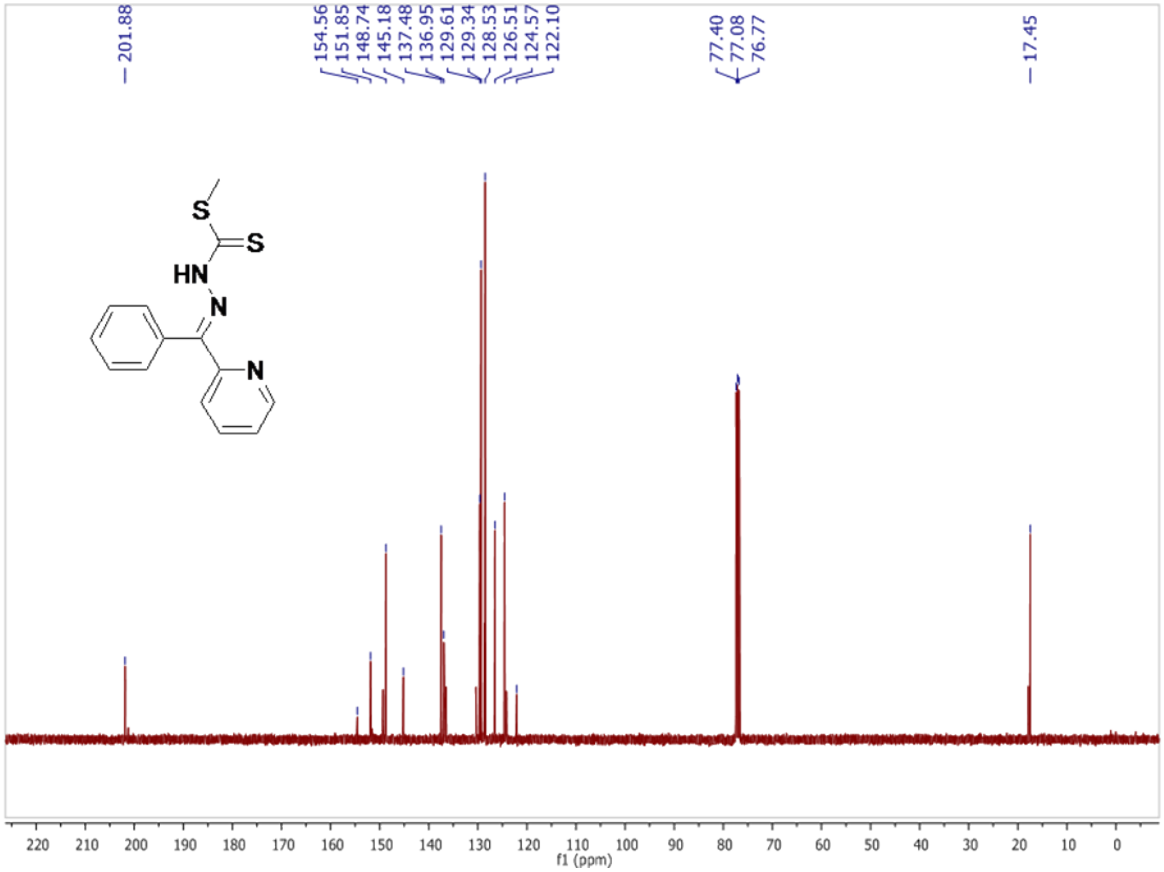

Figure S6. ^{13}C NMR spectrum of H(L3) in $CDCl_3$

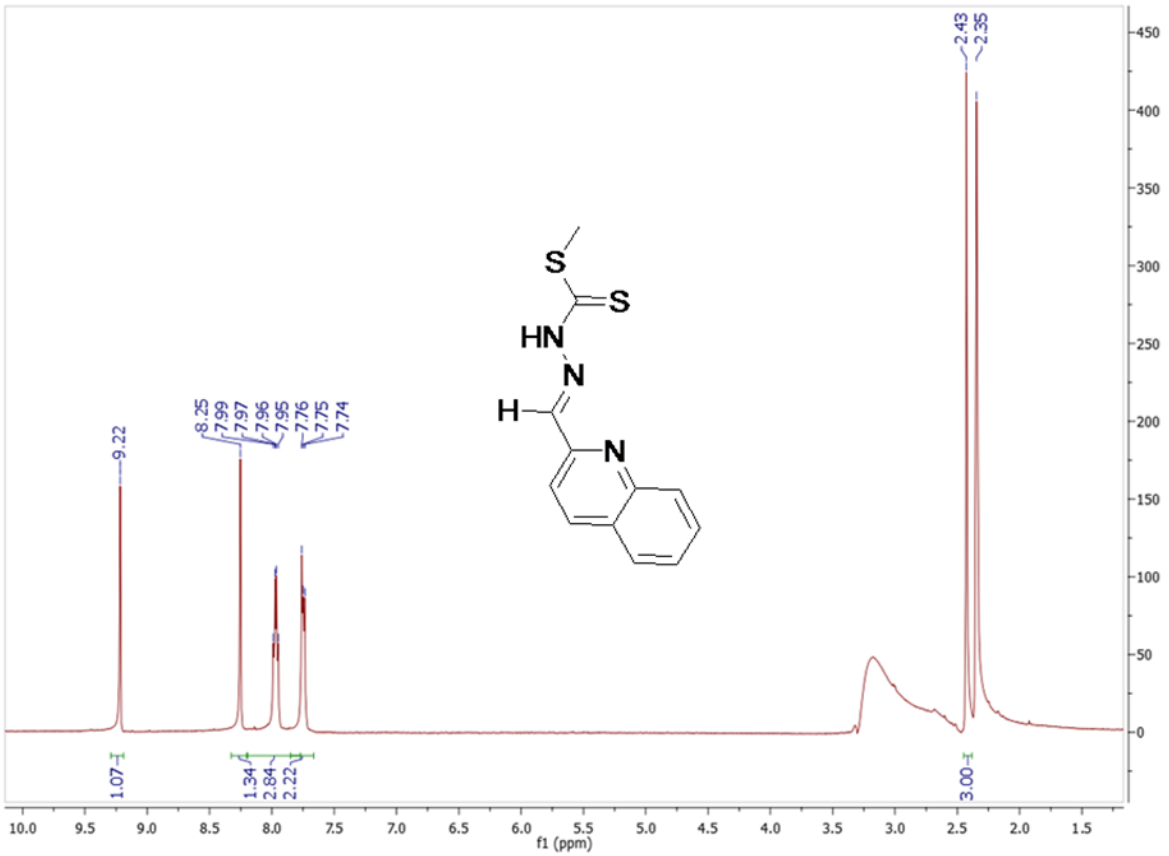

Figure S7. ^{1}H NMR spectrum of H(L4) in DMSO-d_6

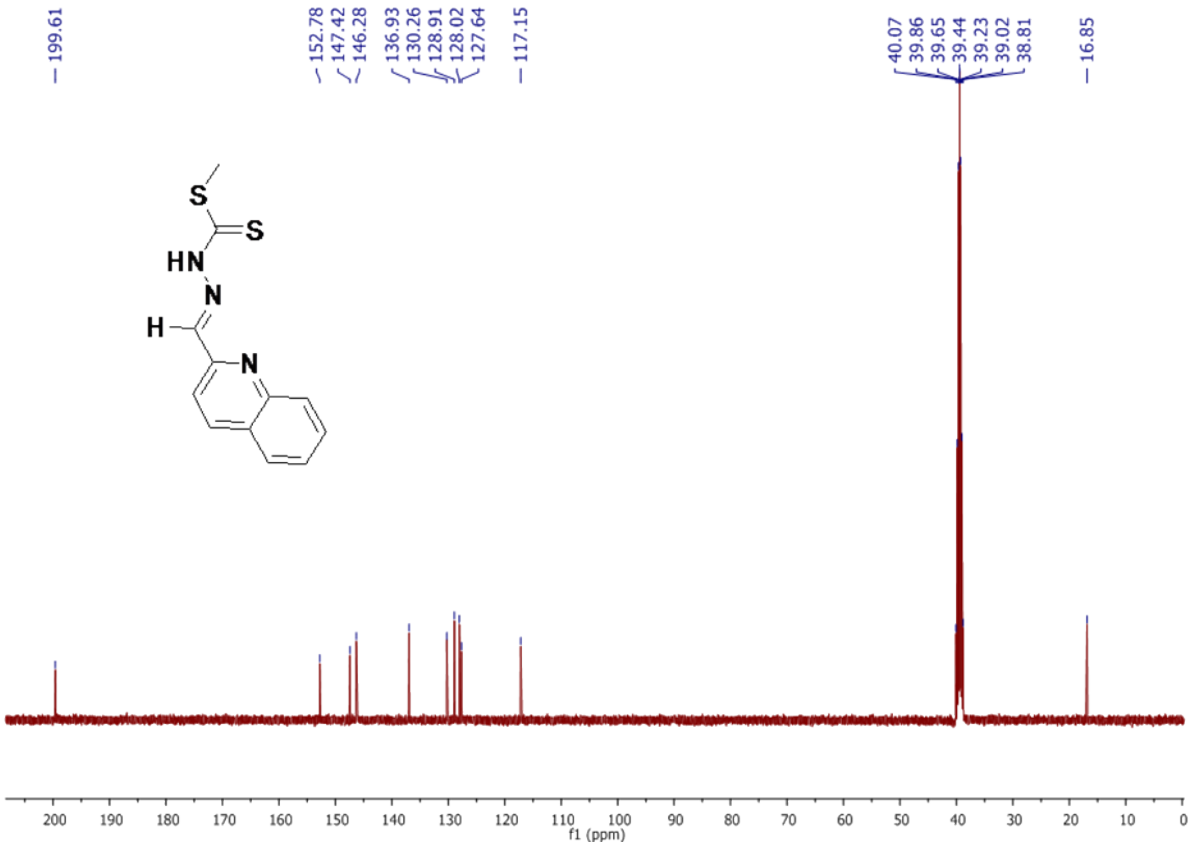

Figure S8. ^{13}C NMR spectrum of H(L4) in DMSO-d_6

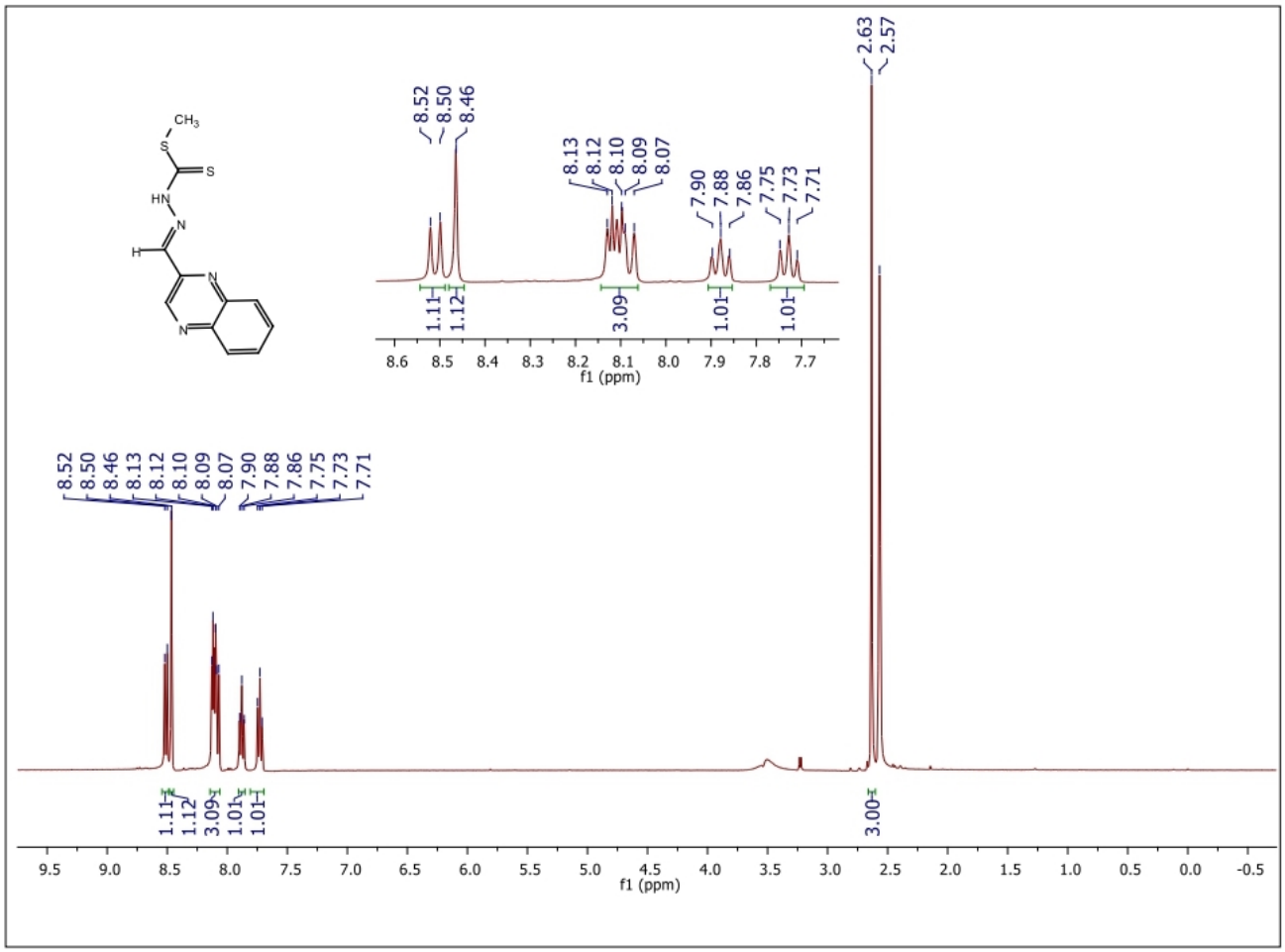

Figure S9. ^{1}H NMR spectrum of H(L5) in DMSO-d_6

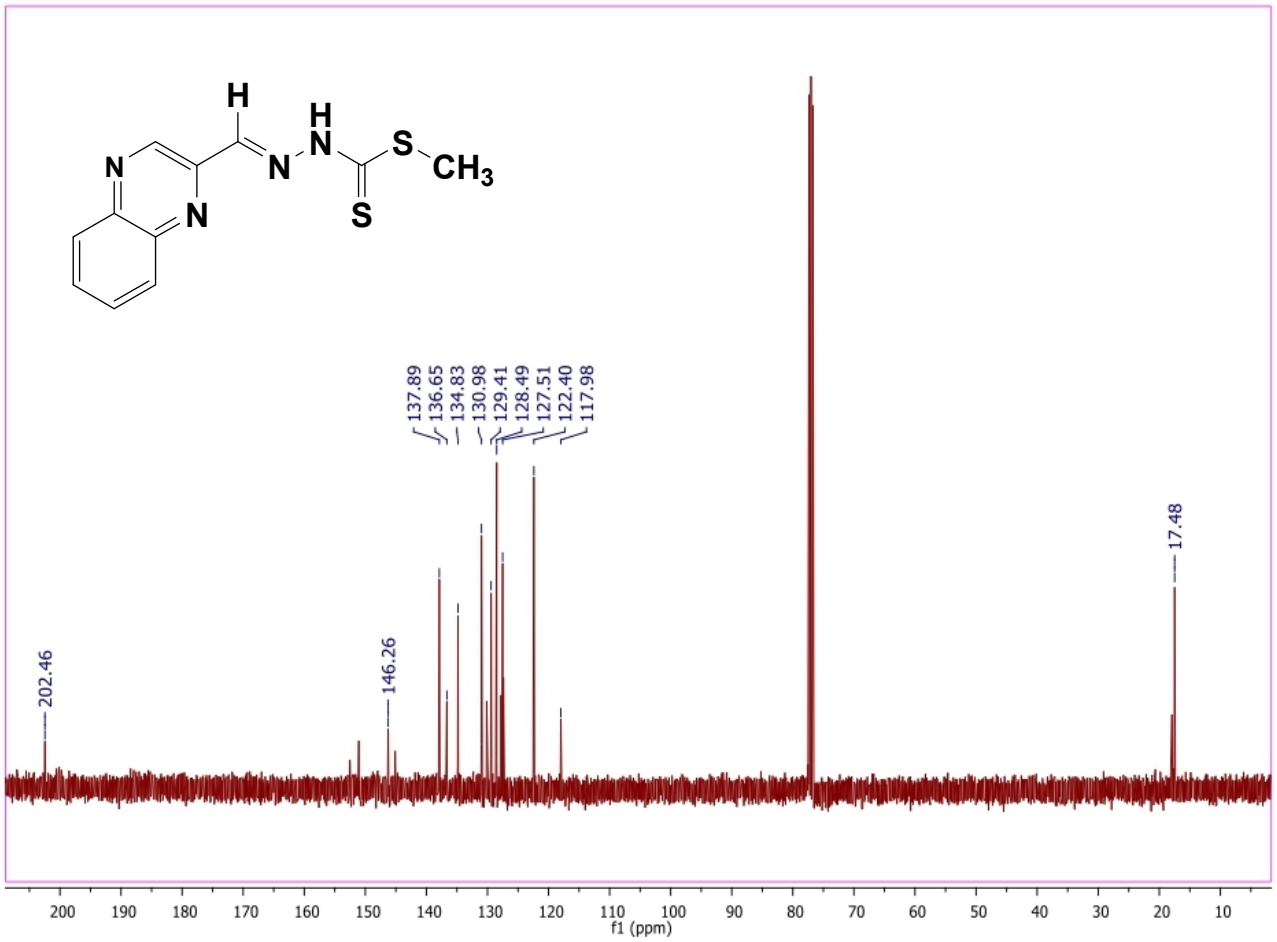

Figure S10. ^{13}C NMR spectrum of H(L5) in DMSO-d_6

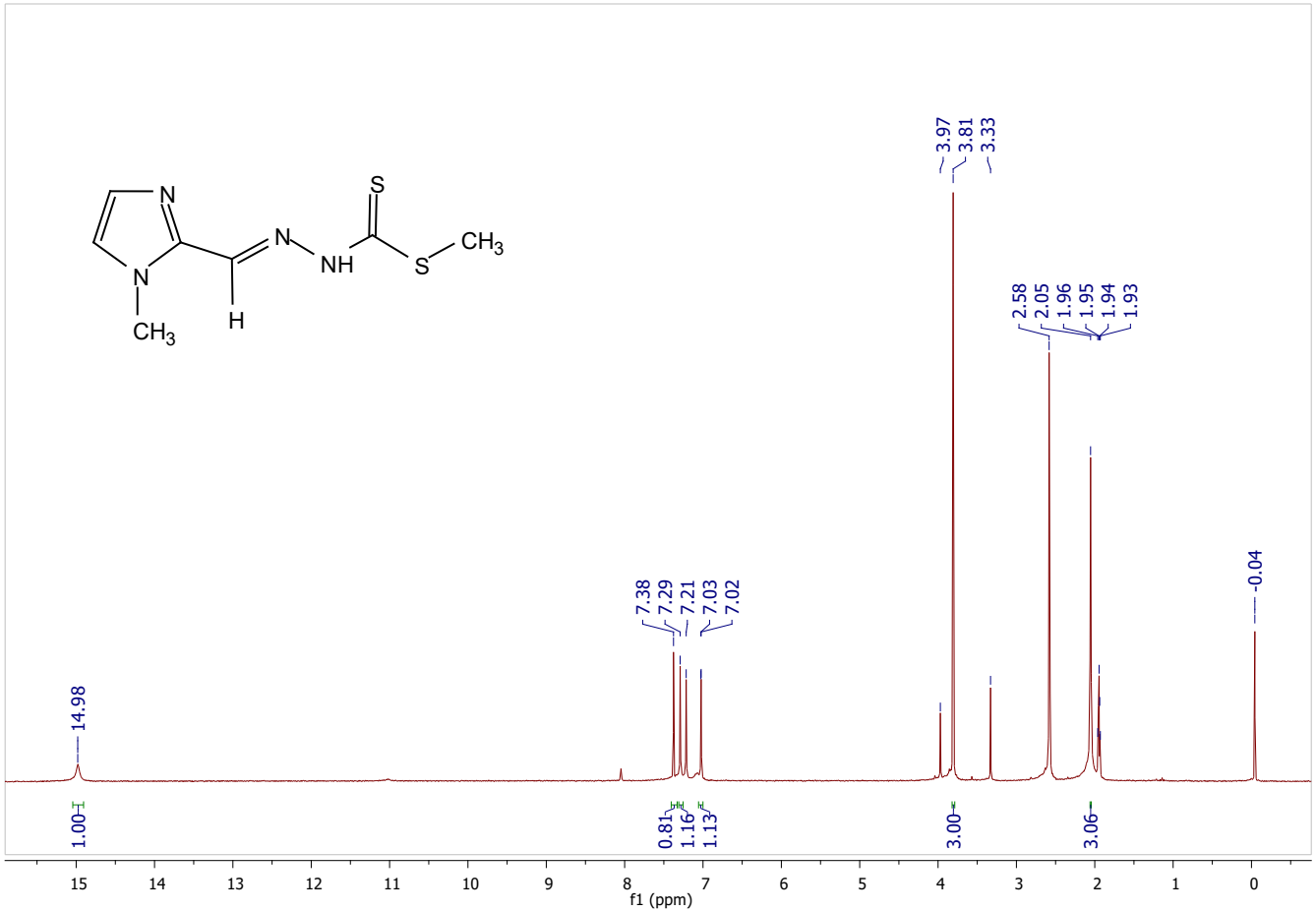

Figure S11. ^{1}H NMR spectrum of H(L6) in CD_3CN

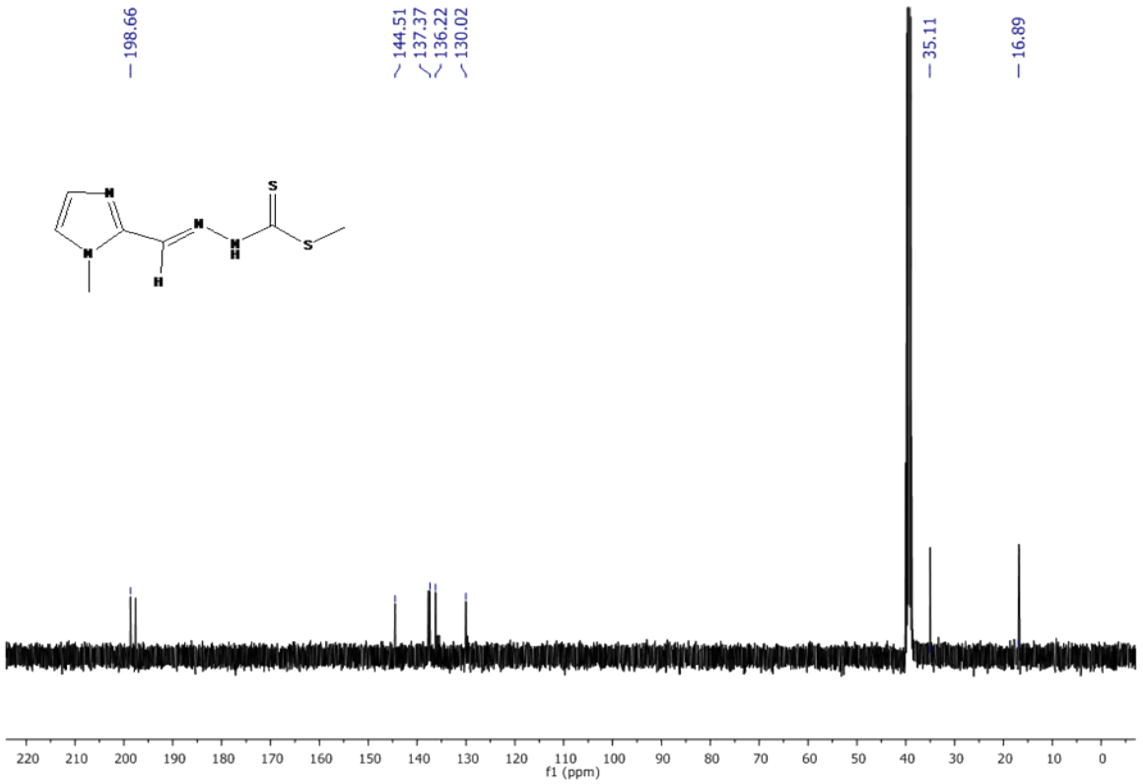

Figure S12. ^{13}C NMR spectrum of H(L6) in CD_3CN

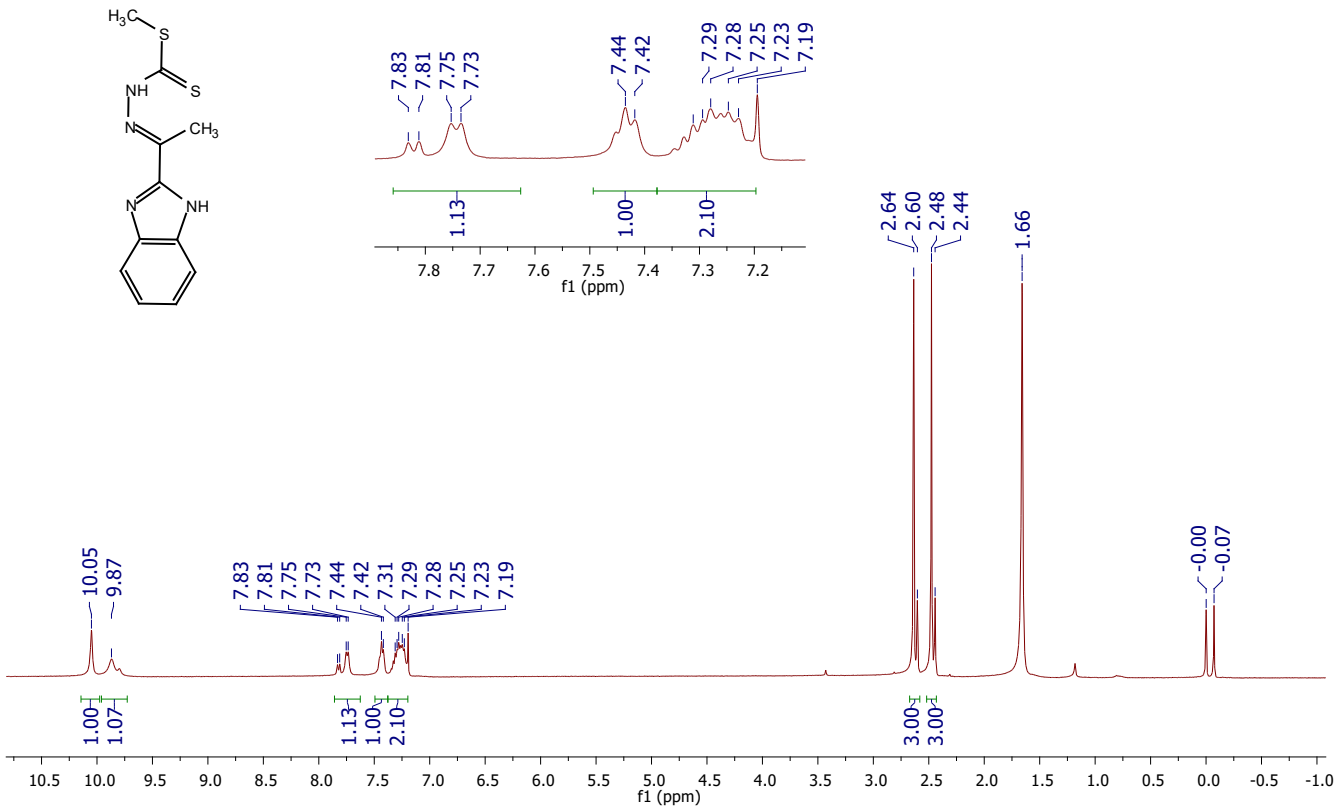

Figure S13. ^{1}H NMR spectrum of H(L7) in DMSO-d_6

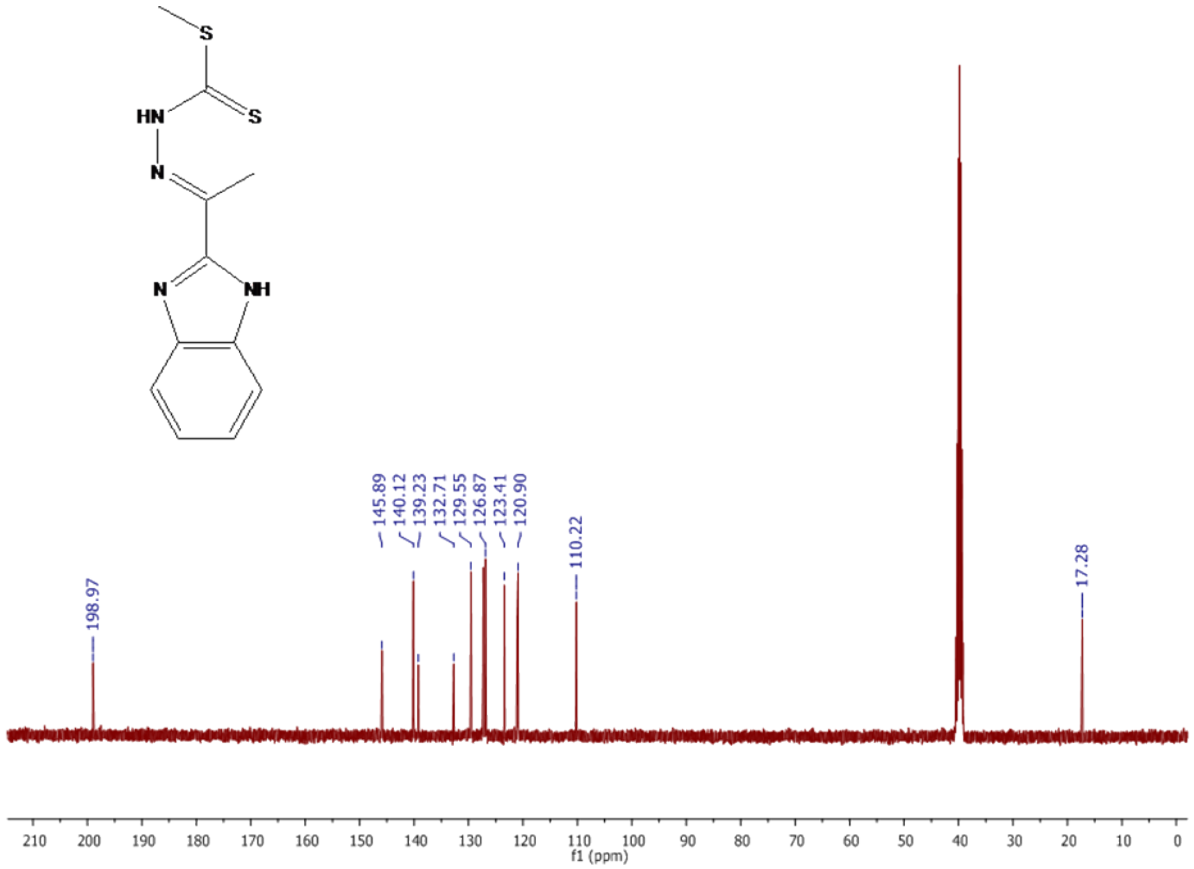

Figure S14. ^{13}C NMR spectrum of H(L7) in DMSO-d_6

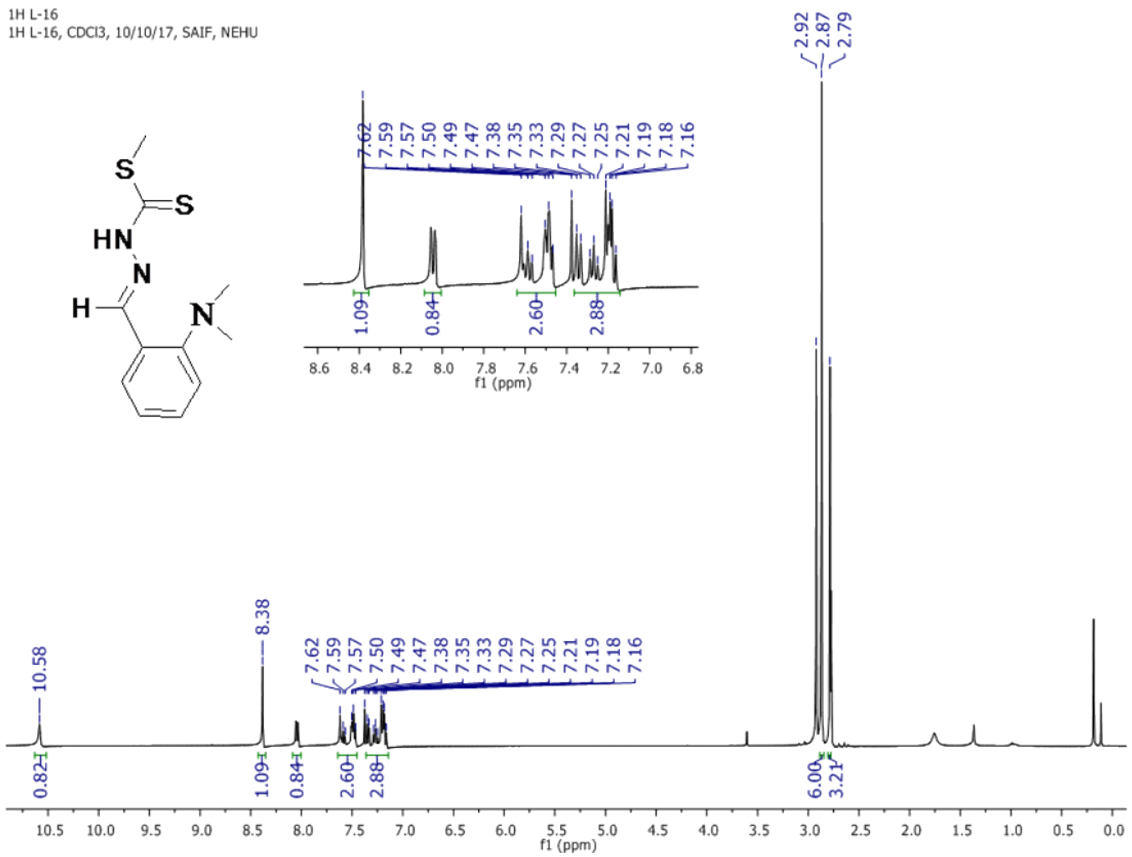

Figure S15. ^{1}H NMR spectrum of H(L8) in $CDCl_3$

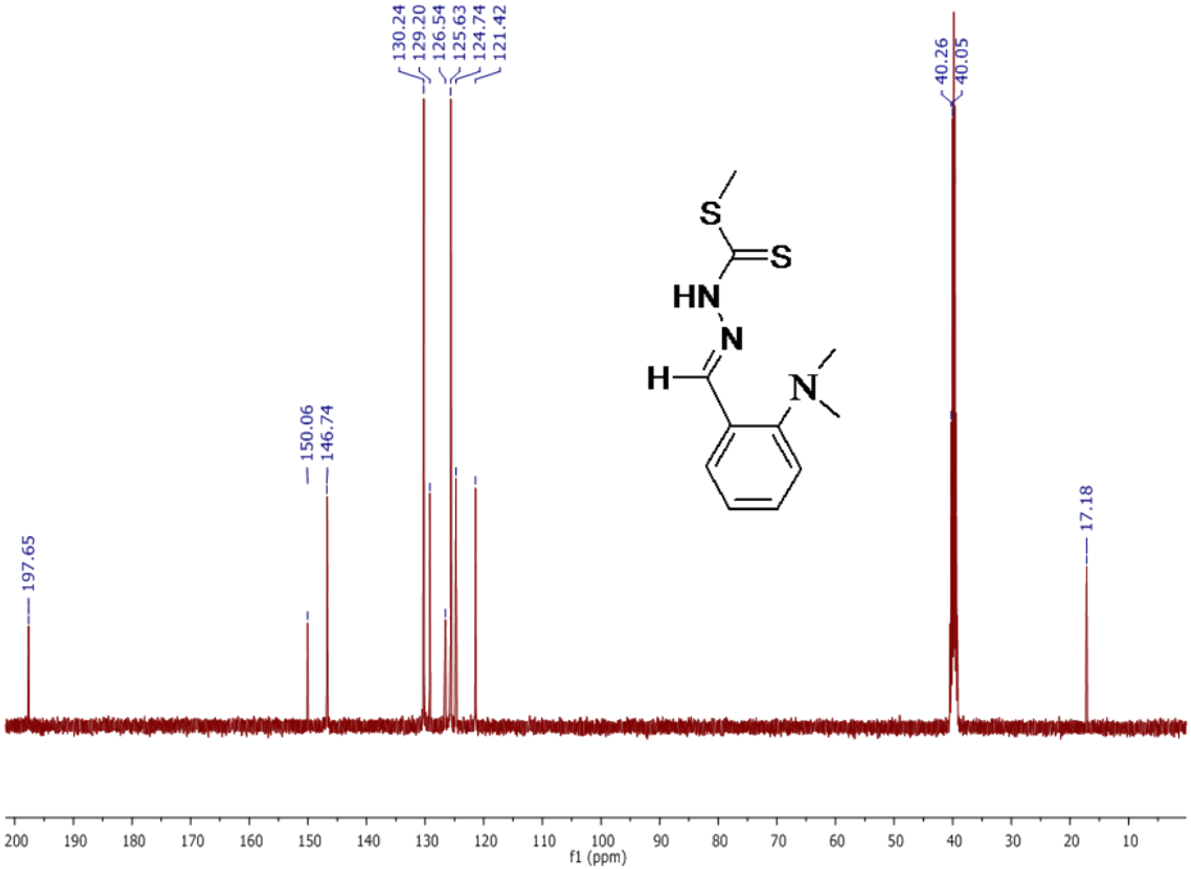

Figure S16. ^{13}C NMR spectrum of H(L8) in $CDCl_3$.

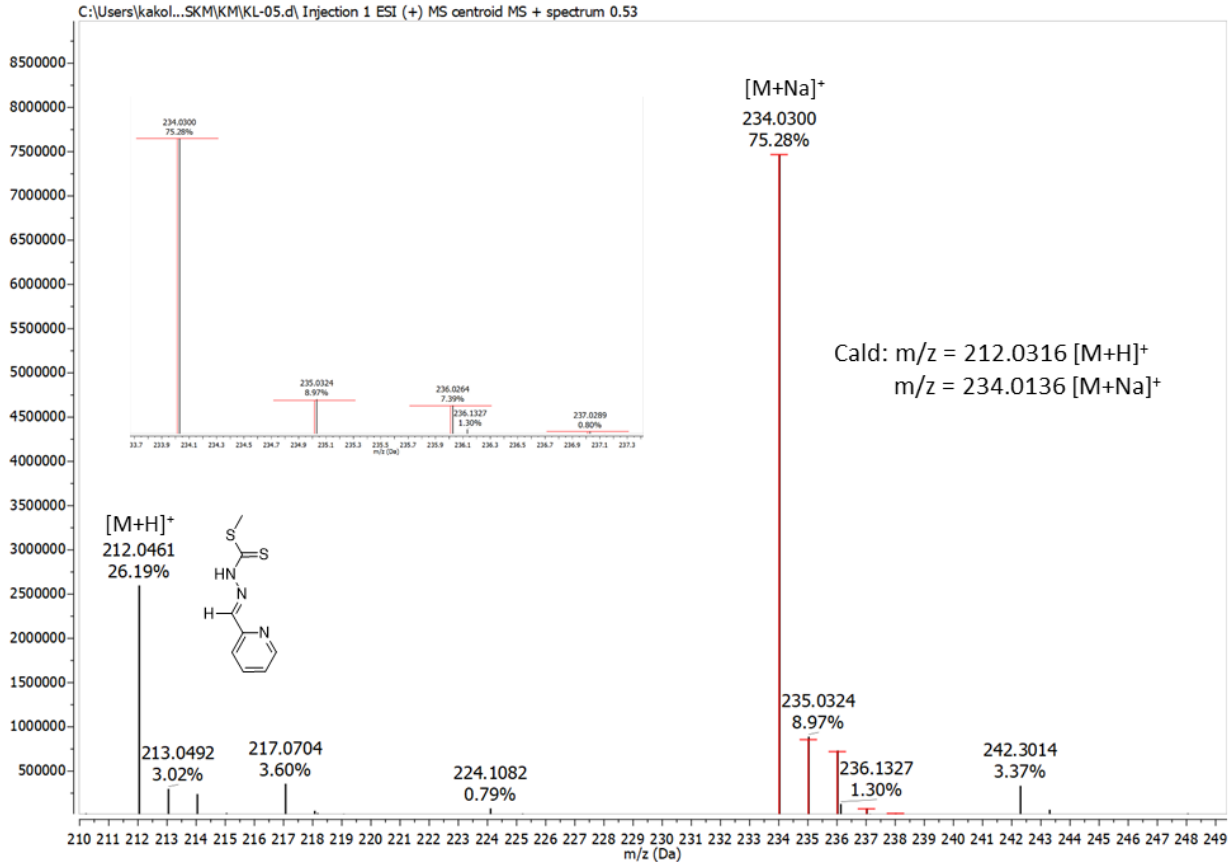

Figure S17. High Resolution Mass spectrum of H(L1) in acetonitrile (Concentration, 0.1 mg/mL).

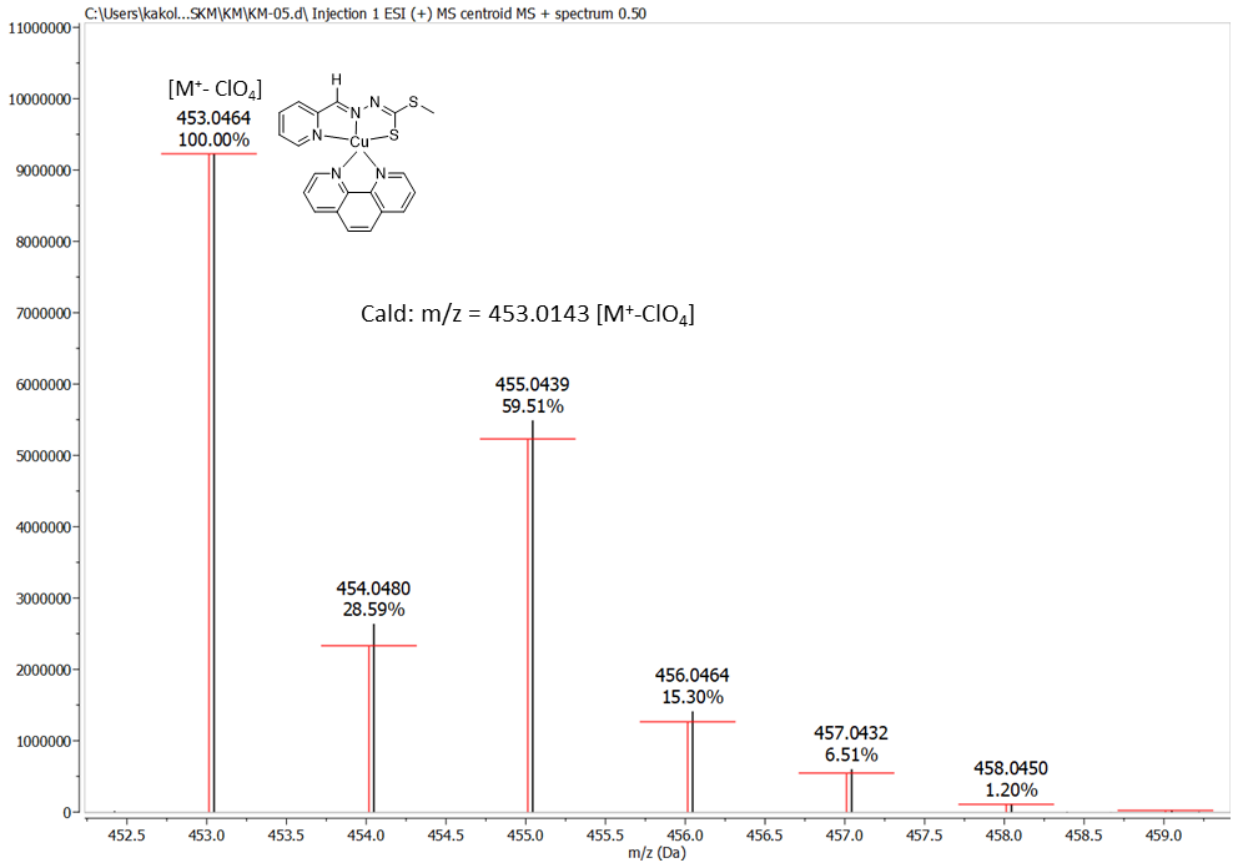

Figure S18. High Resolution Mass spectrum of [Cu(L1)(Phen)]ClO_4 (**1**) in acetonitrile (Concentration, 0.1 mg/mL).

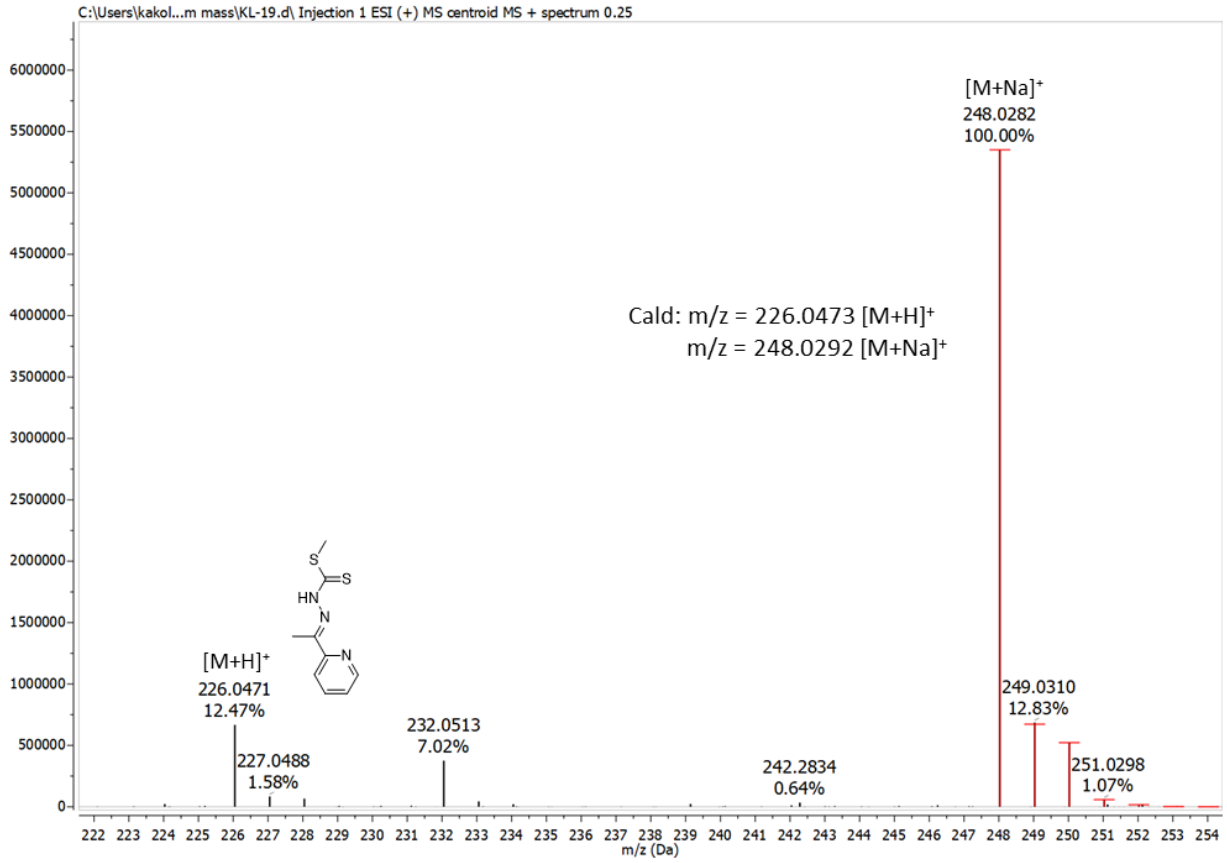

Figure S19. High Resolution Mass spectrum of H(L2) in acetonitrile (Concentration, 0.1 mg/mL).

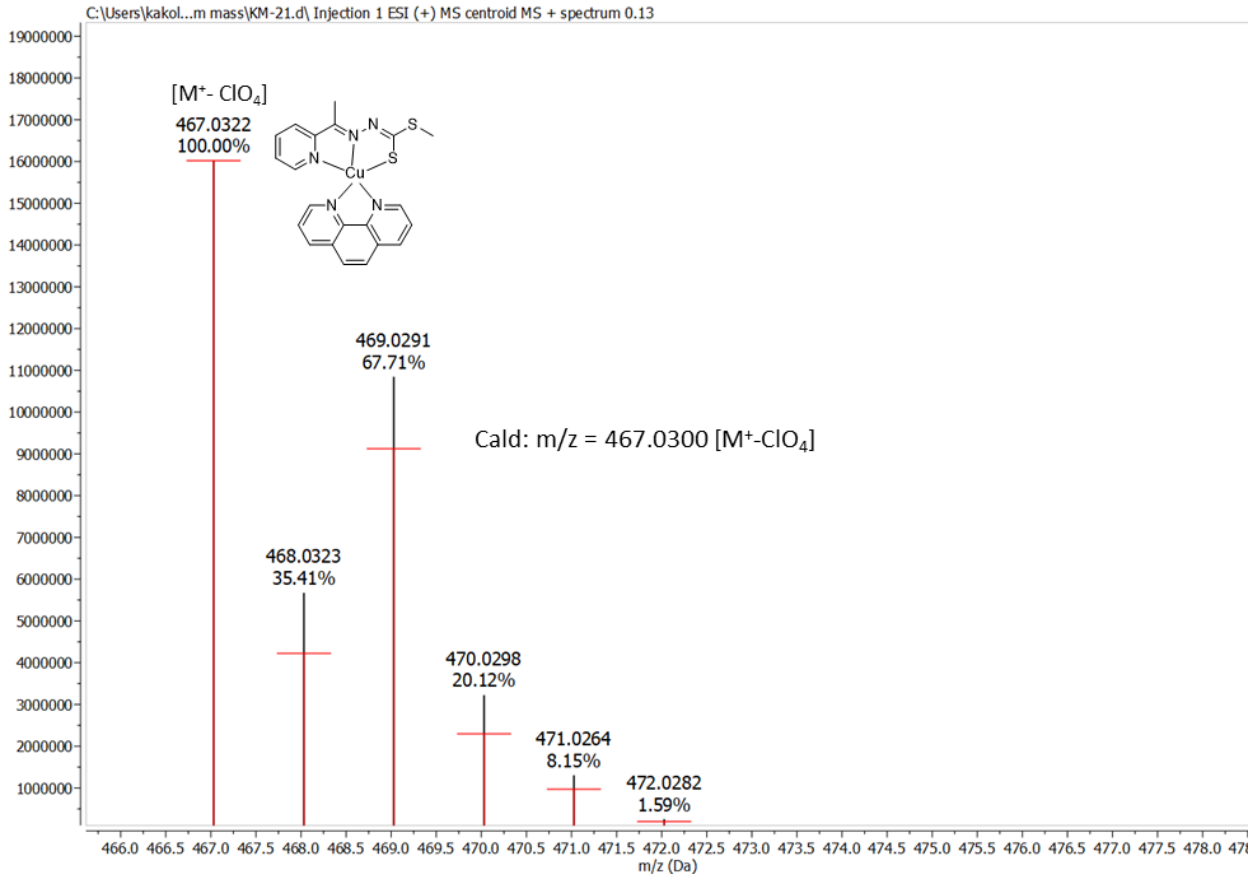

Figure S20. High Resolution Mass spectrum of [Cu(L2)(Phen)]ClO_4 (**2**) in acetonitrile (Concentration, 0.1 mg/mL).

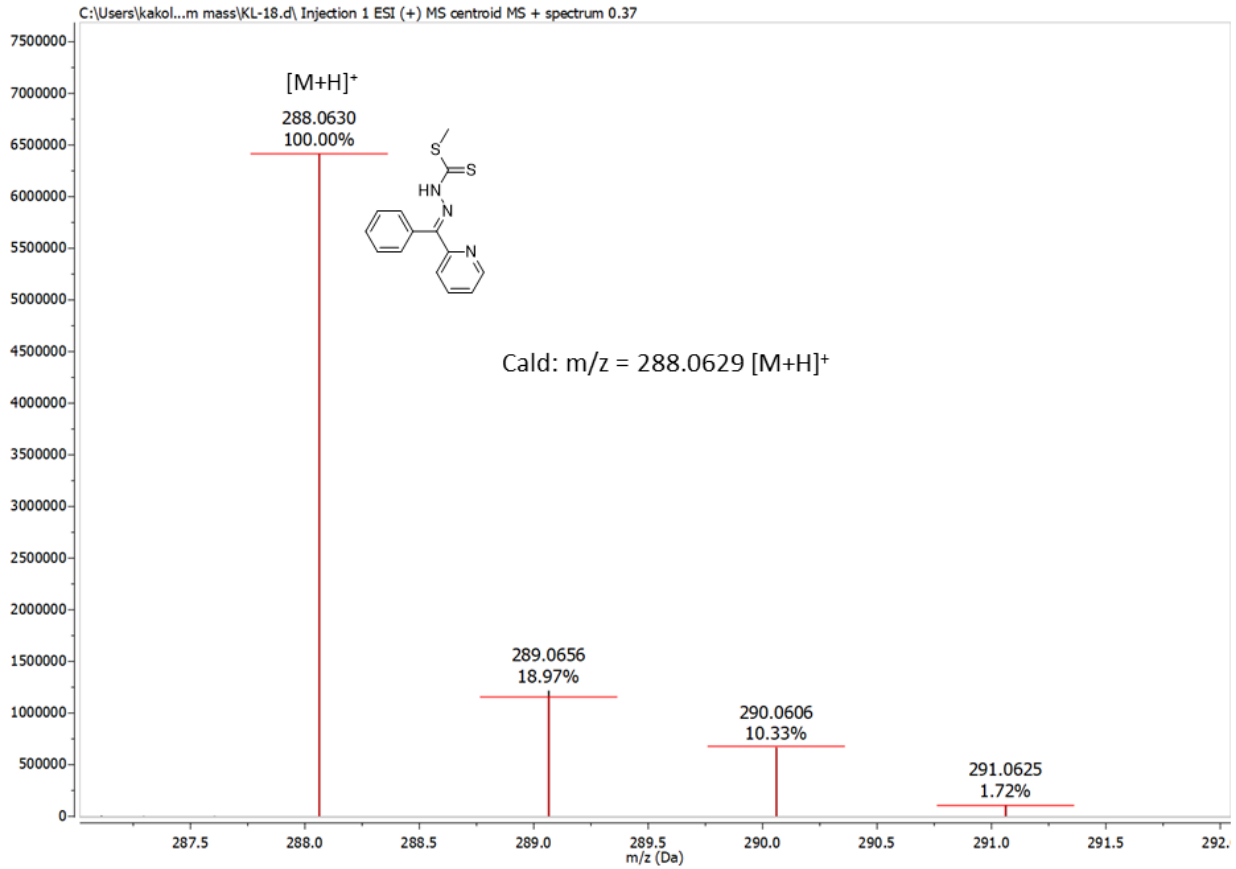

Figure S21. High Resolution Mass spectrum of H(L3) in acetonitrile (Concentration, 0.1 mg/mL).

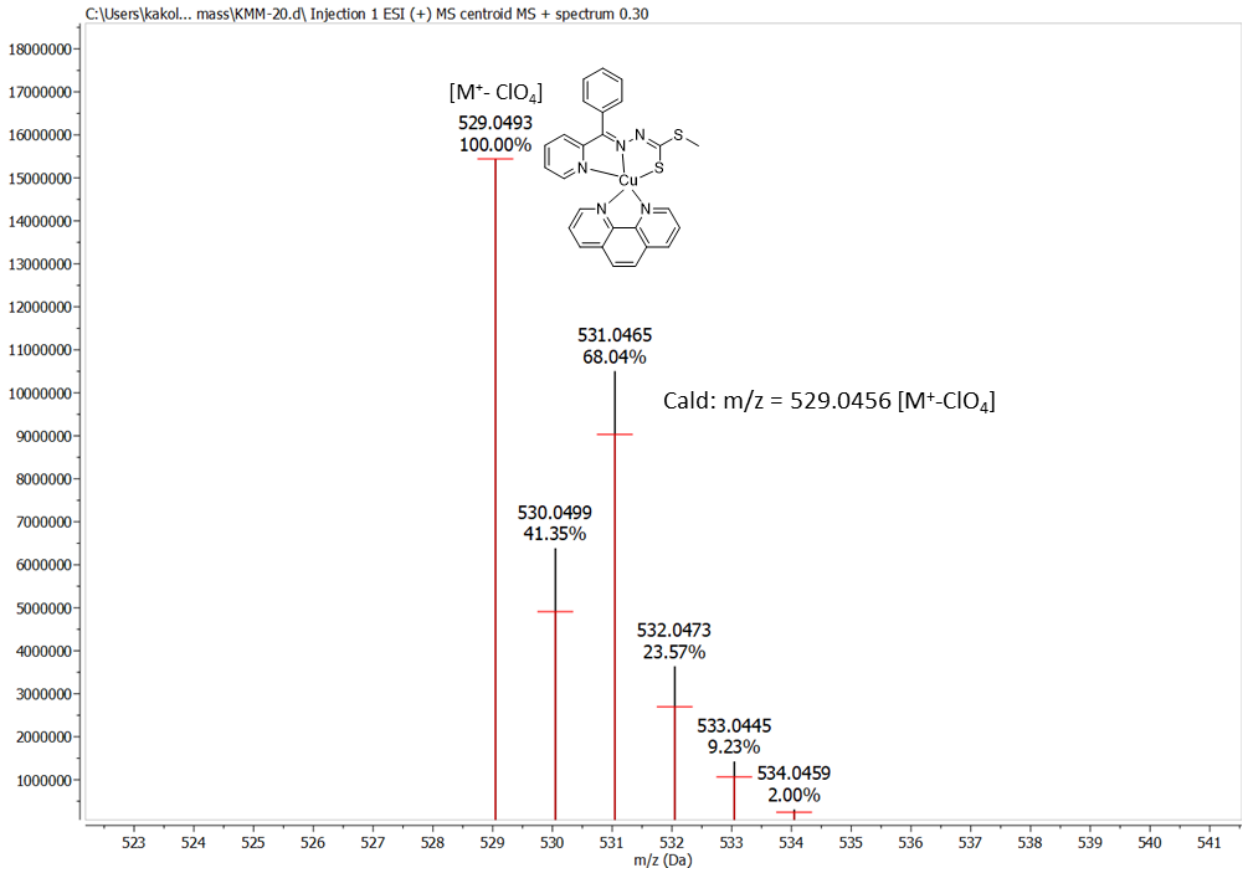

Figure S22. High Resolution Mass spectrum of [Cu(L3)(Phen)]ClO_4 (**3**) in acetonitrile (Concentration, 0.1 mg/mL).

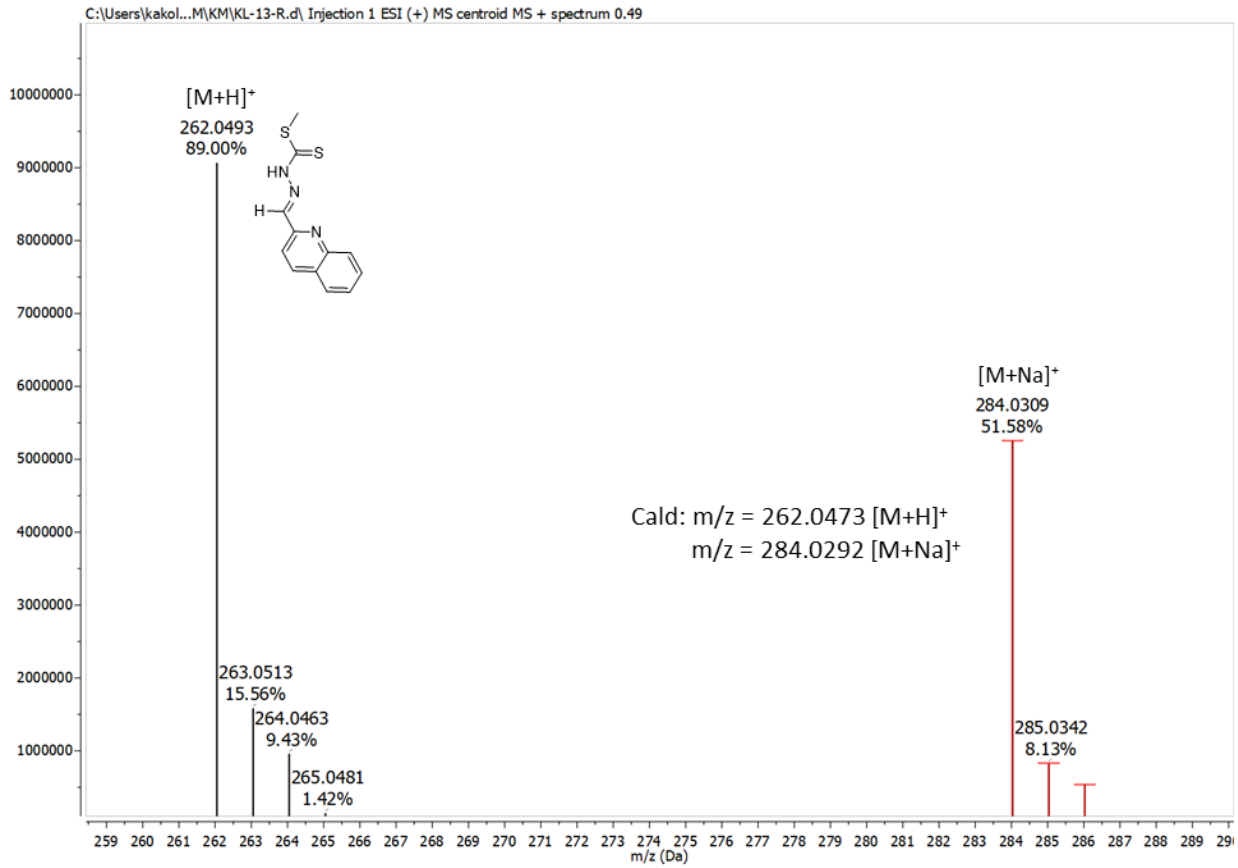

Figure S23. High Resolution Mass spectrum of H(L4) in acetonitrile (Concentration, 0.1 mg/mL).

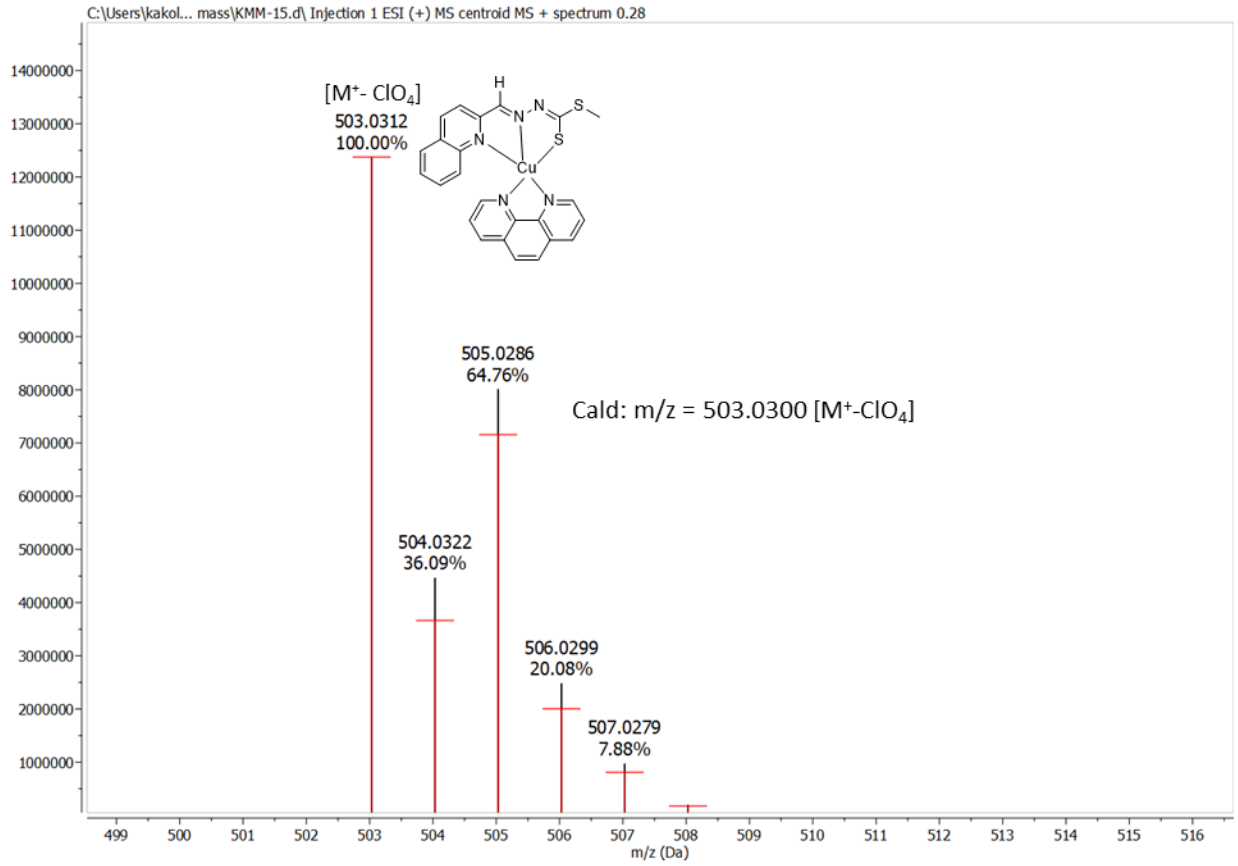

Figure S24. High Resolution Mass spectrum of [Cu(L4)(Phen)]ClO_4 (**4**) in acetonitrile (Concentration, 0.1 mg/mL).

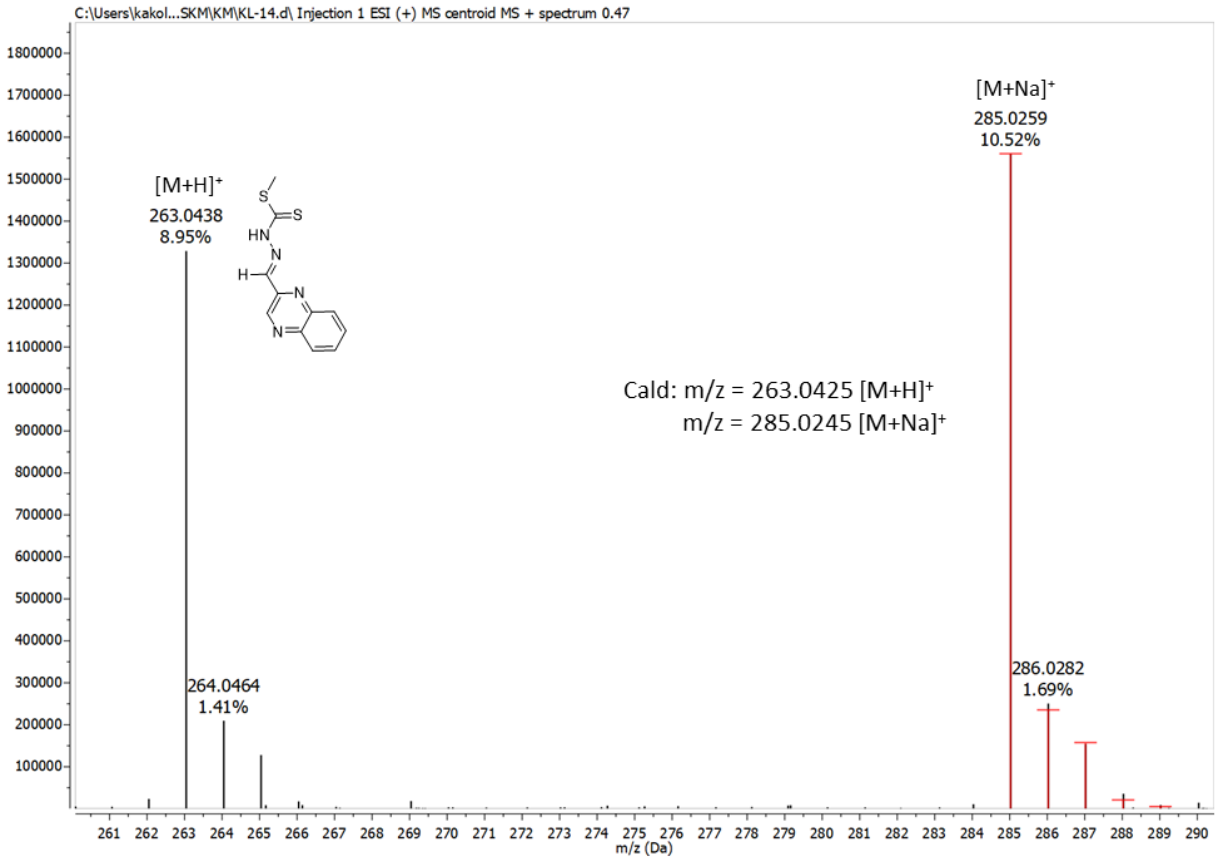

Figure S25. High Resolution Mass spectrum of H(L5) in acetonitrile (Concentration, 0.1 mg/mL).

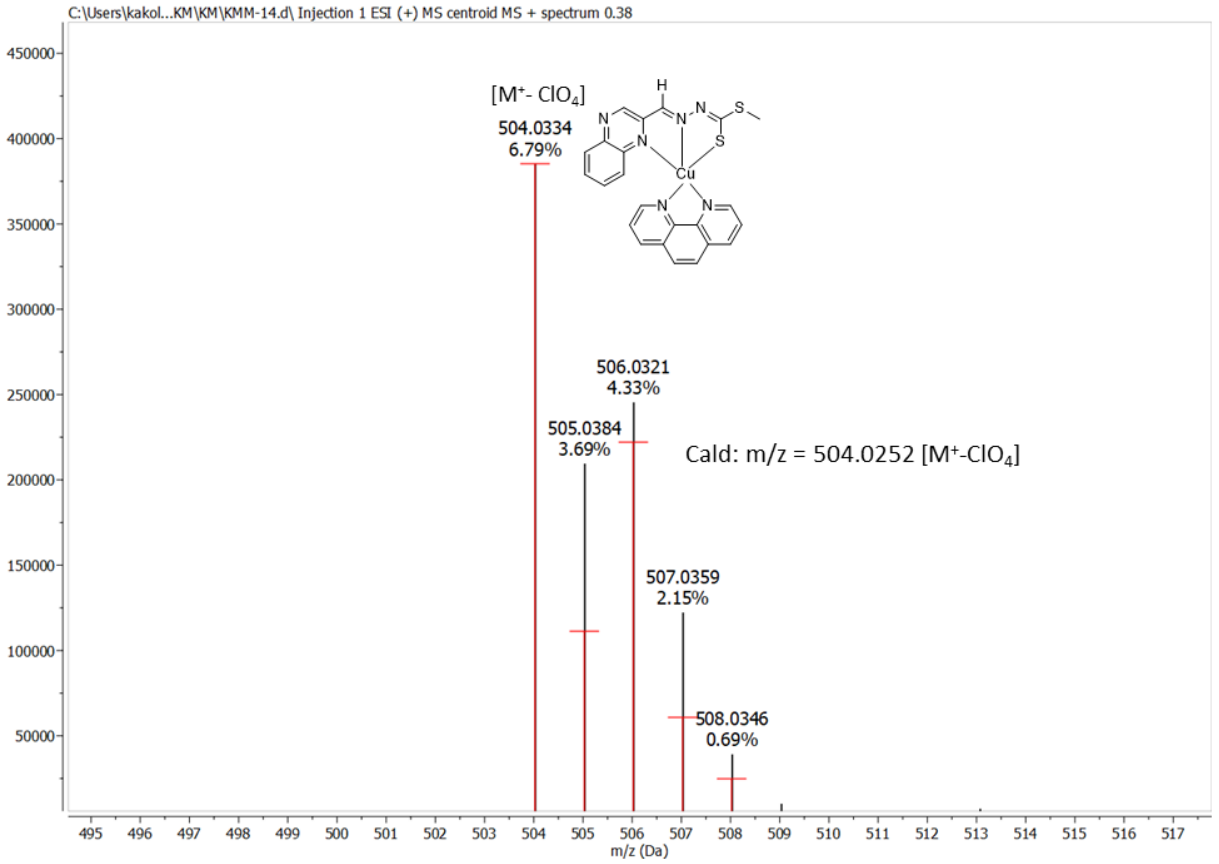

Figure S26. High Resolution Mass spectrum of [Cu(L5)(Phen)]ClO_4 (**5**) in acetonitrile (Concentration, 0.1 mg/mL).

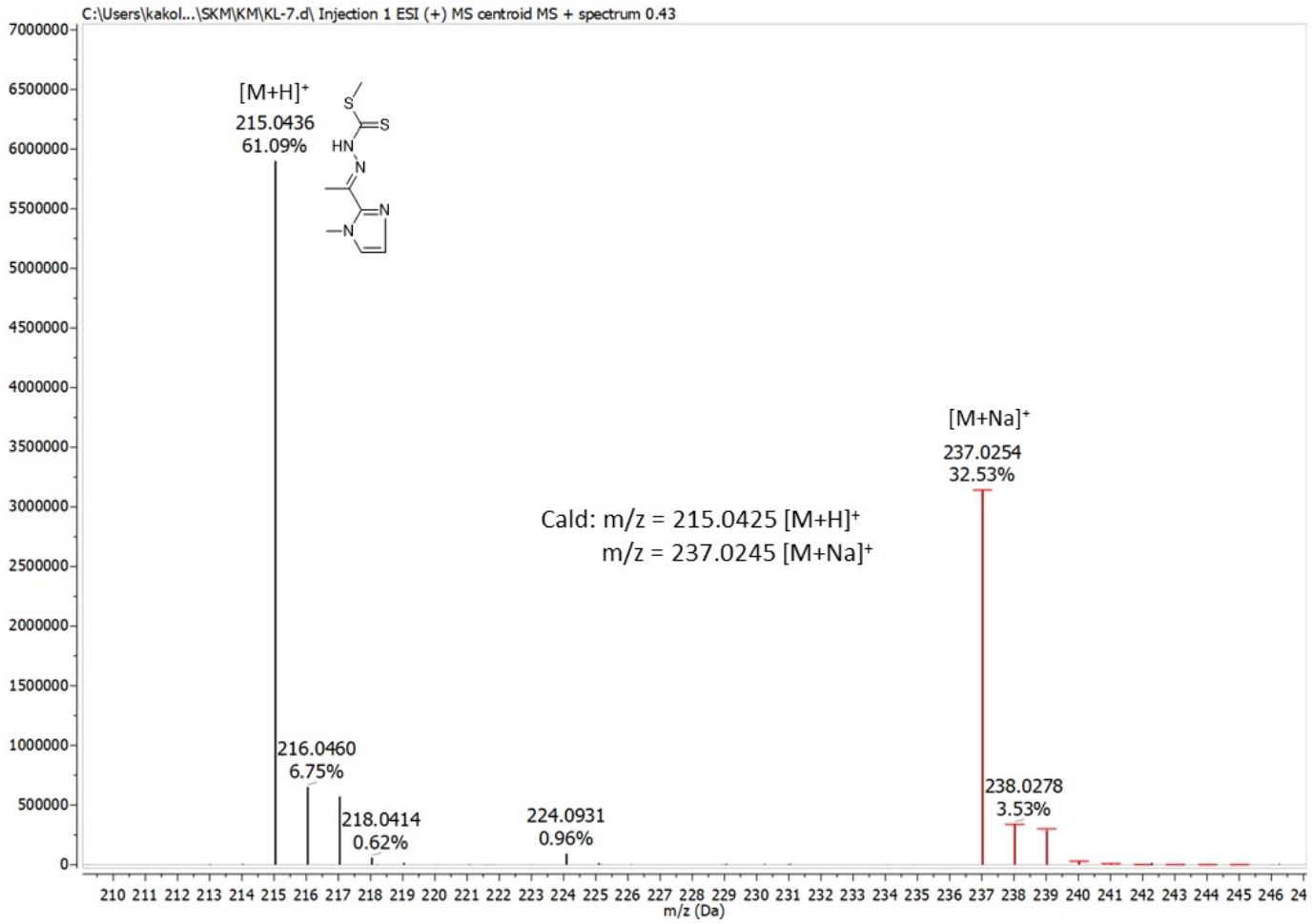

Figure S27. High Resolution Mass spectrum of H(L6) in acetonitrile (Concentration, 0.1 mg/mL).

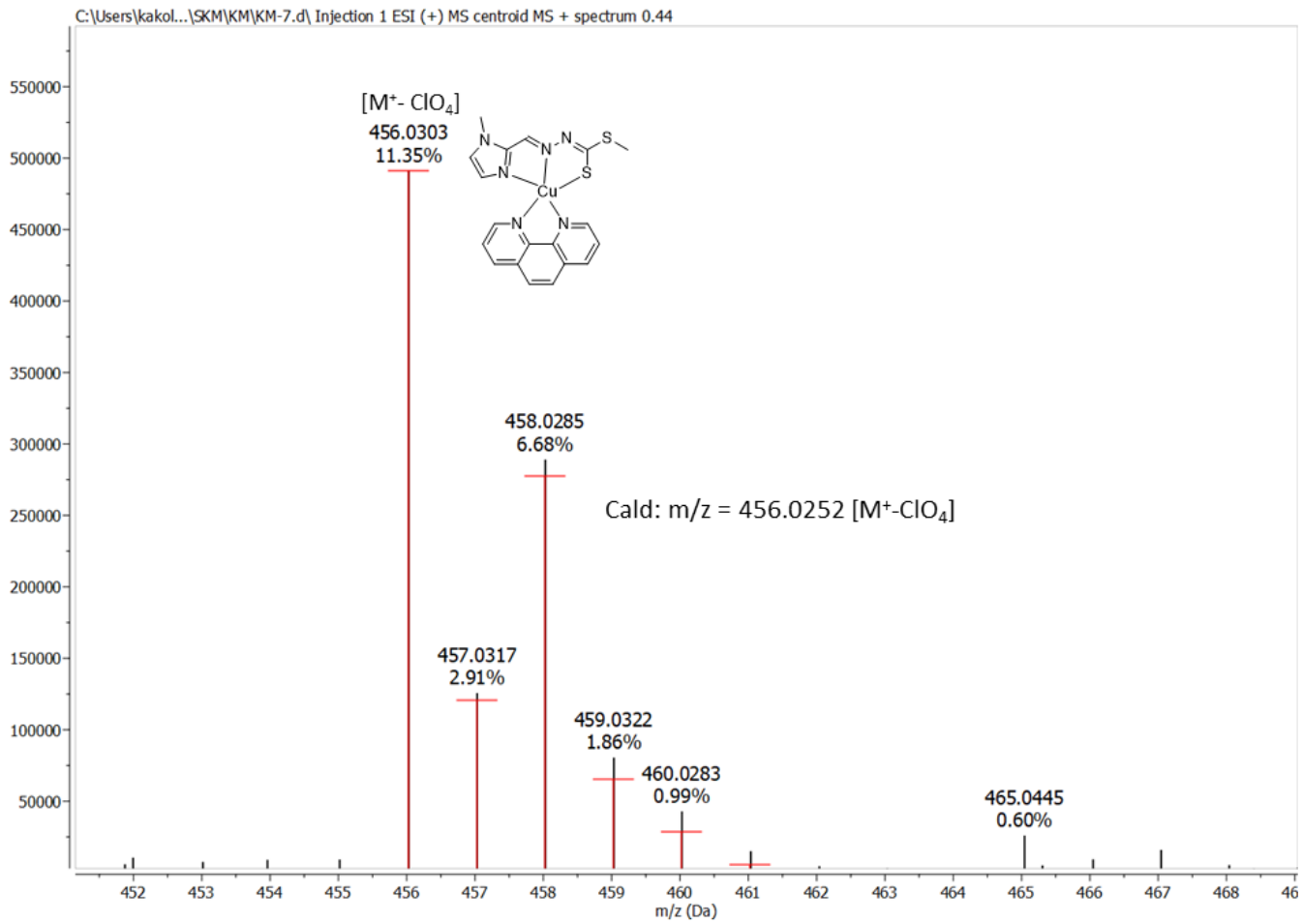

Figure S28. High Resolution Mass spectrum of [Cu(L6)(Phen)]ClO_4 (**6**) in acetonitrile (Concentration, 0.1 mg/mL).

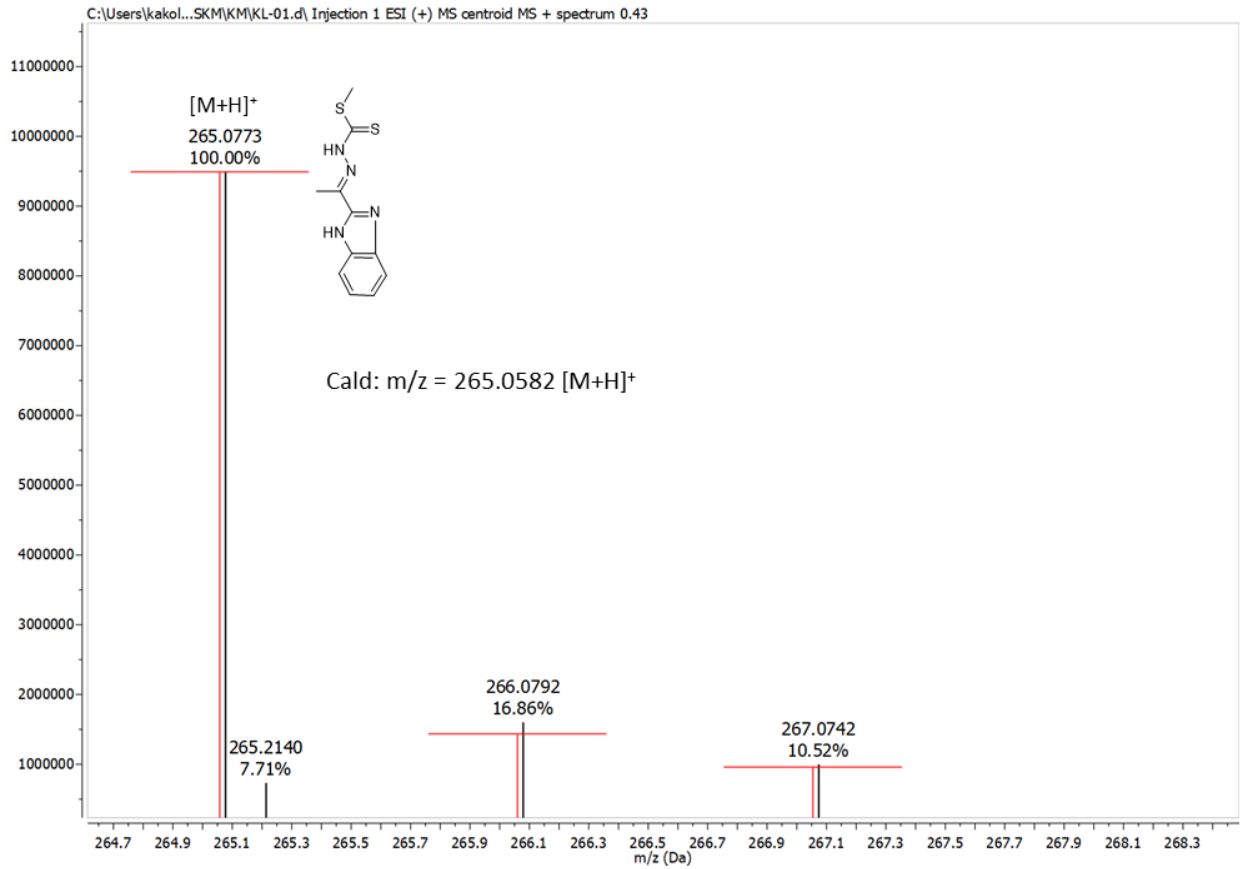

Figure S29. High Resolution Mass spectrum of H(L7) in acetonitrile (Concentration, 0.1 mg/mL).

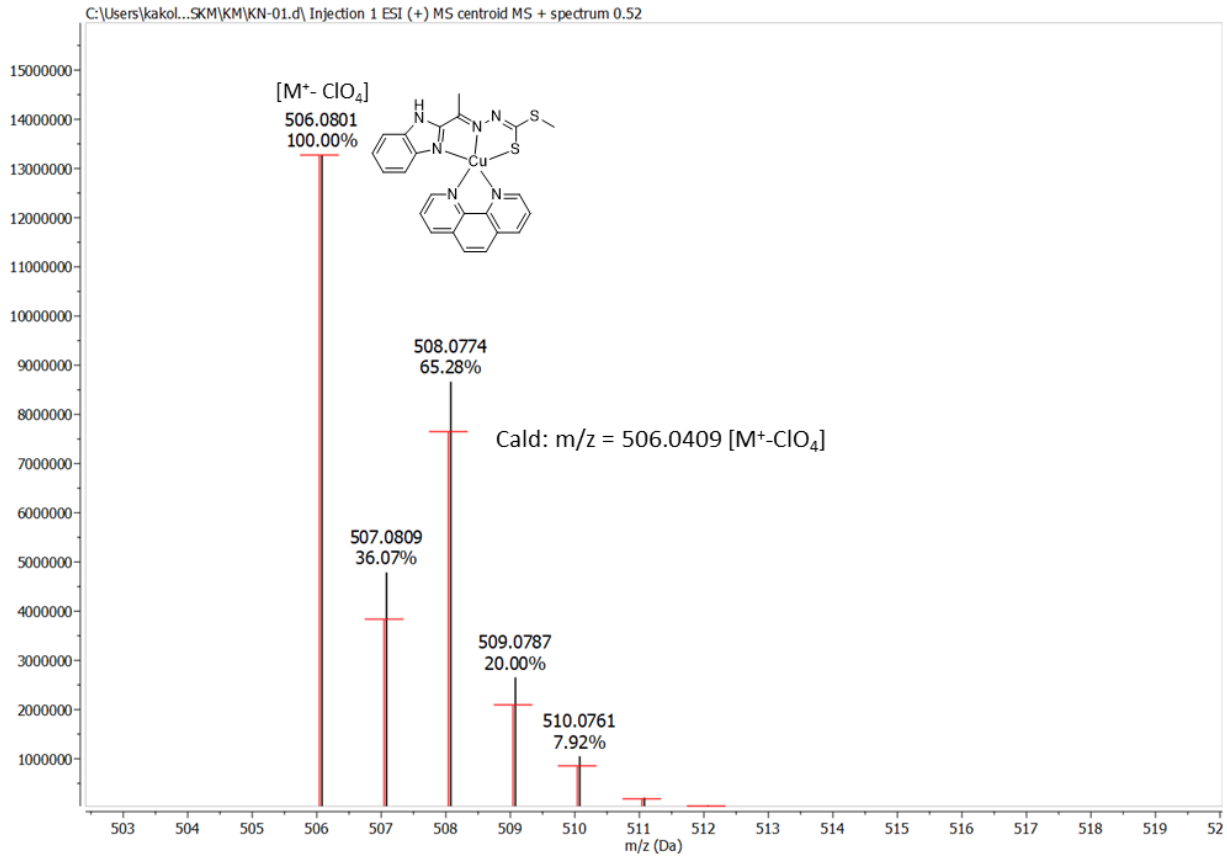

Figure S30. High Resolution Mass spectrum of [Cu(L7)(Phen)]ClO_4 (**7**) in acetonitrile (Concentration, 0.1 mg/mL).

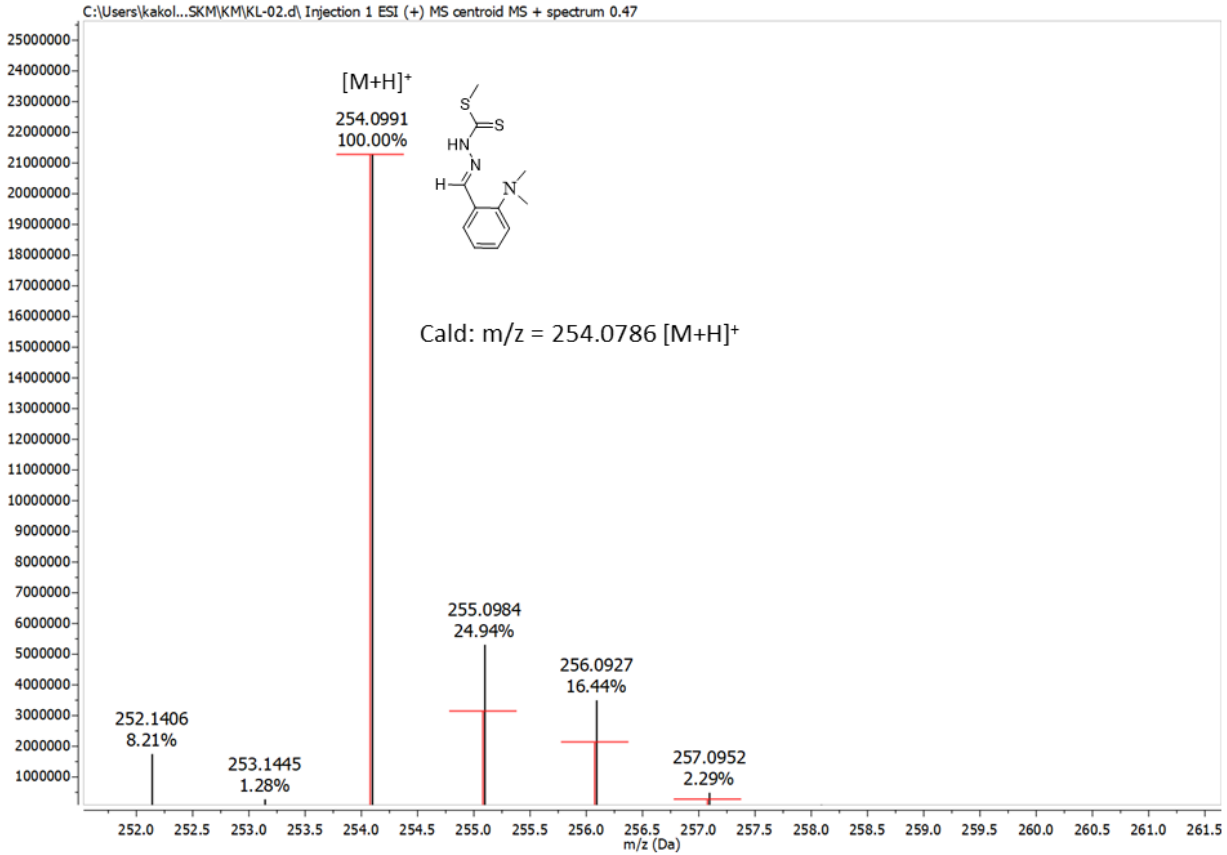

Figure S31. High Resolution Mass spectrum of H(L8) in acetonitrile (Concentration, 0.1 mg/mL).

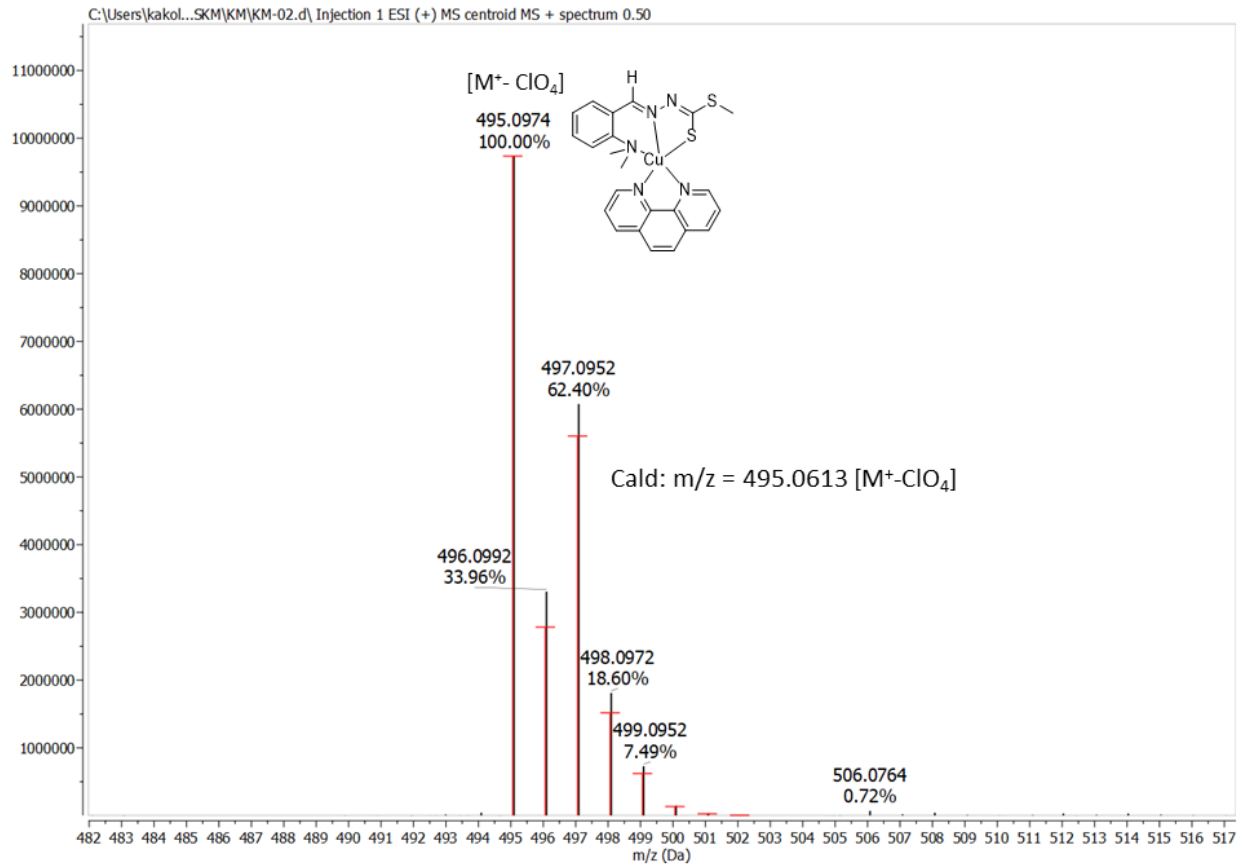

Figure S32. High Resolution Mass spectrum of [Cu(L8)(Phen)]ClO_4 (**8**) in acetonitrile (Concentration, 0.1 mg/mL).

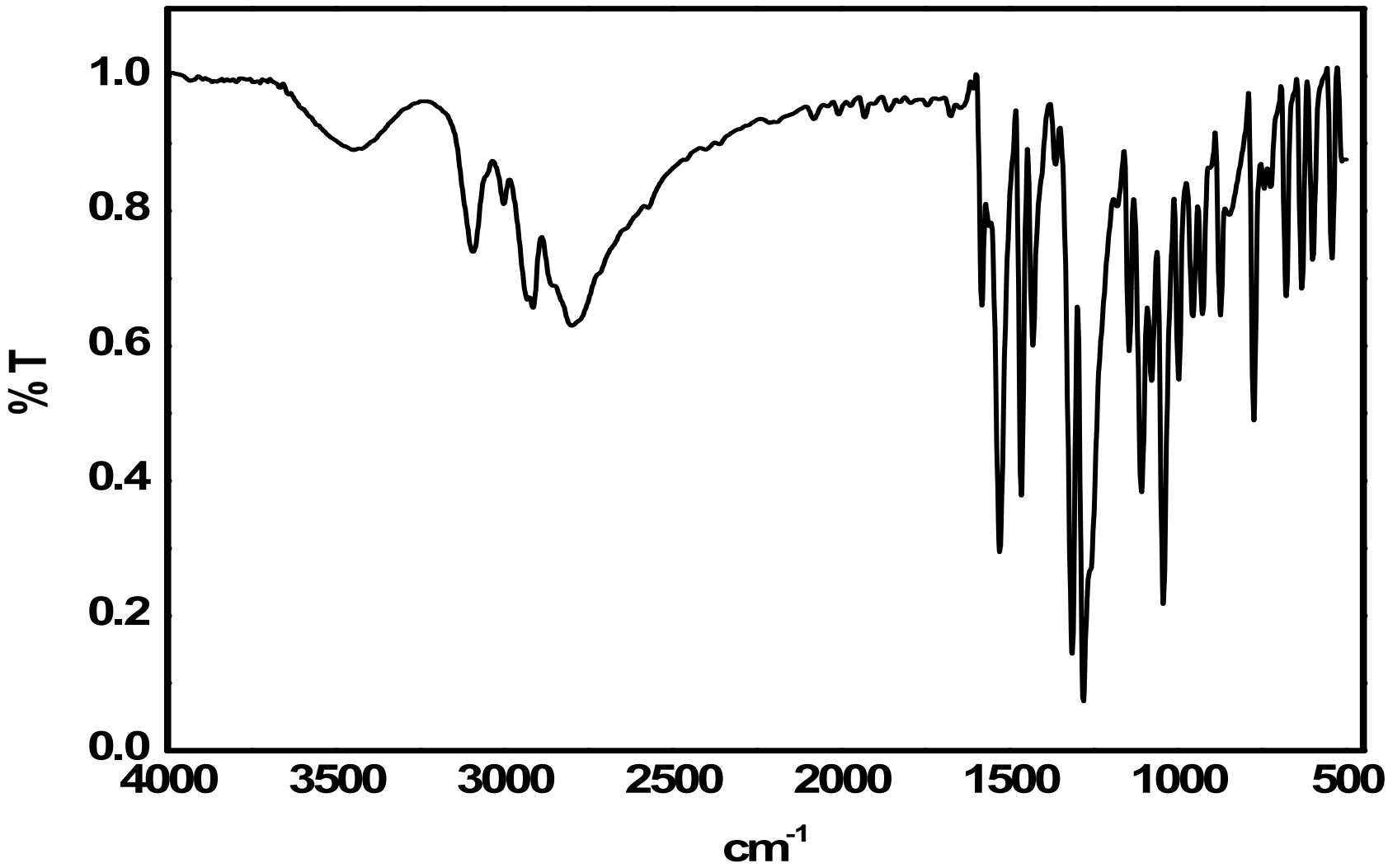

Figure S33. FTIR spectrum of H(L1).

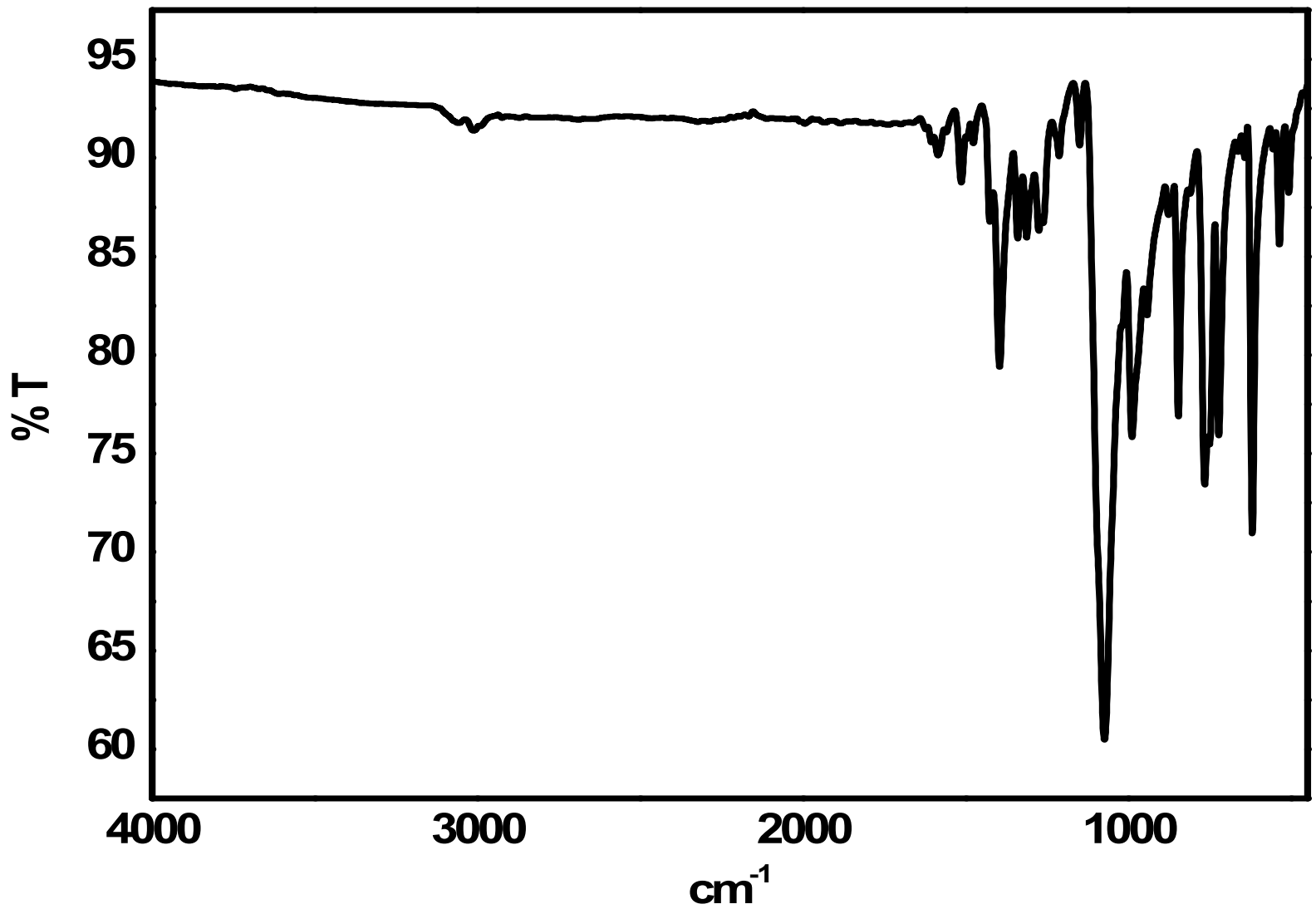

Figure S34. FTIR spectrum of [Cu(L1)(Phen)]ClO_4 (**1**).

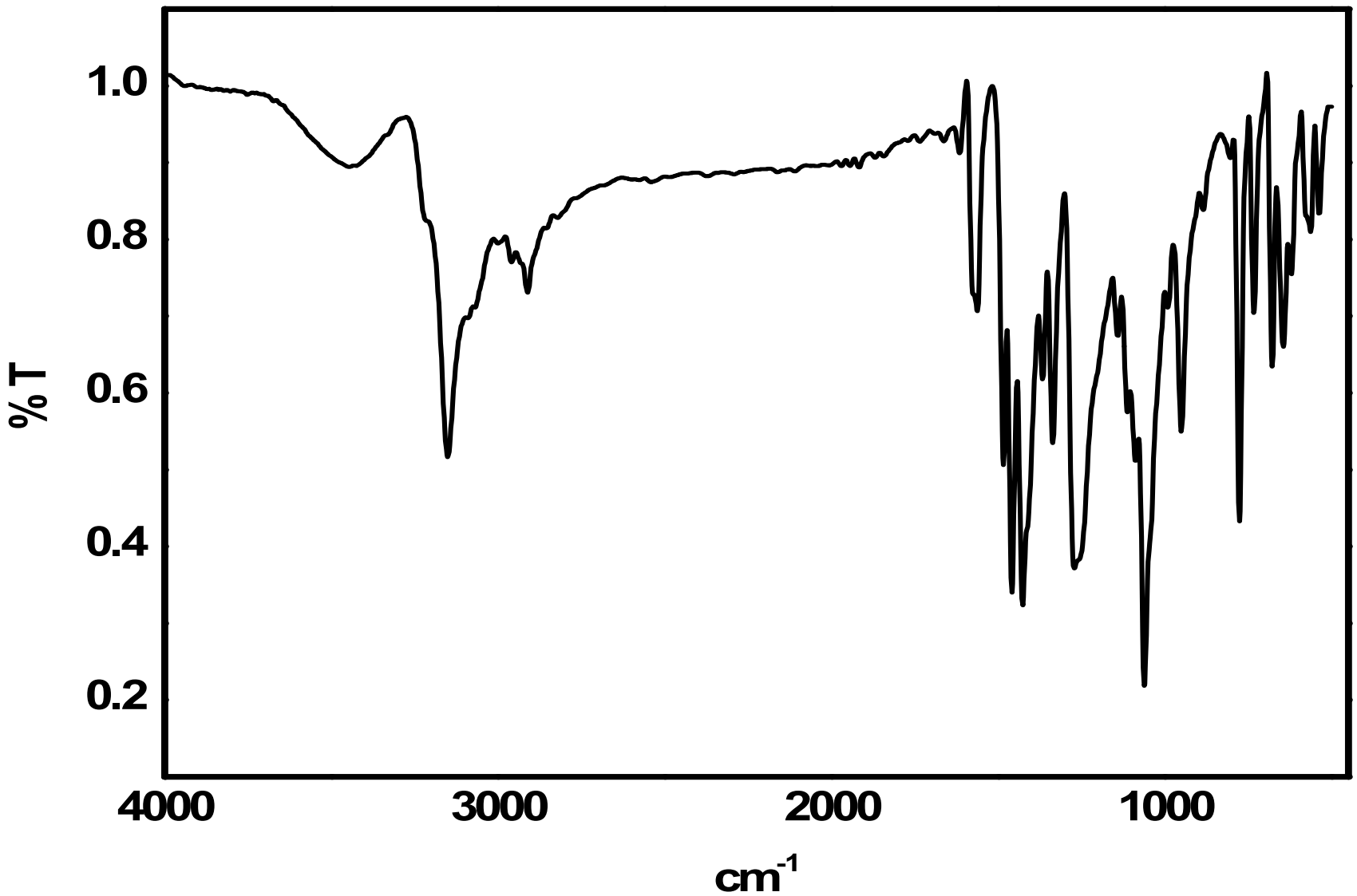

Figure S35. FTIR spectrum of H(L2).

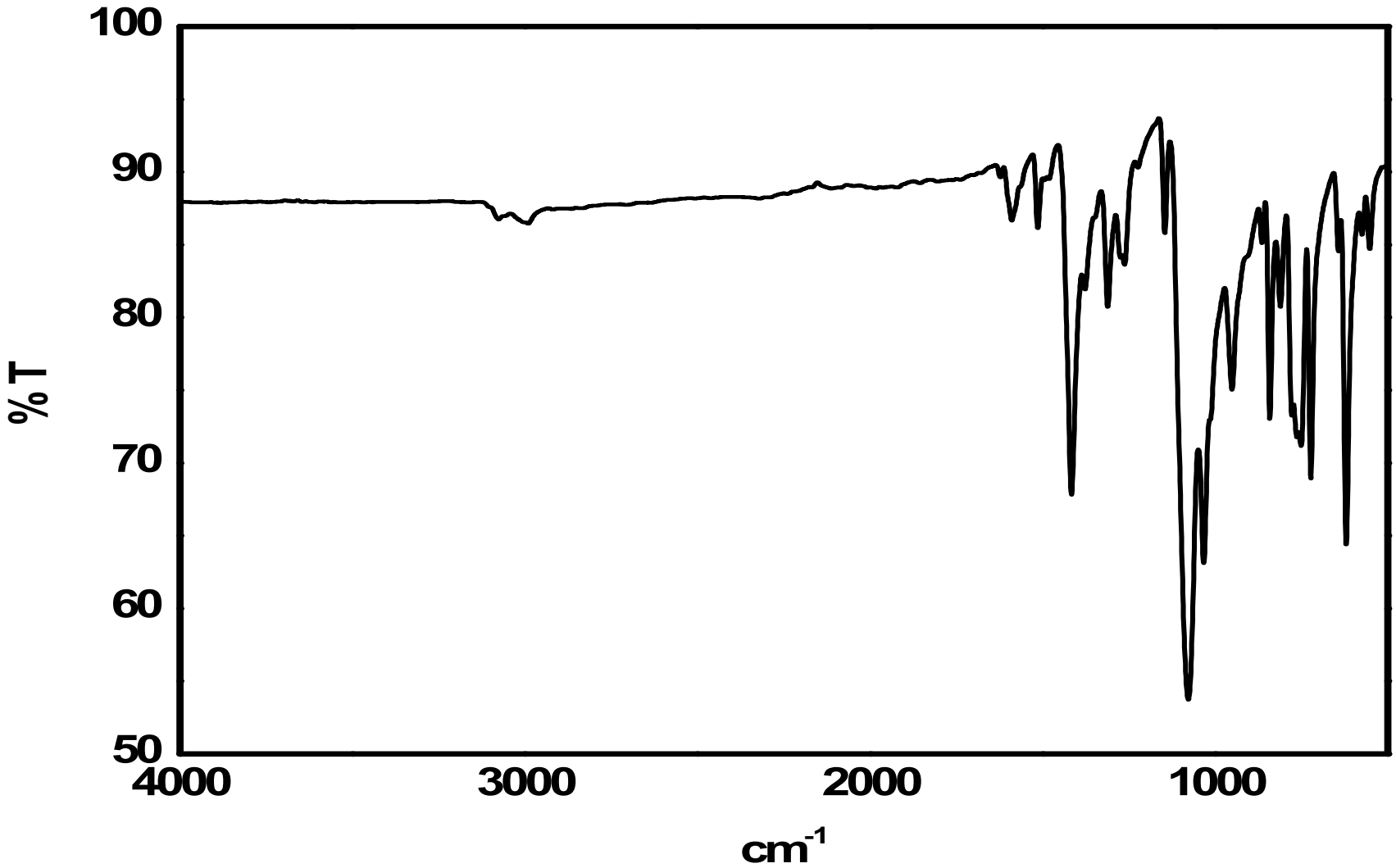

Figure S36. FTIR spectrum of [Cu(L2)(Phen)]ClO_4 (**2**).

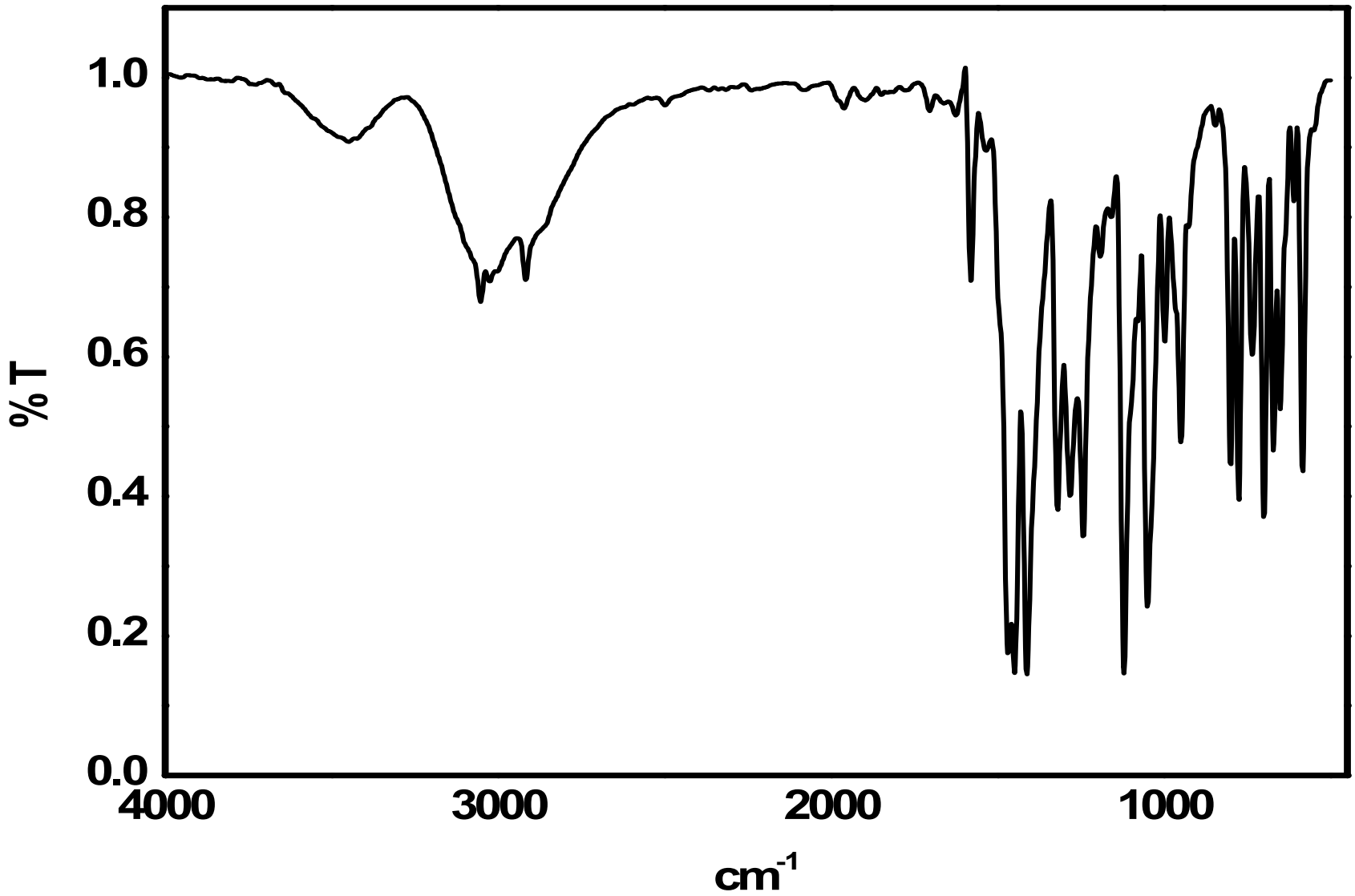

Figure S37. FTIR spectrum of H(L3).

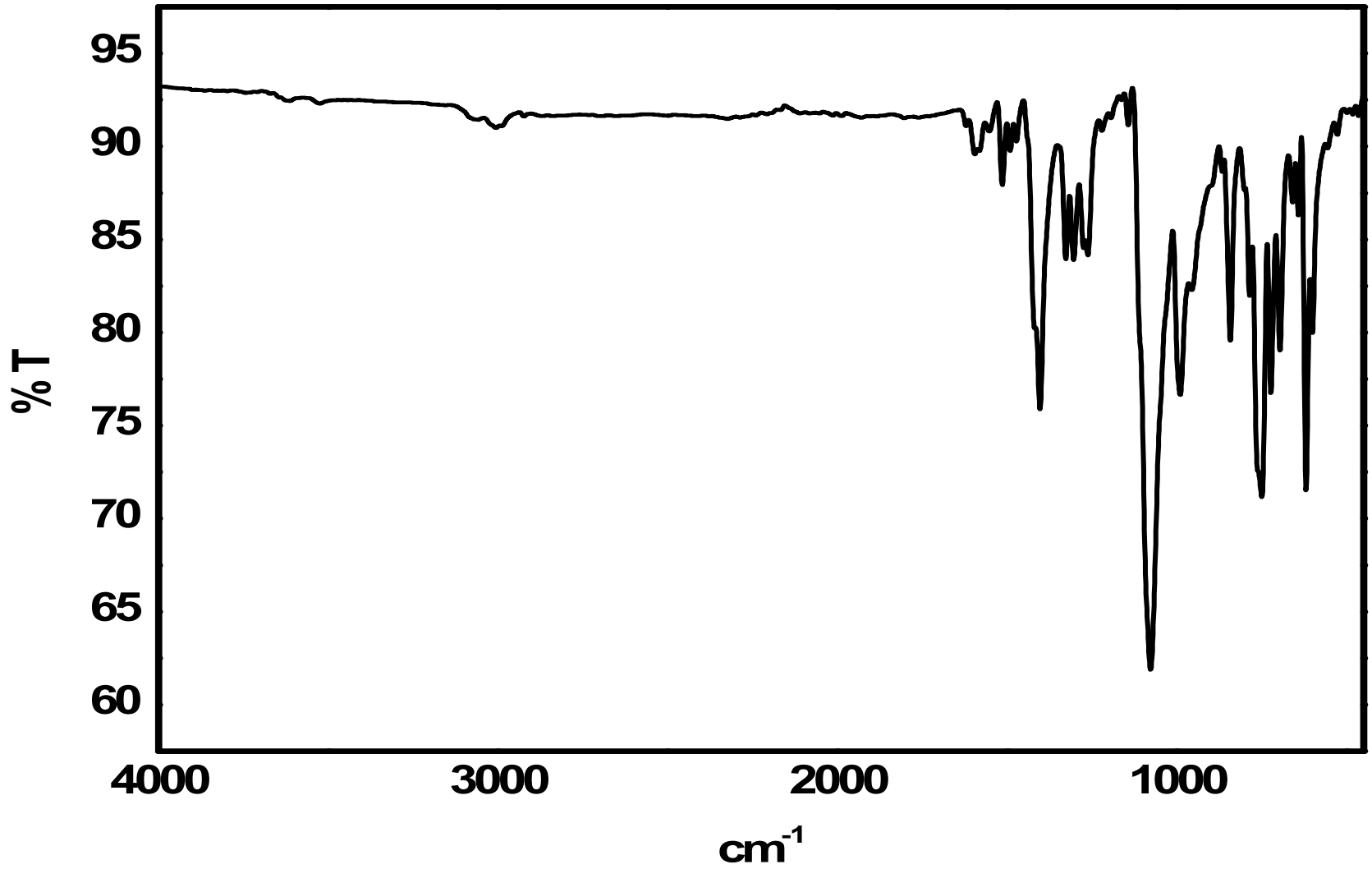

Figure S38. FTIR spectrum of [Cu(L3)(Phen)]ClO_4 (**3**).

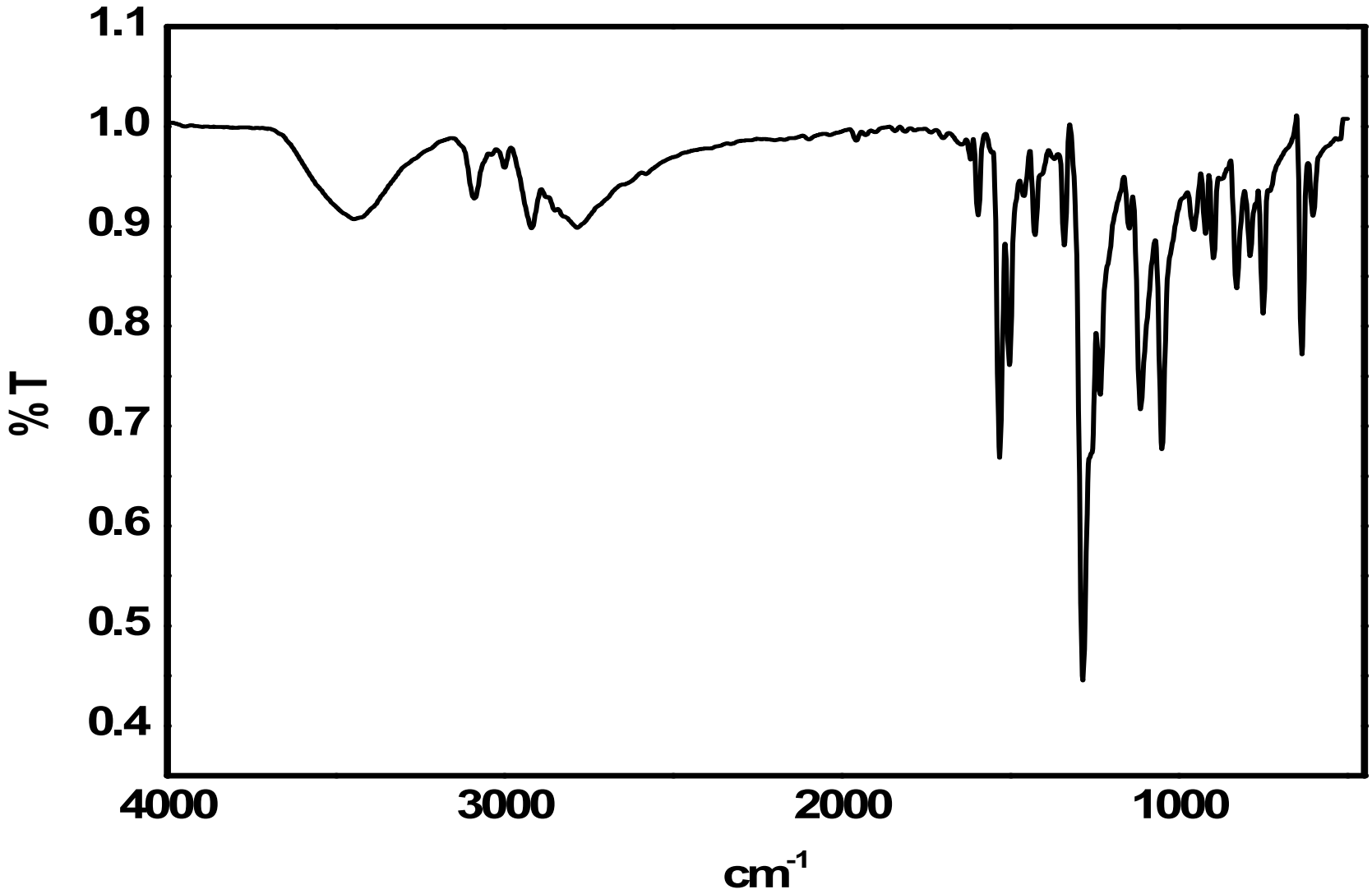

Figure S39. FTIR spectrum of H(L4).

.

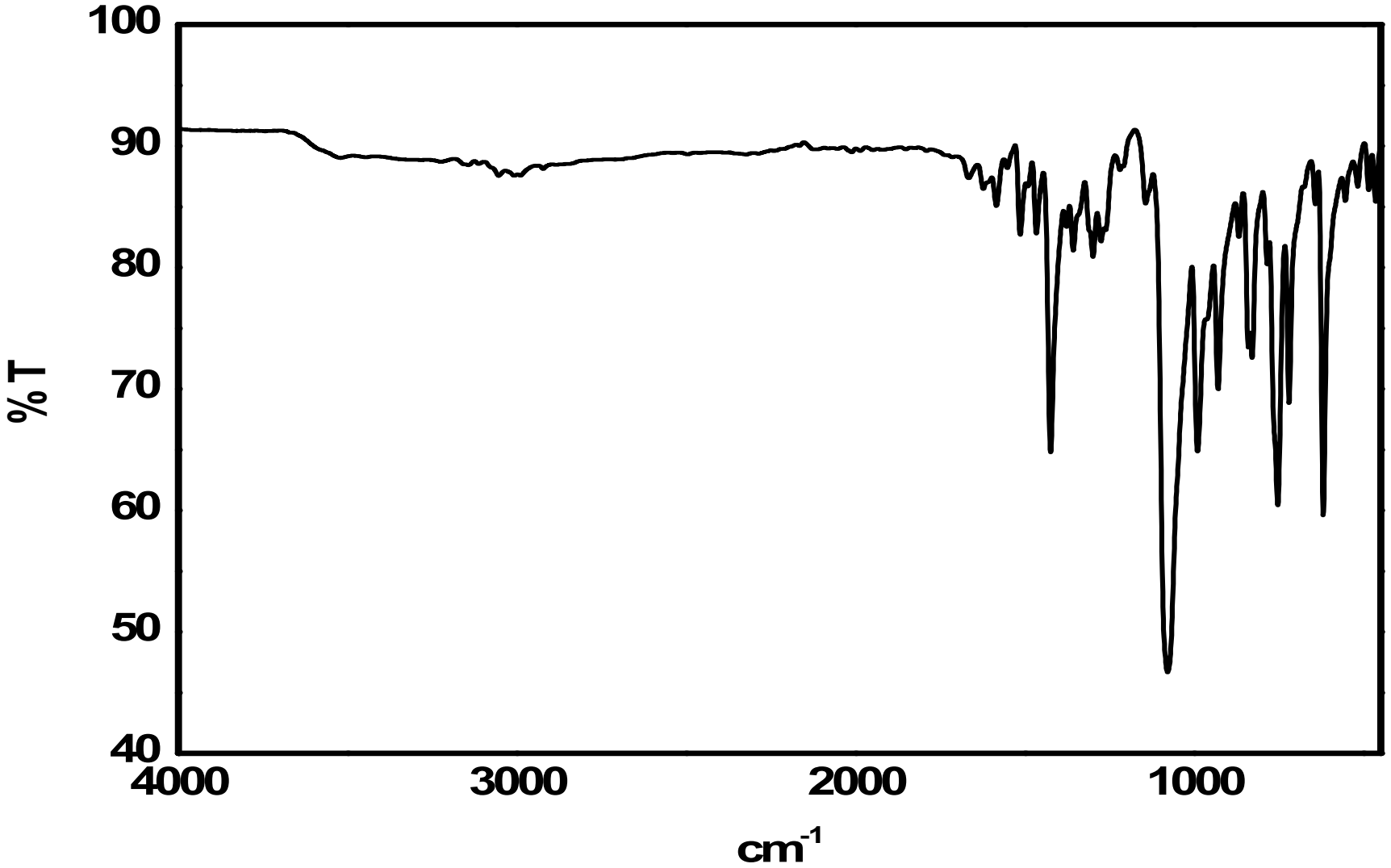

Figure S40. FTIR spectrum of [Cu(L4)(Phen)]ClO_4 (**4**).

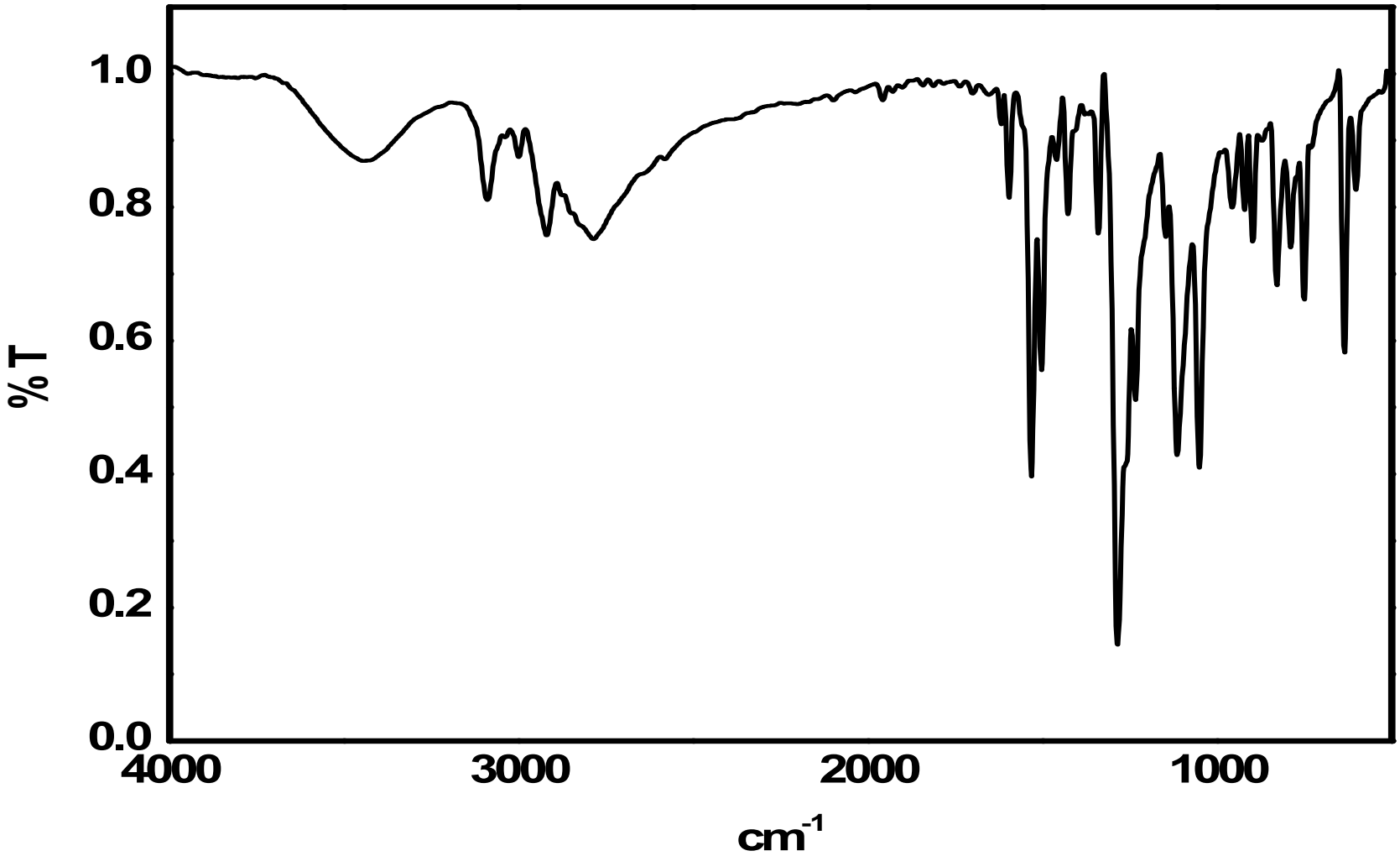

Figure S41. FTIR spectrum of H(L5).

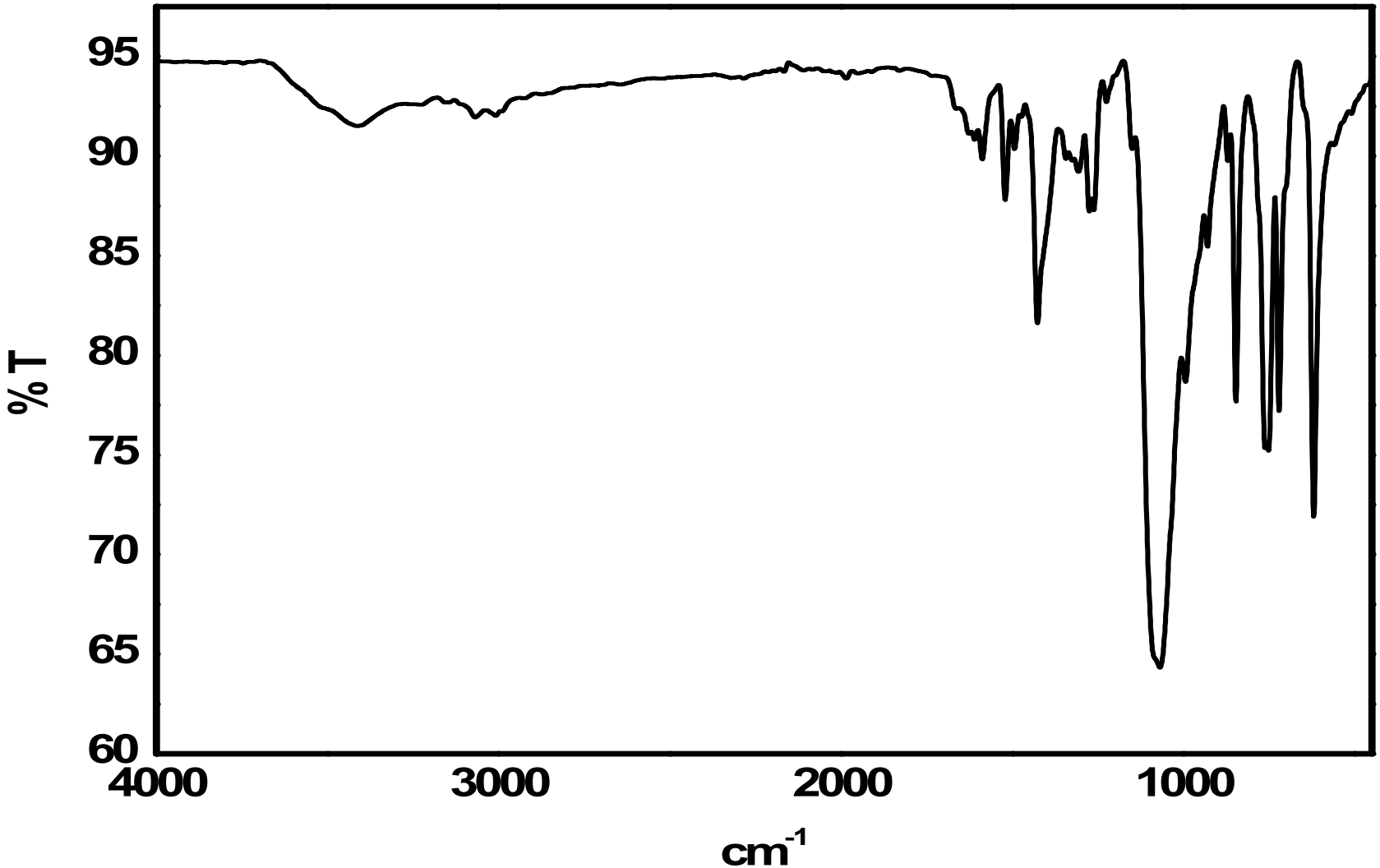

Figure S42. FTIR spectrum of [Cu(L5)(Phen)]ClO_4 (**5**).

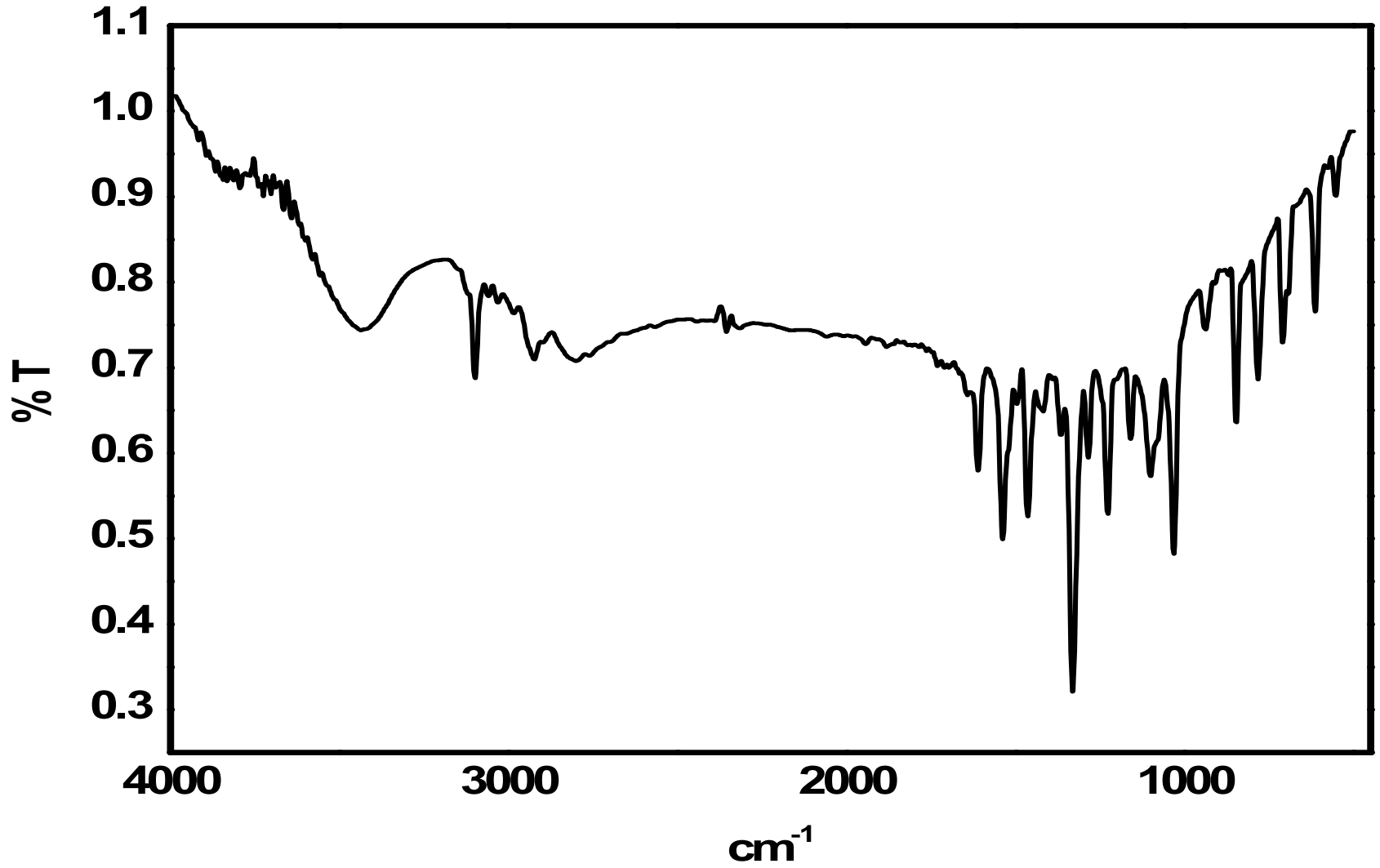

Figure S43. FTIR spectrum of H(L6).

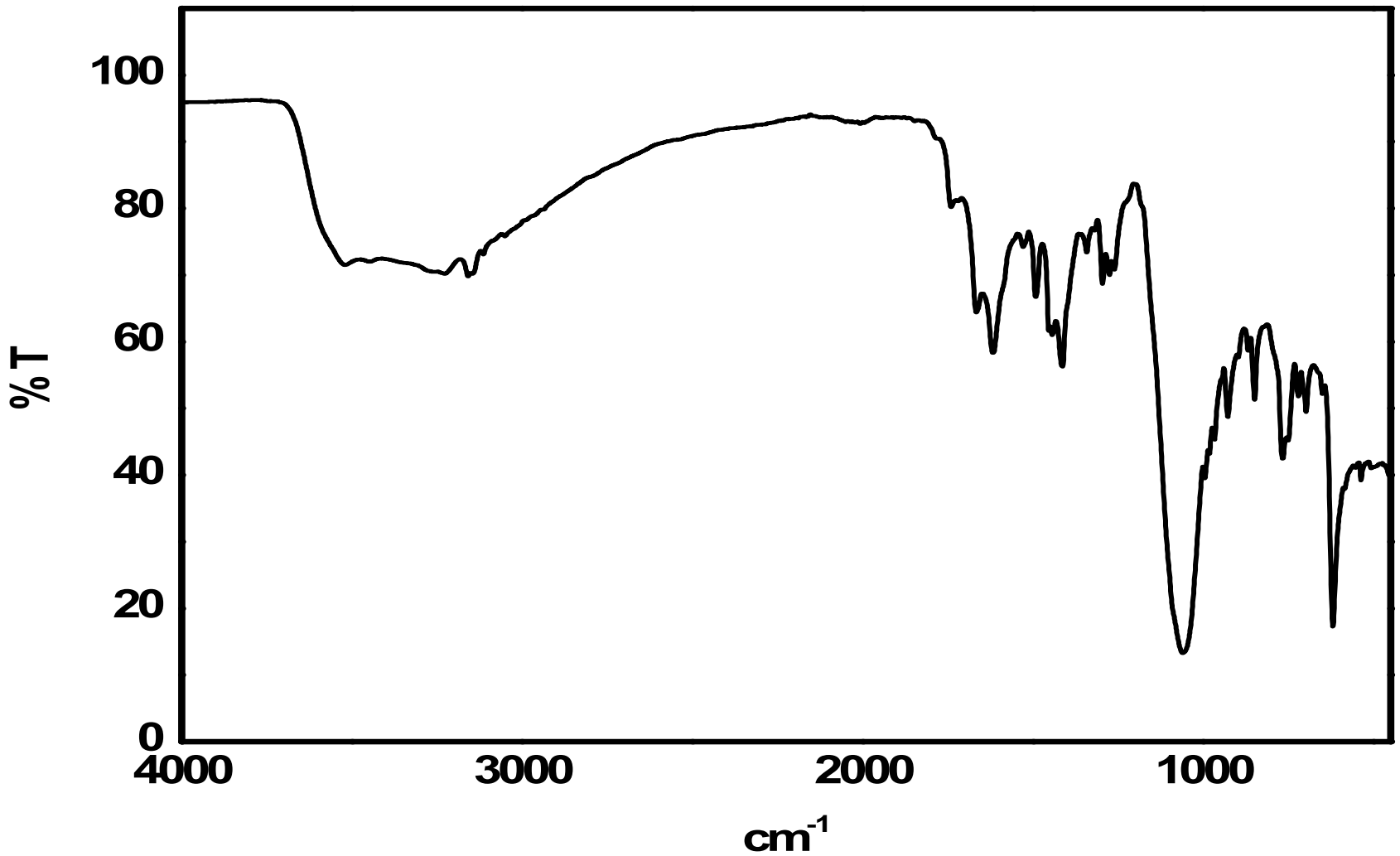

Figure S44. FTIR spectrum of [Cu(L6)(Phen)]ClO_4 (**6**).

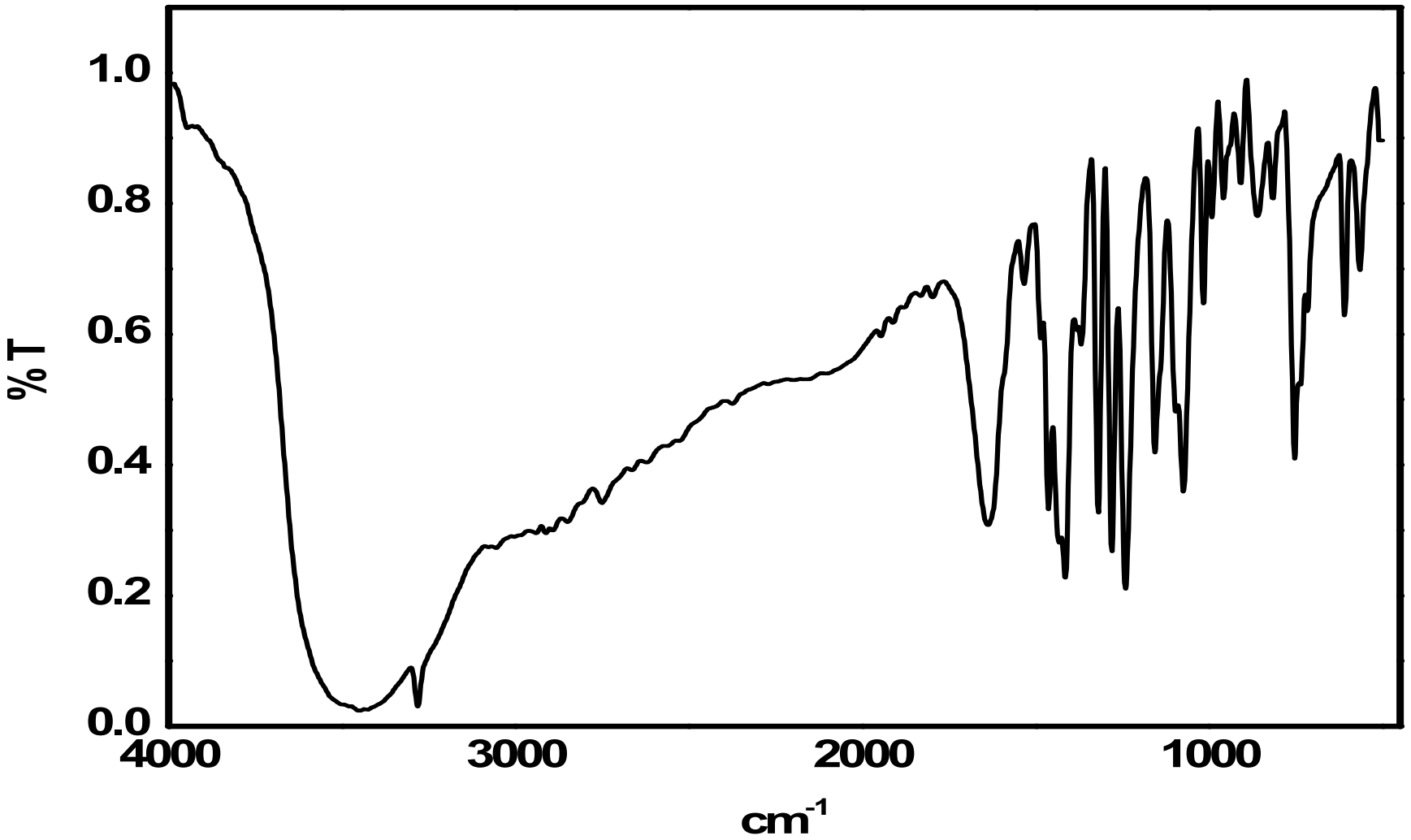

Figure S45. FTIR spectrum of H(L7).

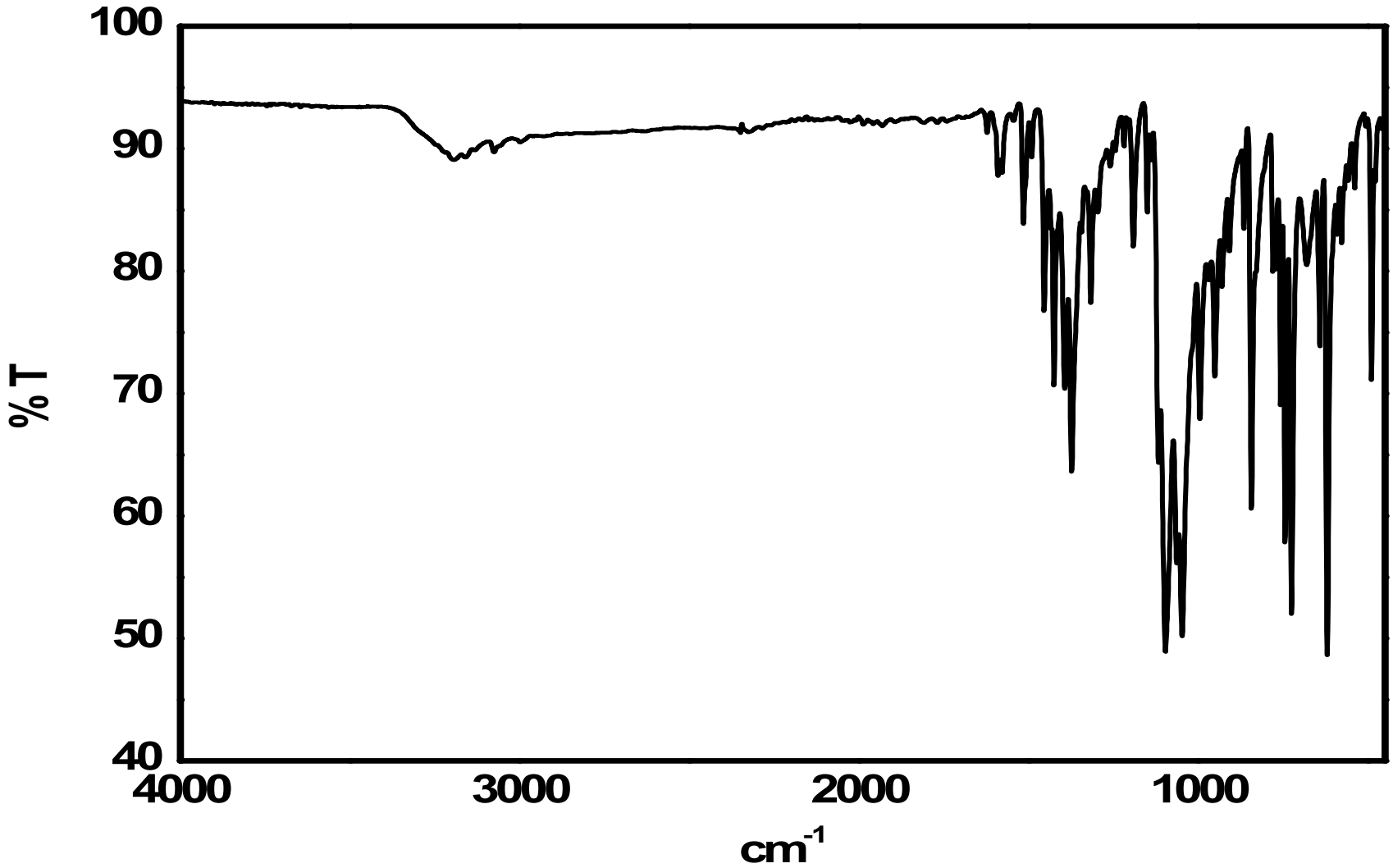

Figure S46. FTIR spectrum of [Cu(L7)(Phen)]ClO_4 (**7**).

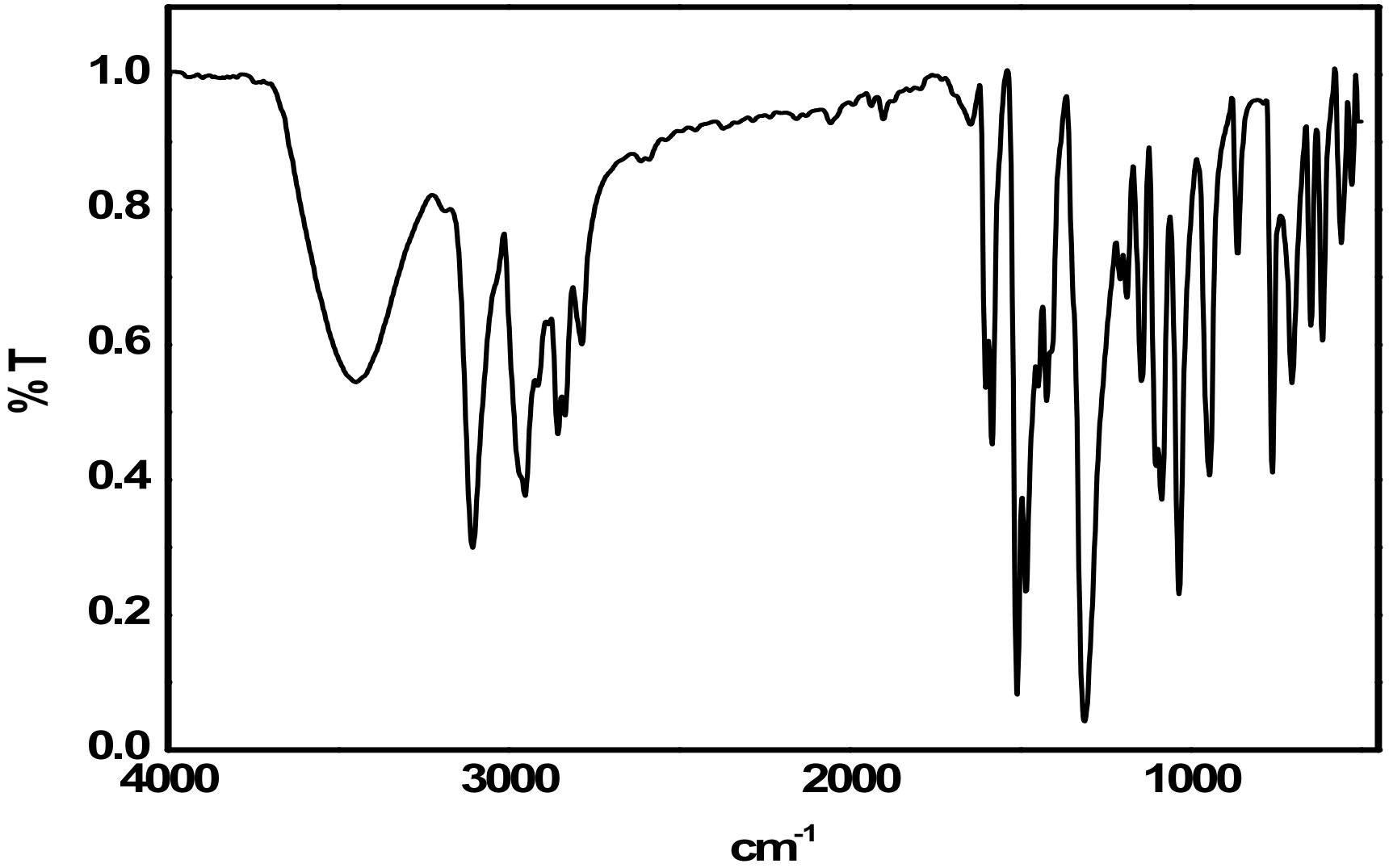

Figure S47. FTIR spectrum of H(L8).

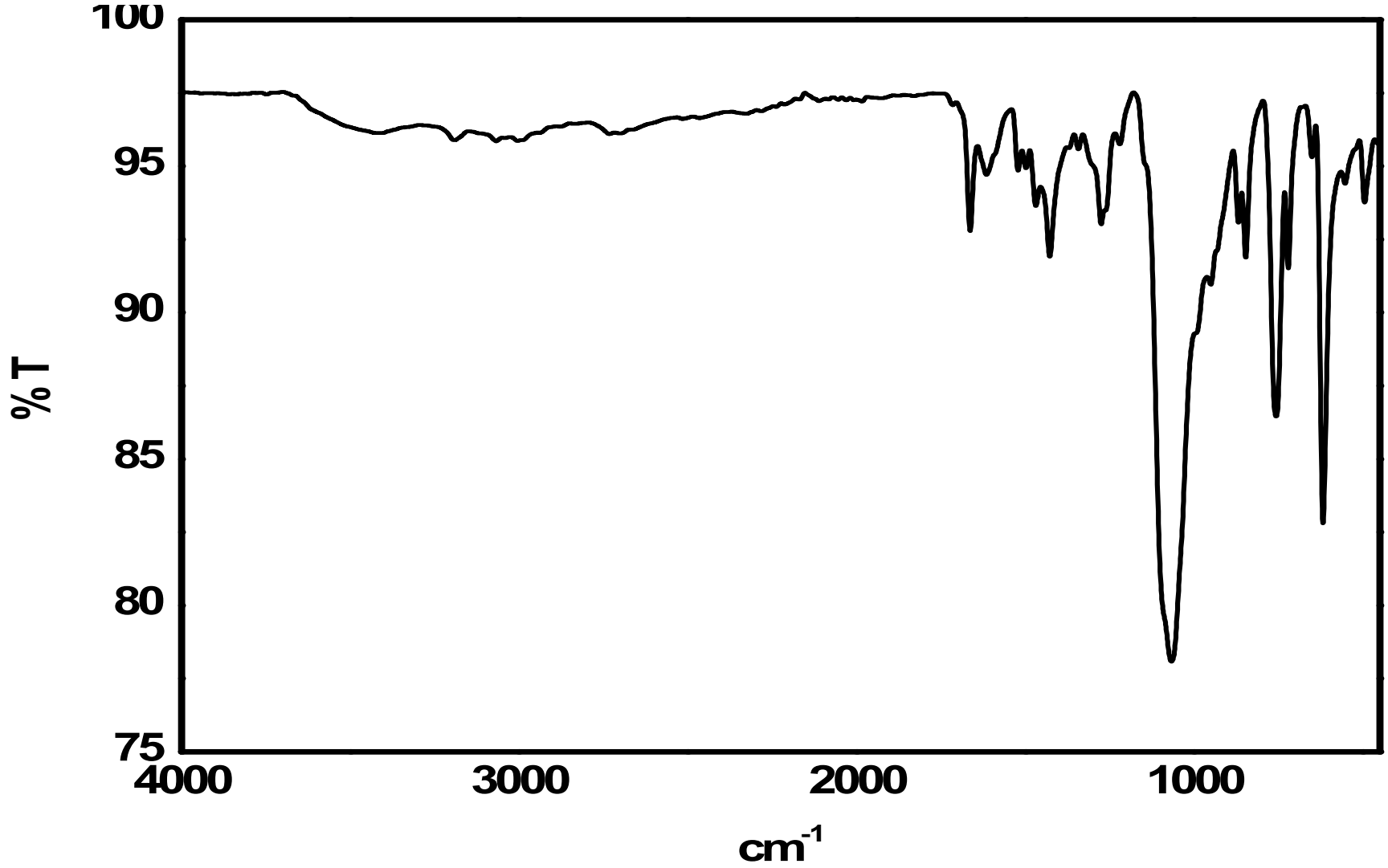

Figure S48. FTIR spectrum of [Cu(L8)(Phen)]ClO_4 (**8**).

Table S3 UV-Visible data for copper(II) complexes (**1**-**8**)

complex	medium	λ_{max} (ε_{max}); nm ($M^{-1}cm^{-1}$)		
		d-d band	CT band	LB band
1	DMSO	637 (90), 818 sh	417 (7510), 393 (9900)	331 (9800)
	MeOH	643 (60), 817 sh	416 (5640), 392 (6320)	334 (9310)
	MeCN	642 (70), 820 sh	416 (5390), 392 (7400)	331 (10290)
	aq. MeOH	641 (75), 821 sh	414 (6600), 392 (8400)	334 (9840)
2	DMSO	621 (90), 890 sh	410 (2092), 395 (3760)	328 (25590)
	MeOH	624 (90), 887 sh	412 (2830), 392 (3520)	327 (21070)
	MeCN	642 (70), 888 sh	416 (4390), 393 (3380)	323 (20300)
	aq. MeOH	641 (75), 886 sh	414 (6600), 392 (8400)	323 (8960)
3	DMSO	615 (80), 870 sh	423 (3560), 393 (3620)	337 (5570)
	MeOH	618 (80), 882 sh	424 (2930), 392 (3490)	338 (6000)
	MeCN	614 (70), 870 sh	422 (3330), 392 (3360)	332 (3460)
	aq. MeOH	616 (80), 868 sh	420 (4010), 393 (3010)	330 (7530)
4	DMSO	650(100), 918 sh (30)	438 (3590), 368 (7260)	
	MeOH	649 (100), 916 sh (30)	440 (3250), 365 (6510)	
	MeCN	649 (80), 906 sh (30)	438 (3030), 368 (8780)	
	aq. MeOH	650 (100), 908 sh (30)	437 (3270), 365 (6130)	
5	DMSO	655 (60), 920 (20)	464 (2180), 370 (5250)	
	MeOH	658 (70), 930 (20)	457 (1790), 379 (5460)	
	MeCN	655 (60), 925 (20)	461 (1930), 378 (5970)	
	aq. MeOH	653 (80), 930 (30)	458 (2010), 373 (6010)	
6	DMSO	666 (70), 926 sh	412 (6990), 323 (6820)	
	MeOH	667 (70), 931 sh	418 (5750), 326 (9400)	
	MeCN	668 (70), 925 sh	414 (5520), 325 (11030)	
	aq. MeOH	667 (50), 928 sh	416 (4070), 324 (10350)	

7	DMSO	686 (80), 925 sh	414 (5600), 394 (6370)	337 (9550)
	MeOH	683 (70), 938 sh	412 (4600), 394 (7940)	338 (8700)
	MeCN	682 (90), 936 sh	413 (6100), 394 (7630)	327 (9700)
	aq. MeOH	684 (80), 930 sh	413 (5570), 392 (6630)	339 (6300)
8	DMSO	666 (90), 944 (30)	368 (3050)	
	MeOH	663 (70), 943 (25)	369 (5110)	
	MeCN	662 (80), 938 (30)	365 (5010)	
	aq. MeOH	666 (70), 936 (30)	365 (4950)	

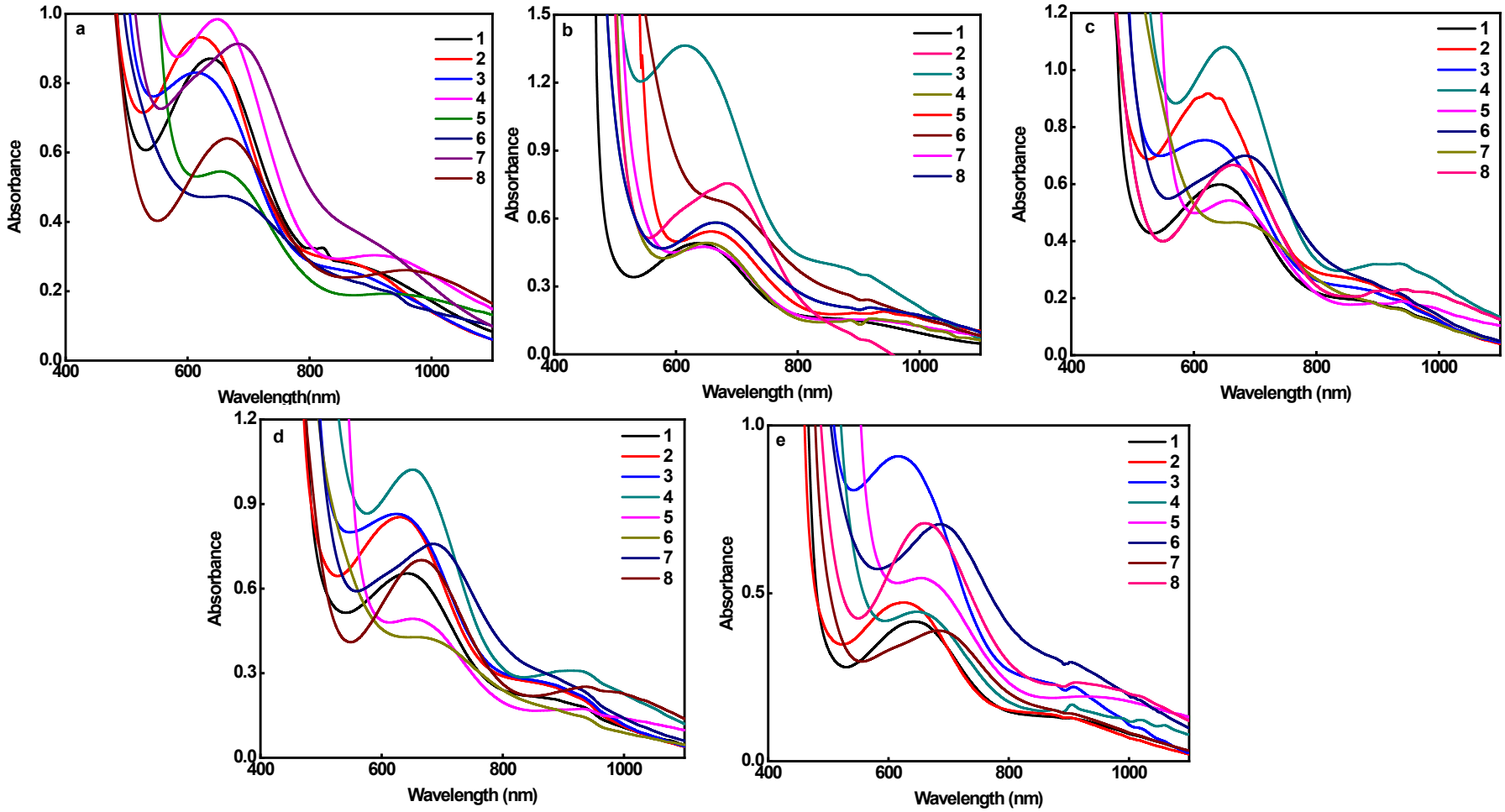

Figure S49. Electronic spectrum of [Cu(**L1**/**L2**/**L3**/**L4**/**L5**/**L6**/**L7**/**L8**)(phen)](ClO_4) (**1**-**8**) in (a) DMF (Concentration, 1×10^{-2} M), (b) DMSO (Concentration, 1×10^{-2} - 5×10^{-3} M), (c) MeOH (Concentration, 1×10^{-2} - 5×10^{-3} M), (d) MeCN (Concentration, 1×10^{-2} - 5×10^{-3} M) and (e) aq. MeOH (Concentration, 1×10^{-2} - 5×10^{-3} M).

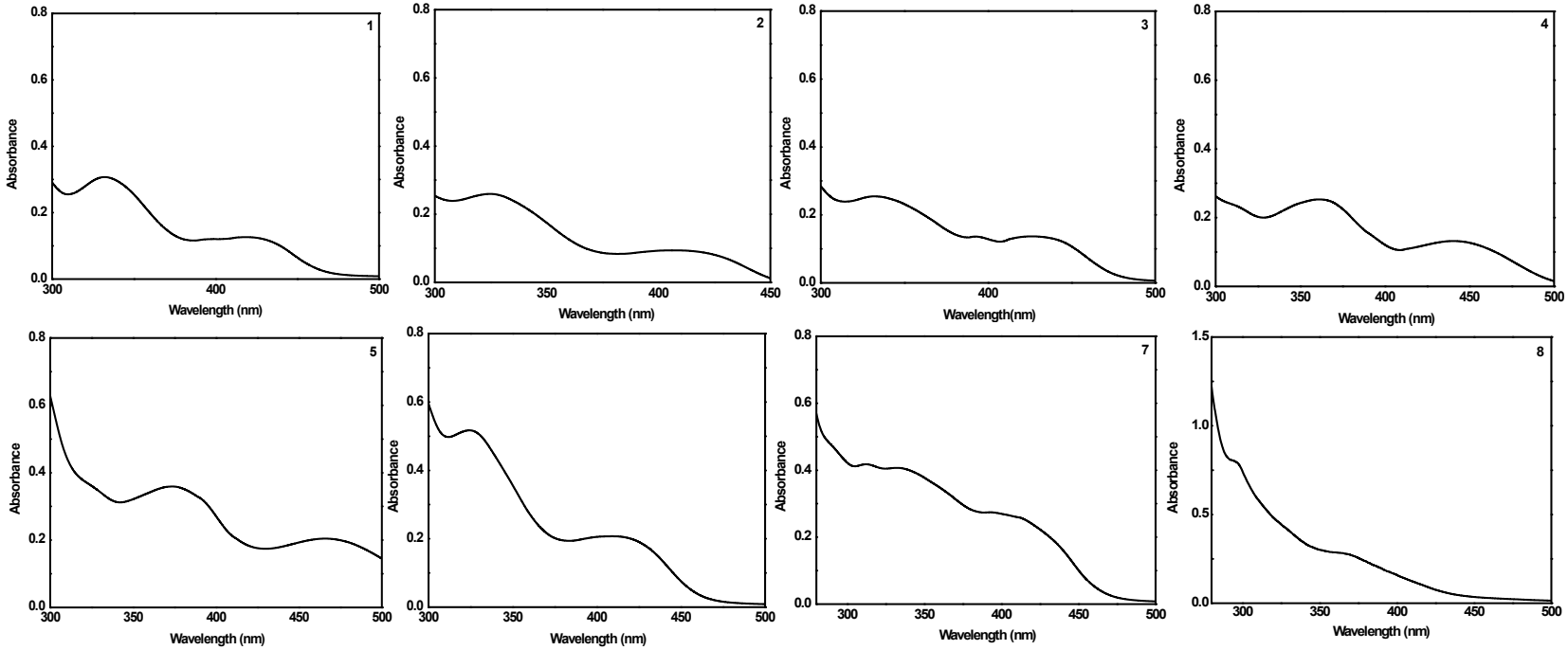

Figure S50. Electronic spectrum of [Cu(**L1**/**L2**/**L3**/**L4**/**L5**/**L6**/**L7**/**L8**)(phen)](ClO_4) (**1**-**8**) in DMF (Concentration, 4.1- 4.3×10^{-5} M).

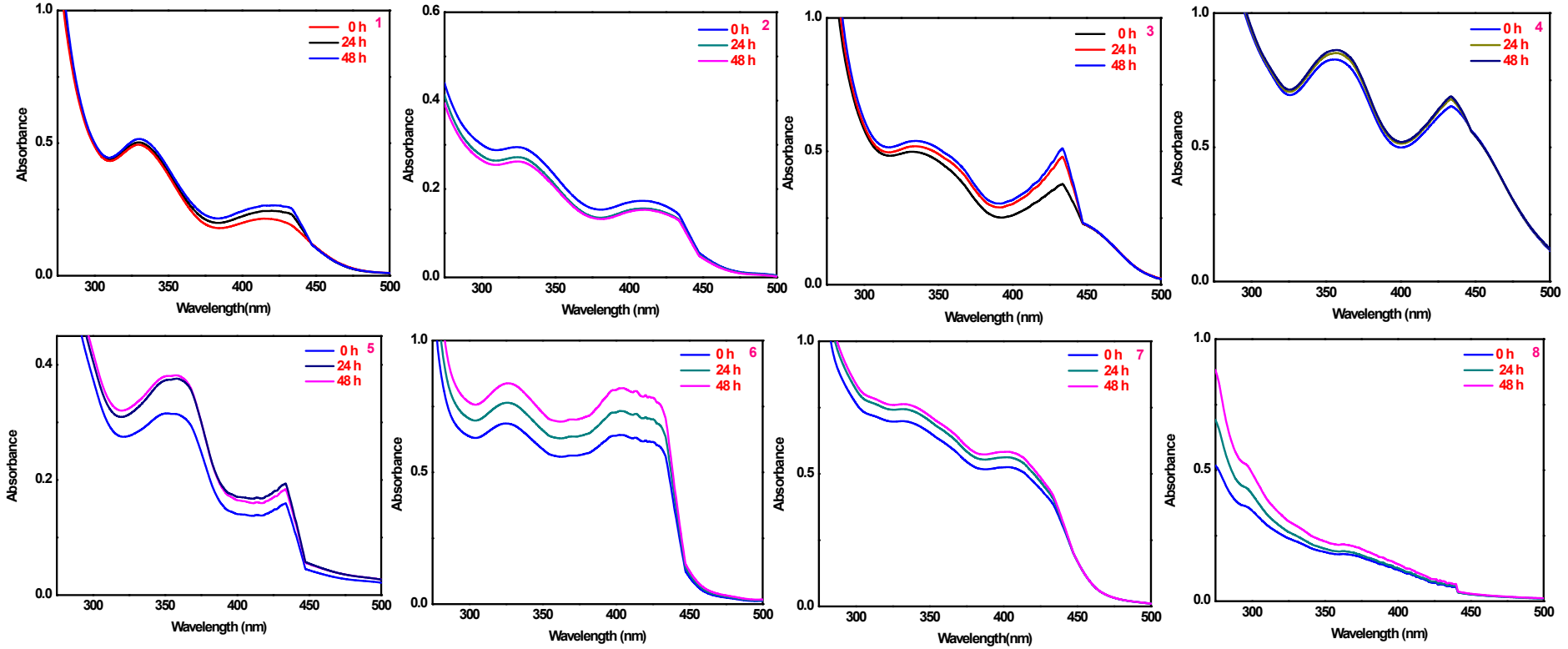

Figure S51. Electronic spectrum of [Cu(**L1**/**L2**/**L3**/**L4**/**L5**/**L6**/**L7**/**L8**)(phen)](ClO_4) (**1**-**8**) in 2% DMF/5 mM Tris-HCl/50 mM NaCl buffer solution in 0 h, 24 h and 48 h (Concentration, 4.1- 4.3×10^{-5} M).

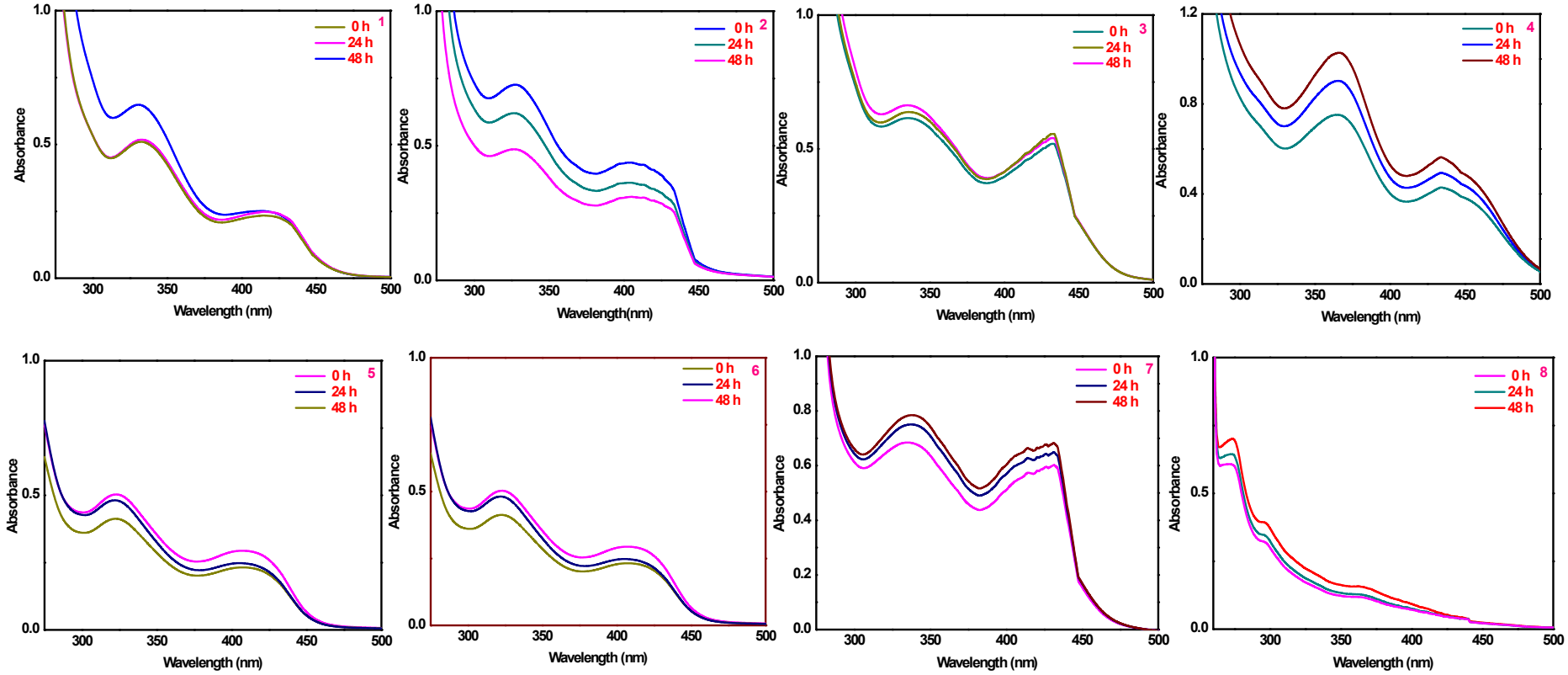

Figure S52. Electronic spectrum of [Cu(**L1**/**L2**/**L3**/**L4**/**L5**/**L6**/**L7**/**L8**)(phen)](ClO_4) (**1**-**8**) in cell culture media (DMEM) in 0 h, 24 h and 48 h (Concentration, 4.1- 4.3×10^{-5} M).

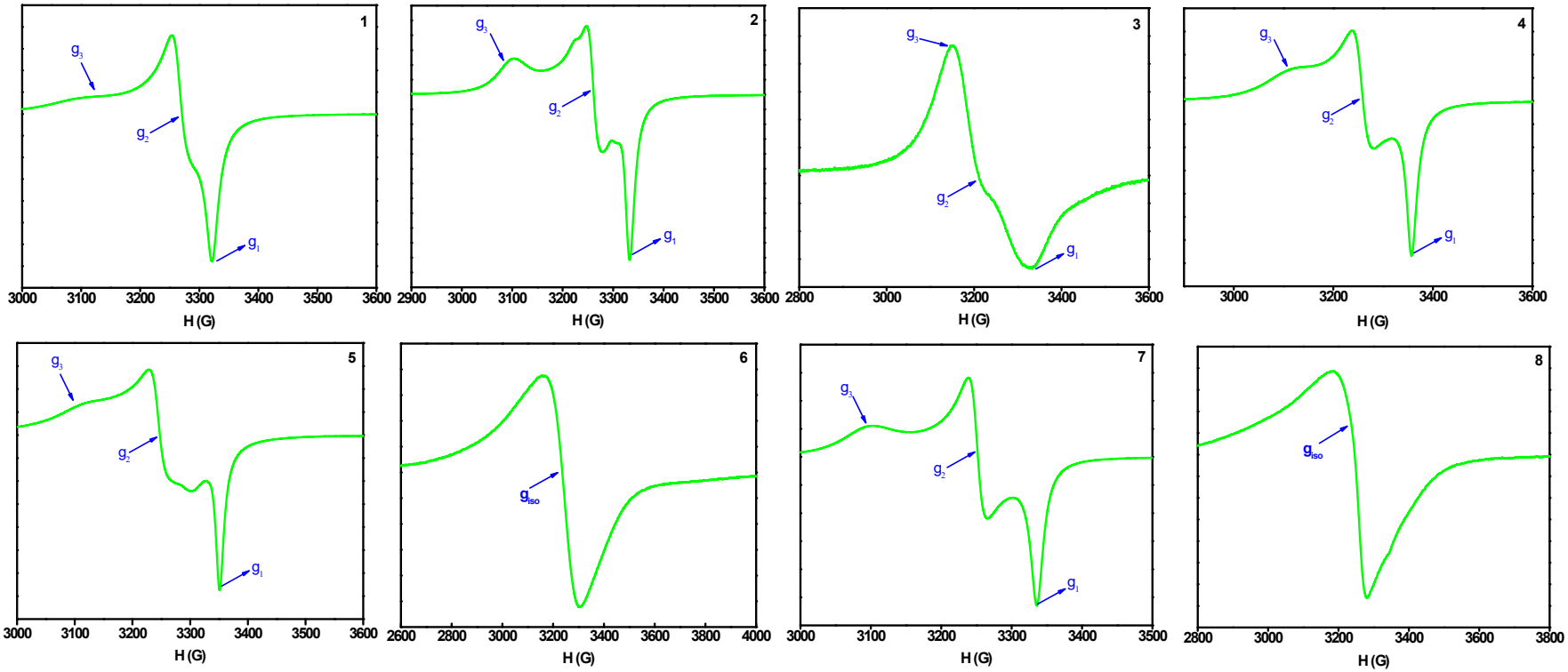

Figure S53. Polycrystalline EPR spectra of [Cu(L1/L2/L3/L4/L5/L6/L7/L8)(phen)](ClO_4) (**1**-**8**) at room temperature.

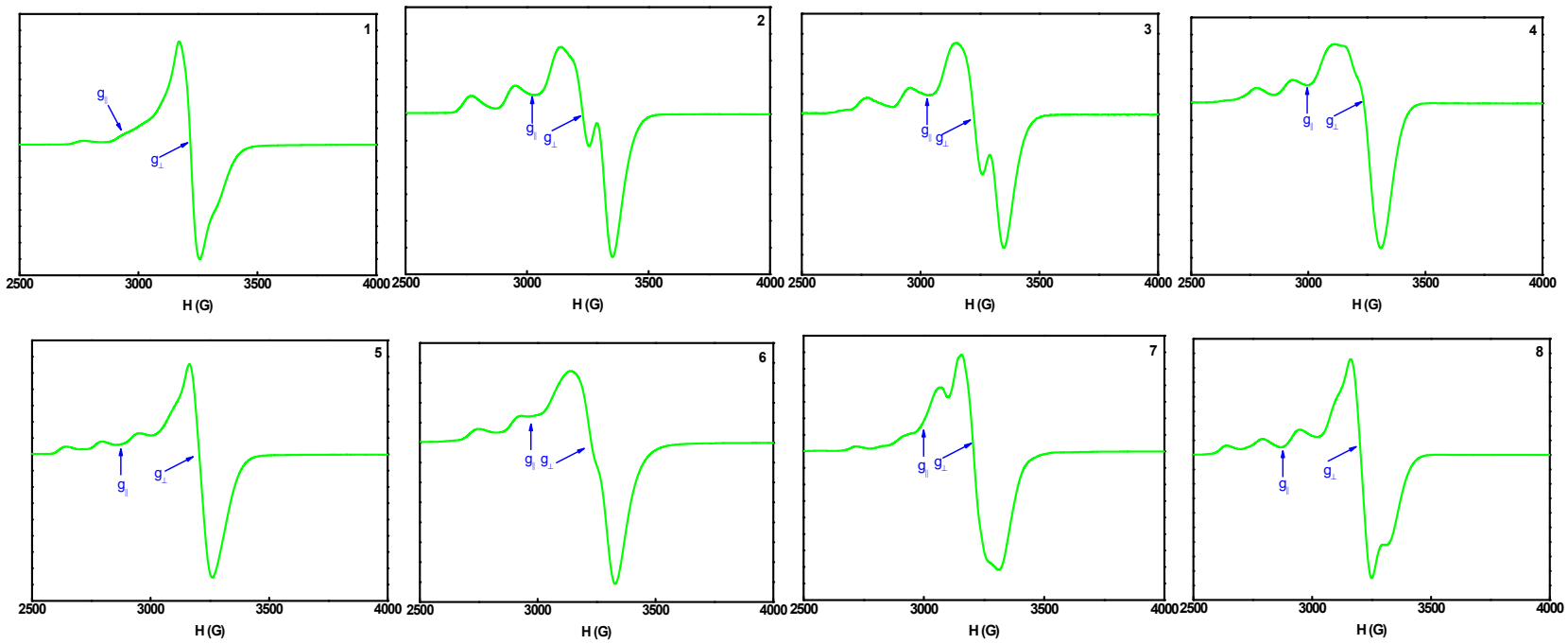

Figure S54. EPR spectrum for frozen solutions of [Cu(L1/L2/L3/L4/L5/L6/L7/L8)(phen)](ClO_4) (**1-8**) in DMF at 77K.

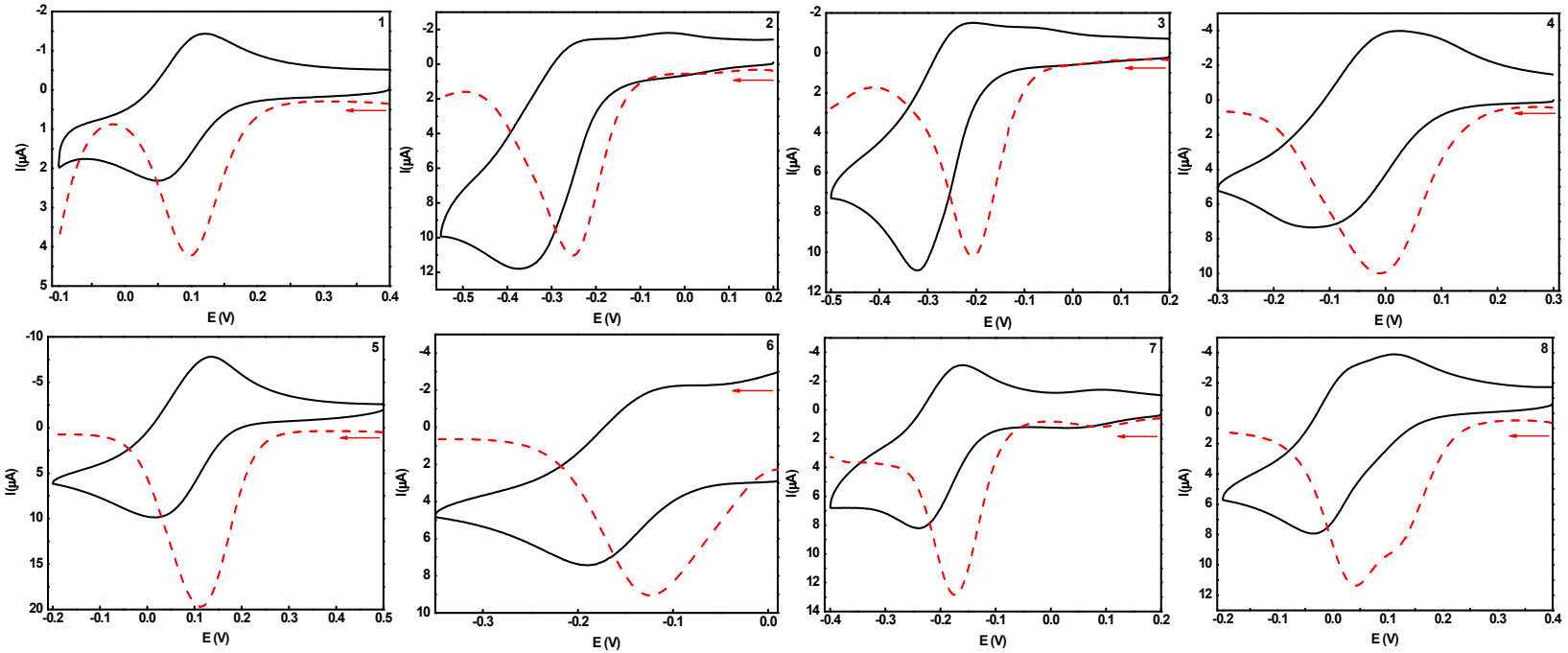

Figure S55. Cyclic (CV) (▬▬) and differential pulse (DPV) (-----) voltammograms of [Cu(L1/L2/L3/L4/L5/L6/L7/L8)(phen)]-(ClO_4) (**1-8**) (Concentration, 1×10^{-3} M) in DMF at 25 °C at 0.05 and 0.002 V s^{-1} scan rates respectively.

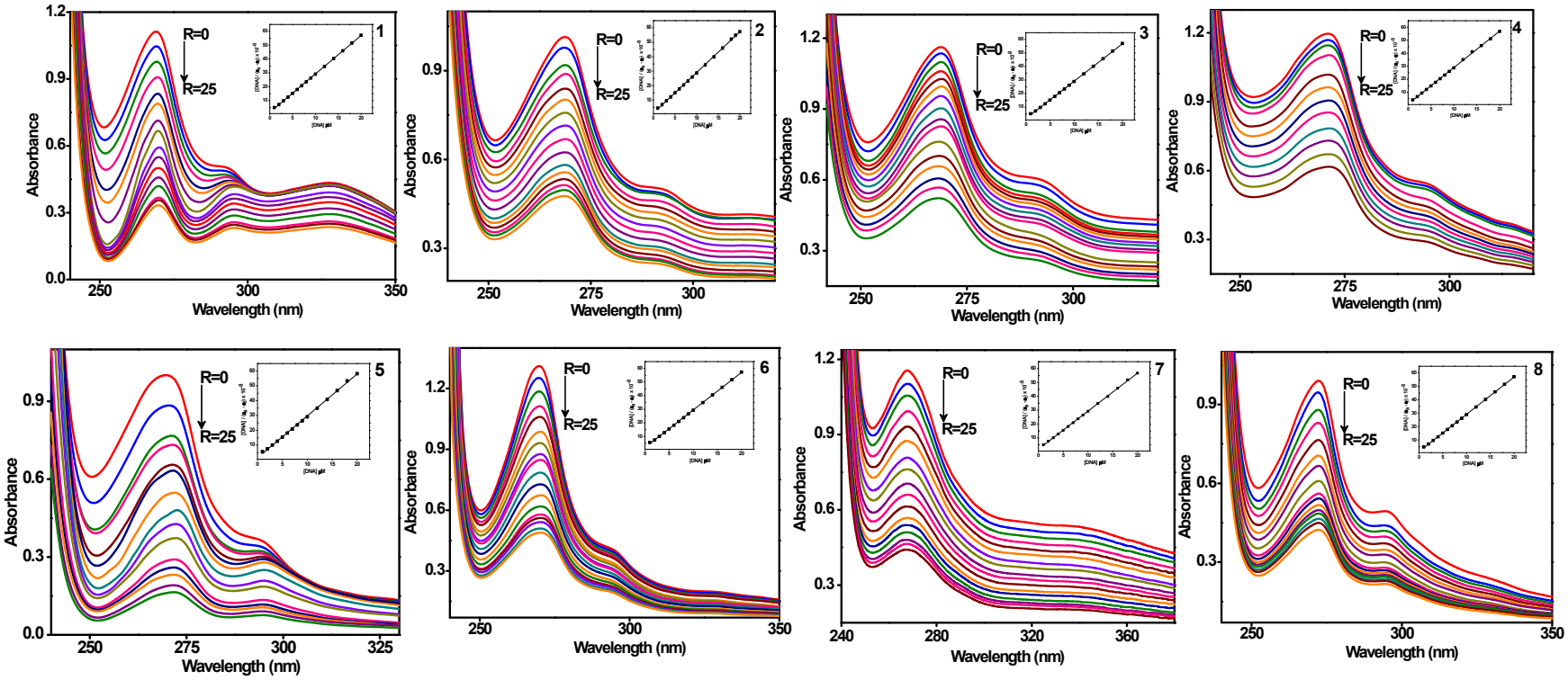

Figure S56. Absorption spectra of **1-8** (10×10^{-6} M) in 2% DMF/5 mM Tris-HCl/50 mM NaCl buffer at pH 7.1 in the absence (R = 0) and presence (R = 25) of increasing amounts of CT DNA. Inset: Plot of [DNA] vs [DNA]/(ε_a - ε_f) at R = 25 of **1-8.**

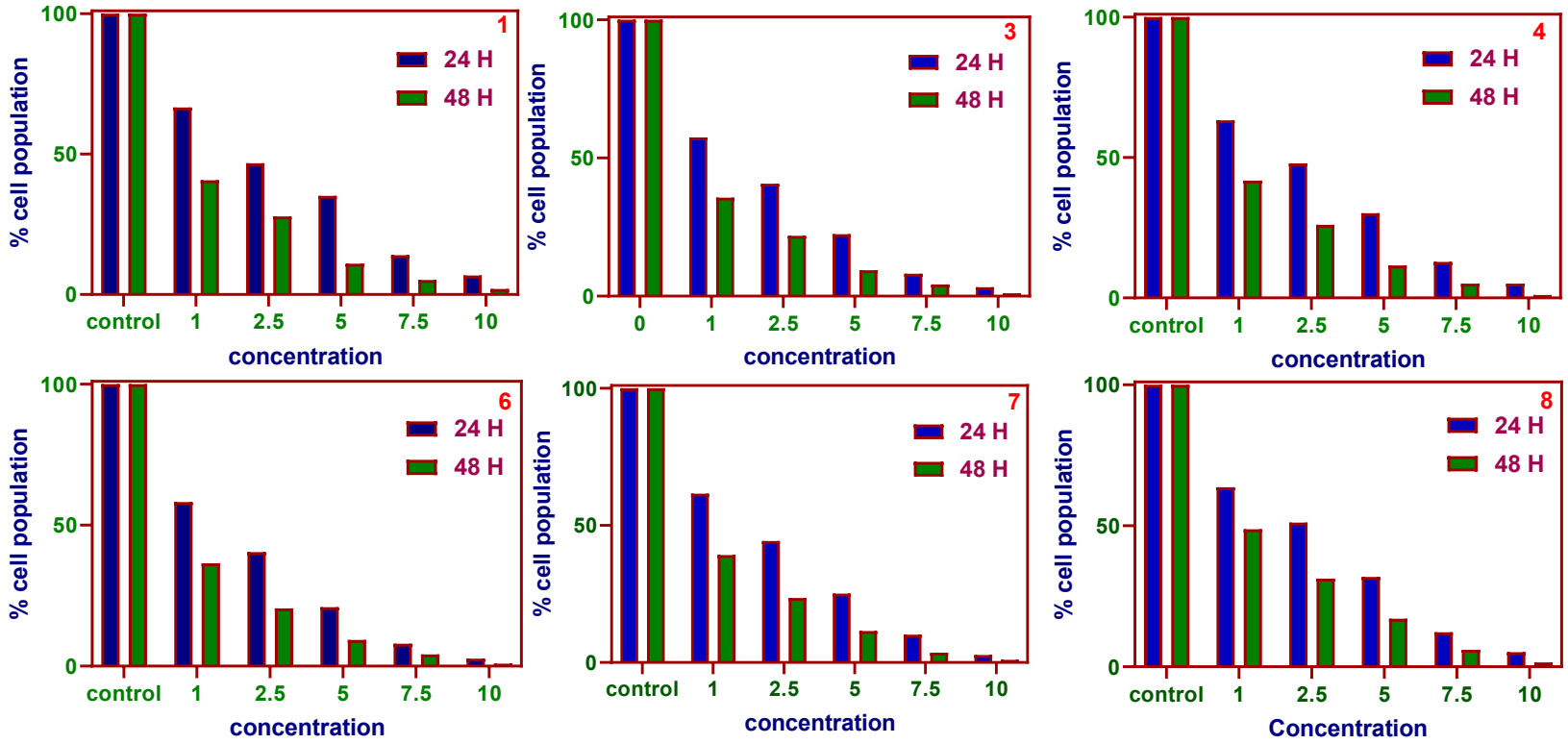

Figure S57. Cell viability of A549 Cancer cells after exposure with copper(II) complex (**1,3,4,6,7,8**) for 24 h and 48 h.

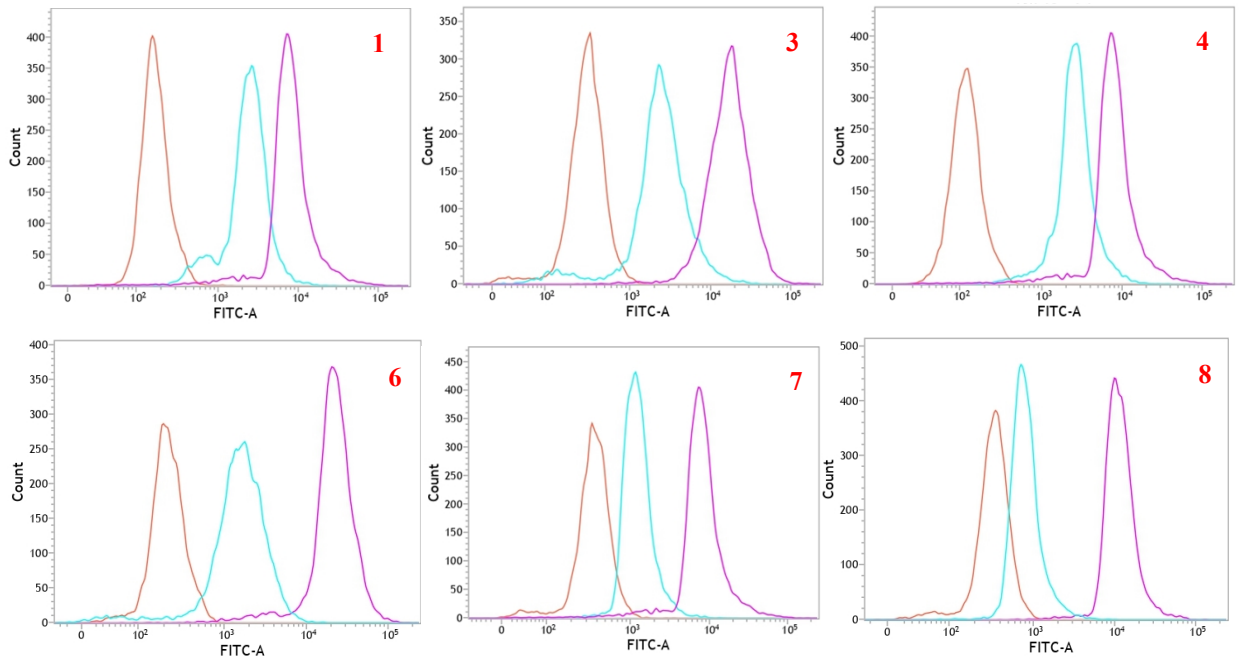

Figure S58. DCFDA assay in A549 cells for generation of ROS using copper(II) complex (**1,3,4,6,7,8**) in a time-dependent manner (orange; 0 h, pink; 12 h, blue; 24 h).

Table S4.
In vitro cytotoxicities (IC_{50} values in μM) for ligands [H(**L1**)-H(**L8**)] and Cu(II) complexes (**1**-**8**) in cancerous (A549) cell line

	24 h	**48 h**
L1	19 ± 1	14 ± 1
L2	22 ± 2	15 ± 1
L3	16 ± 1	12 ± 1
L4	15 ± 1	11 ± 1
L5	14 ± 1	11 ± 1
L6	14 ± 1	11 ± 1
L7	38 ± 2	13 ± 1
L8	22 ± 1	11 ± 1

DNA binding experiment

The UV absorbance ratio of DNA solutions (5 mM Tris HCl/50 mM NaCl buffer) at 260 and 280 nm (A_{260}/A_{280}) was 1.9,[1] showing that the DNA was adequately free of protein. In the buffer, concentrated stock solutions of DNA (13.5 mol dm^3) were made, and 25 cycles of sonication were carried out, each cycle lasting 30 s with a 1 min break. The DNA solutions were pretreated with mixed-ligand copper(II) complex(es) (1-8) in 2% DMF/5 mM Tris-HCl/50 mM NaCl buffer solution to confirm that the concentration of the complex for the absorption spectral investigations were not altered. The complex was kept at a constant concentration while the nucleic acid concentration was changed to conduct absorption spectral titration experiments. This was accomplished by dissolving a suitable quantity of the stock solutions for the metal complex and DNA while keeping the total volume constant (1 mL). As a result, a series of solutions with various DNA concentrations and the same concentration of the complex were produced. After adding CT DNA incrementally, the absorbance (A) of the band resulting from the ligand-centered π-π* transition of the complex was measured.

DNA Binding: Absorption Spectral Titration

Table S12

Absorption[a] titration of copper(II) complexes (**1**-**8**) bound to CT DNA

complex	λ_{max}	R	shift	Quenching	K_b	ΔG
	(nm)		(nm)	%	$\times 10^5$ $M^{-1)}$	
1	269	25	2	78	2.78	-13.49
2	268	25	-	58	2.81	-13.50
3	269	25	-	64	2.76	-13.48
4	270	25	1	59	2.80	-13.50
5	269	25	2	89	2.82	-13.51
6	269	25	1	83	2.76	-13.48
7	267	25	-	72	2.74	-13.47
8	272	25	-	58	2.78	-13.49

[a]Measurements were made at R = 25, where R = [DNA]/[complex], concentration of solutions of Copper(II) complexes = 30×10^{-6} M (**1**-**8**).

Understanding the tumor inhabitation mechanism is vital for cancer therapy,[2] and DNA binding is a key phase.[3] Any molecule that interacts with DNA changes the polarity of the environment and conformation in the DNA helix. The hypochromism and hypochromicity of the absorption spectrum served as a reflection of this. Therefore, using the absorption spectral technique, the mode and propensity of binding of the mixed ligand copper(II) complexes to DNA were examined. When CT DNA is gradually added to complexes at R = 25 (R = [DNA]/[Cu]), the absorption band resulting from the ligand-centered π-π* transition in the range of 269-272 nm exhibits hypochromism (**1**, 78; **2**, 58; **3**, 64; **4**, 59; **5**, 89; **6**, 83; **7**, 72; **8**, 58%) with no or minimal red-shifts in the band position (Fig. S8). The change in absorbance and shift in wavelength can be used to describe the intercalation of the complexes and DNA because the intercalation mode involves a strong stacking interaction between the aromatic plane and the DNA base pairs.

The strength of the intercalative interaction is frequently consistent with the degree of hypochromism.[4] Hypochromism and a little or nonexistent red shift are seen when CT DNA concentration increases, indicating that the mixed-ligand copper(II) complexes have a higher propensity for DNA binding due to partial intercalative interaction between the planar phen ring of the complexes and CT DNA. The interaction between the electronic states of the DNA bases

and the compound chromophores is known as hypochromicity. After the complex binds to DNA, the energy difference between the highest occupied and lowest unoccupied molecular orbitals (HOMO and LUMO) decreases, which has been linked to the red shift.[5,6] The intrinsic binding constants, K_b, of the complexes (**1**-**8**) are comparable, demonstrating that the DNA binding affinity is determined by the hydrophobic tendency of the primary ligand. The electron-releasing methyl substituent on the sulfhydryl group of the primary ligand would interact with hydrophobic DNA, increasing the affinity of **1**-**8** for binding to DNA. This is noteworthy because the size and shape of the complex are tailored to tightly fit between the base pairs, resulting in a strong hydrophobic interaction with the DNA surface, which increases the tendency of the phen ring for DNA binding. As a result, the DNA binding structure is dictated by the minute changes in coordination geometry brought about by the bonding of the nitrogens from the phen co-ligand to copper(II), and the hydrophobic propensity of the primary ligand is dependent upon the coordination geometry, increasing the DNA binding affinity. It is already known that copper(II) complexes with a higher affinity for DNA exhibit greater cytotoxicity.[7] Therefore, it is anticipated that the present mixed-ligand copper(II) complexes, which incorporate a planar phen ligand with a higher DNA binding affinity, will exhibit a higher level of cytotoxicity. The equation: $G = -RT \ln K_b$, where $R = 8.314$ J K^{-1} mol^{-1} and $T = 298$ K [8,9] was used to compute the Gibbs free energy of the binding of complexes **1**-**8** (Table S12) with CT DNA (**1**, -13.49; **2**, -13.50; **3**, -13.48; **4**, -13.50; **5**, -13.51; **6**, -13.48; **7**, -13.47; **8**, -13.49 kJ mol^{-1}). While G denotes whether the complex-DNA interaction is spontaneous or non-spontaneous, the constant K_b measures the stability of the complex-DNA adduct. Indicating spontaneous binding between these mixed-ligand copper(II) complexes and CT DNA, all G values for **1**-**8** were found to be negative.

References

1 J. Marmur, *J. Mol. Biol.* 1961, **3**, 208-218.

2 M. Chauhan, K. Banerjee, F. Arjmand, *Inorg. Chem.* 2007, **46**, 3072.

3 F. Arjmand, M. Aziz, M. Chauhan, *J. Inclusion Phenom. Macrocyclic Chem.* 2008, ***61***, 265.

4 P. Krishnamoorthy, P. Sathyadevi, A.H. Cowley, R.R. Butorac, N. Dharmaraj, *Eur. J. Med. Chem.* 2011, **46**, 3376.

5 V.M. Manikandamathavan, R.P. Parameswari, T. Weyherműller, H.R. Vasanthi, B.U. Nair, *Eur. J. Med. Chem.* 2011, **46**, 4537.

6 W.J. Mei, J. Liu, C.K. Zheng, L.J. Lin, H. Chao, A.X. Li, F.C. Yun, L.N. Ji, *Dalton Trans*. 2003, **7**, 1352.

7 R. Loganathan, S. Ramakrishnan, E. Suresh, M. Palaniandavar, A. Riyasdeen, M.A. Akbarsha, *Dalton Trans*. 2014, **43**, 6177.

8 P. Ghorai, R. Saha, S. Bhuiya, S. Das, P. Brandão, D. Ghosh, T. Bhaumik, P. Bandyopadhyay, D. Chattopadhyay, A. Saha, *Polyhedron* 2018, **141**, 153.

9 M.N. Zafar, S. Masood, G.-S. Chaudhry, T.ST. Muhammad, A.F. Dalebrook, M.F. Nazar, F.P. Malik, E.U. Mughal, L.J. Wright, *Dalton Trans*. 2019, **48**, 15408.